Mechanisms that relate transverse loading of muscle to changes in contractile performance.

by

David Stephen Ryan

M.Sc., Wageningen UR, 2012

Thesis Submitted in Partial Fulfillment of the
Requirements for the Degree of
Doctor of Philosophy

in the
Department of Biomedical Physiology and Kinesiology
Faculty of Science

SIMON FRASER UNIVERSITY
Summer 2020

Approval

Name:	**David Stephen Ryan**
Degree:	**Doctor of Philosophy**
Title:	**Mechanisms that relate transverse loading of muscle to changes in contractile performance.**
Examining Committee:	**Chair:** Sam Doesburg Associate Professor
	James M. Wakeling Senior Supervisor Professor
	Tobias Siebert Supervisor Professor Institut für Sport- und Bewegungswissenschaft Universität Stuttgart
	Nilima Nigam Supervisor Professor Department of Mathematics
	Dan Marigold Internal Examiner Associate Professor
	Glen Lichtwark External Examiner Associate Professor School of Human Movement and Nutrition Sciences The University of Queensland
Date Defended/Approved:	July 9, 2020

Ethics Statement

The author, whose name appears on the title page of this work, has obtained, for the research described in this work, either:

a. human research ethics approval from the Simon Fraser University Office of Research Ethics

or

b. advance approval of the animal care protocol from the University Animal Care Committee of Simon Fraser University

or has conducted the research

c. as a co-investigator, collaborator, or research assistant in a research project approved in advance.

A copy of the approval letter has been filed with the Theses Office of the University Library at the time of submission of this thesis or project.

The original application for approval and letter of approval are filed with the relevant offices. Inquiries may be directed to those authorities.

Simon Fraser University Library
Burnaby, British Columbia, Canada

Update Spring 2016

Abstract

Research has shown that factors such as the contraction of surrounding muscle, resistance to radial expansion, and external transverse loading have an effect on the way that muscle performs. Such factors are often ignored when doing muscle experiments, yet they can have significant effects on the force and power that a muscle is able to produce. The aim of this thesis is to determine to what degree external loading affects muscle force and to study the changes in muscle architecture due to external loading. The purpose of this thesis was to determine whether external transverse loading causes force reduction in humans, how external transverse loading affects muscle architecture, and describe the mechanisms involved. We applied an external transverse load to the medial gastrocnemius of prone participants as a point loaded mass. Transverse loading reduced ankle torque with higher loads resulting in greater reductions. Passive transverse loading caused a decrease in the resting pennation angle and muscle thickness, with higher loads leading to greater decreases. During activation of the muscle the pennation angle, muscle thickness, and fascicle thickness increase transiently relative to the amount of transverse loading. Alterations to the design of the experiment were made by applying a multi-directional external transverse load and changing the position of the participants from prone to seated, where sitting changed the resting length of the muscle. Our altered experiments showed no change in ankle torque. Minor differences were shown for pennation angle and muscle thickness both at passive resting values and peak active values, but not for fascicle thickness and fascicle. Fascicle thickness decrease transiently, and fascicle length increased. We replicated the external transverse loading experiments using a three-dimensional finite element model of a fibre-reinforced, non-linearly-elastic transversely isotropic composite biomaterial. The model consists of active and passive force-length properties of muscle fibre as well as passive force-length properties of base material. Results show external transverse loading causes architecture changes and reductions in muscle force. Muscle force reduction is dependent on direction of loading, initial pennation, and initial muscle length.

Keywords: transverse loading; ultrasound; force; muscle architecture; finite element method

Acknowledgements

First and foremost I would like to thank my supervisor James for accepting me into his lab and allowing me to work towards getting my Ph.D.. You have always been available and willing to discuss my work and your enthusiasm and guidance have always motivated me to perform to the best of my ability. You provided amazing opportunities during my research to travel and collaborate with others. It has truly been inspiring to work for you and has encouraged me to pursue a career in academia. Thank you for all the time and effort you have spent on me and my research over the past years.

I would like to thank Tobias Siebert for his contributions to my research. Thank you for the opportunity to visit and work for you. Thank you for accepting me into your lab and into your home. It was a wonderful experience and I was able to learn a lot. Thank you for your support and all you have done.

Thank you to Nilima Nigam for the work she has provided towards my research. You have provided me with a great opportunity to work outside of my field. As such I was able to learn more than would have otherwise been possible. Thank you for all your effort and encouragement.

Thank you to Norman Stuzig for working with me on my research. Thank you for accepting me into your home and the time spent together.

To all the current and former lab members thank you for kindness and support during my time in the lab. You provided a great work environment and it was wonderful working with all of you. Thank you to Basant Chana, Dr Oliver Blake, Dr Taylor Dick, Dr Avleen Randhawa, Dr Hadi Rahemi, Dr Adrian Lai, Dr Courtney Pollock, Stephanie Ross, Sebastián Domínguez, Amy Robinson, Jaylene Pratt, Ryan Konno, and Cassidy Tam.

Last but not least I would like to thank my family (Tim, Nel, and Andrew) for their continues support. Without you this would not have been possible. Thank you for everything. Also, to my friends, thank you for your encouragement.

Table of Contents

Approval ..... **Error! Bookmark not defined.**
Ethics Statement ii
Abstract iv
Acknowledgements v
Table of Contents vi
List of Tables ix
List of Figures xi
List of Symbols xiv
Published studies xvi

Chapter 1. Introduction 1
1.1. Muscle Structure and Function 2
1.1.1. Sarcomere structure 2
1.1.2. Sliding filament theory 3
1.1.3. Isovolumetric properties 3
1.1.4. Link between longitudinal and transverse forces 4
1.1.5. Force-length 4
1.1.6. Muscle fibre pennation 5
1.2. Transverse loading of muscle 7
1.3. Experimental quantification of muscle architecture 10
1.3.1. Ultrasound Imaging 11
1.3.2. Automated tracking of muscle architecture 13
1.3.3. Digital Image Processing 13
Image convolution 14
Frangi filter 15
Hough transform 16
Fourier transform 17
Fascicle curvature 18
1.4. Computational simulations of muscle force 19
1.5. Specific Aims 22

Chapter 2. Passive and dynamic muscle architecture during transverse loading for gastrocnemius medialis in man 25
2.1. Introduction 25
2.2. Materials and Methods 27
2.3. Results 30
2.4. Discussion 34
2.4.1. Force reduction 35
2.4.2. Muscle deformation 35
2.4.3. Fascicle pennation and length 36
2.4.4. Intramuscular pressure 36
2.4.5. Muscle models 37

2.4.6. Fascicle length calculation 38
2.4.7. Limitations 38
2.4.8. Conclusion 39

Chapter 3. The effect of multidirectional loading on contractions of the medial gastrocnemius 40
3.1. Introduction 40
3.2. Material and Methods 43
3.3. Results 49
3.4. Discussion 57
3.4.1. Muscle length compared to the force-length relationship 57
3.4.2. Knee angle related to muscle force 58
3.4.3. Pennation angle of transversely loaded muscle 58
3.4.4. Anisotropic deformation 59
3.4.5. Fascicle curvature 59
3.4.6. Limitations 61
3.4.7. Conclusion 63

Chapter 4. External transverse loading of muscle using the finite element method 64
4.1. Introduction 64
4.2. Methods 66
4.3. Results 75
4.4. Discussion 84
4.4.1. Changes in muscle architecture 84
4.4.2. Muscle force reduction 85
4.4.3. Initial muscle length 86
4.4.4. Loading direction 87
4.4.5. Initial pennation angle 87
4.4.6. Comparison of physical experiments and example computational experiments 88
4.4.7. Muscle energies 88
4.4.8. Limitations 89
4.4.9. Conclusion 91

Chapter 5. Discussion 92
5.1. Thesis Summary 92
5.1.1. Comparing unidirectional against multidirectional loading 93
5.1.2. The effect of muscle length 94
5.1.3. Comparing force measurements 95
5.1.4. Transverse expansion of the muscle 96
5.1.5. Pennation angle changes 96
5.1.6. Muscular hydrostats 98
5.1.7. Duration of architecture changes 99
5.1.8. Comparing the finite element model to physical experiments 100

5.1.9. Example computational experiments compared to physical experiments .. 101
5.1.10. Comparison of muscle models 104
5.2. Avenues of Future Research 105
5.2.1. Muscle length measurement 105
5.2.2. Effects of fat accumulation 105
5.2.3. Errors in ultrasound imaging 106
5.2.4. Muscle force measurement from ultrasound 107
5.2.5. Extracellular matrix restrictions to bulging due to aging 108

References 110

Appendix 128

List of Tables

Table 2-1 The values (mean ± SE) for each trial of the measured muscle architecture. The values are given for muscle at rest (passive), at peak active contraction (active), and the change that have occurred. Significant differences between trials are given († - sign. differences between 2 kg and 4.5 kg, ‡ - sign. differences between 4.5 kg and 10 kg, + - sign. differences between 2 kg and 10 kg). The transverse wavelength corresponds to fascicle thickness. 31

Table 3-1 Calculations of the baseline variation between the end and beginning of consecutive twitches compared to the change in muscle architecture. The mean measured change in muscle architecture was compared to thresholds of the baseline variation at the mean plus 1, 2, and 3 times the standard deviation. Comparisons were made for all trials for the pennation angle, muscle thickness, fascicle thickness, and fascicle length. The table indicates changes higher than the threshold (green, clear) and lower than the threshold (red, shaded). 53

Table 3-2 Curvatures for the four trials at resting passive and peak active states. Comparisons of the curvatures are made between the four trials at both passive resting and peak active state. Data show the mean and standard deviation of all twitches. Significances are indicated between pretest and 5 kg (*), pretest and 10 kg (†), pretest and posttest (|), 5 kg and 10 kg (±), 5 kg and posttest (‡), and 10 kg and posttest (+). 55

Table 3-3 Comparisons of the muscle architecture measurements between the four trials at passive resting state, peak active state, and the change between passive and active. Means and standard deviations are given for the pennation angles, muscle thicknesses, transverse wavelengths, and fascicle lengths. Significances are indicated between pretest and 5 kg (*), pretest and 10 kg (†), pretest and posttest (|), 5 kg and 10 kg (±), 5 kg and posttest (‡), and 10 kg and posttest (+). 56

Table 4-1 Details on the example computational experiments. Each computational experiment varies in initial pennation angle, initial muscle length, loading direction, and loading intensity. 80

Table 4-2 The forces calculated for the example computational experiments. Shown are the values at the unloaded, loaded, and maximum active state of each computational experiment. Given are the change in force between the unloaded and loaded state, as well as between the loaded and maximum active state and unloaded and maximum active state. The percentage force reduction between the unloaded and maximum active state is also given. 80

Table 4-3 The length, thickness, and width for the example computational experiments. Shown are the values at the unloaded, loaded, and maximum active state. Also shown are the change between the unloaded and loaded state, as well as between the loaded and maximum active state. 81

Table 4-4 The pennation, volume, and pressure for the example computational experiments. Shown are the values at the unloaded, loaded, and maximum active state. Also shown are the change between the unloaded

and loaded state, as well as between the loaded and maximum active state..... 82

List of Figures

Figure 1-1 A schematic of a sarcomere. The schematic shows the myosin (red), actin (blue), and titin (green) filaments, along with the Z discs (purple), I bands, A band, and H zone. 2

Figure 1-2 Definitions for the different architecture elements as they are used throughout this thesis. Shown are the definitions for muscle thickness, pennation angle, fascicle width, and fascicle length. 12

Figure 2-1 Schematic of the experimental design. Showing the position of the force plate (a) and the point at which load was added (b). The point of contact between the gastrocnemius and the transversal load is at the same position that the ultrasound probe was positioned (c). The calf muscles of the participants were stimulated in the popliteal fossa with a current stimulator (d). 28

Figure 2-2 Mean maximum twitch forces (MTF; mean ± SE), for each trial, given as percentage of pretest twitch force. Statistics showed no significant differences between pretest and posttest force. The forces for each loaded trial were significantly different from one and other as well as from the pre- and posttest. Means with different letters are significantly different ($p < 0.001$). 31

Figure 2-3 Changes in muscle architecture induced by transverse muscle loading. Absolute values for pennation angle (A), muscle thickness (C), and transverse wavelength (E) as well as corresponding changes in pennation angle (B) and strains for muscle thickness (D) and transverse wavelength (F). Twitch force is presented in (G). Note that, the transverse strain of wavelengths corresponds to the transverse strain of the fascicles . The graphs show the mean of all participants with standard errors for the 2 (red), 4.5 (black), and 10 kg (blue) trials. Muscle thickness and transverse wavelength changes were scaled to the 2 kg trials. Higher transverse loads show lower absolute values both for passive values and during contraction. The changes in transverse wavelength were interpreted as fascicle thickness strains. 33

Figure 2-4 Fascicle lengths (A) and fascicle length changes (B) during contraction for the 2 (red), 4.5 (black), and 10 kg (blue) trials (mean ± SE). The changes were scaled to the 2 kg trials. Fascicle length was calculated as a function of pennation angle and muscle thickness. 34

Figure 2-5 Measured values for muscle thickness (A), pennation angle (B), and wavelength (C) for individual measurements. The values are given for muscle at rest (blue), and at peak active contraction (red). The box plots show the mean with 25 and 75 % quantiles with the whiskers showing the minimum and maximum values. 34

Figure 3-1 Experimental design for the collection of force data and ultrasound data. Participants were seated in a custom designed chair with their right foot placed on a force plate (A). Through the use of a pully system weights (B) loaded the sling (C) which was wrapped around the calf to apply transverse loads to the muscle. Ultrasound images (D) were taken of the medial gastrocnemius, and the muscle was stimulated using an electrode (E) in the popliteal nerve. 44

Figure 3-2 Ultrasound example data of the medial gastrocnemius. Ultrasound images for the passive unloaded pretest (A) and the passive 10kg loaded (B) measurements. 46

Figure 3-3 Images illustrating fascicle trajectory calculation. Example of a fascicle trajectory calculated along 11 points (A). Schematic of a fascicle trajectory calculation with a 3 pixel jump distance and 4 jumps along the trajectory. 48

Figure 3-4 The mean changes in muscle architecture and force measured during muscle twitches. The mean and standard error for all measured twitches are plotted for the pre- (green, solid) and posttest (gray, dot-dashed), and the 5 kg (blue, dashed) and 10 kg (red, dotted) loaded trials. Transient increases are shown for the pennation angle (A,B) and muscle thickness (C,D). The transverse wavelength (E,F) and fascicle length (G,H) show transient decreases. The measured twitch force (I) shows an increase with muscle activation. 51

Figure 3-5 The passive loaded and peak active loaded values for all twitches. Passive (blue) and active (red) values are shown for the pennation angle (A), muscle thickness (B), transverse wavelength (C), and fascicle length (D). The dots show individual twitches with the boxes showing the mean and span from the 0.25 to the 0.75 quantile. Significant differences are shown between passive and active states (*, $p < 0.001$). 52

Figure 3-6 Mean resting passive (blue) and peak active (red) curvatures measured for all trials. The error bars indicate the standard deviations. The loaded trials show lower curvatures than the unloaded trials, and for the loaded trials the peak active curvature is higher than the resting passive curvature. Significances between trials are shown (*, $p<0.05$). 54

Figure 4-1 Schematic of the cubes on which the model will be computed. The cubes vary in initial pennation angle and initial strain. 67

Figure 4-2 Force-length relationship of the muscle fibres as they are used in the finite element model. Shown are the active force-length properties (solid) and the passive force-length properties (dashed). 72

Figure 4-3 Initially the model is set to lengthen or shorten the muscle (A). Following is the compression of the muscle with top (B), side (C), and all (D) compression. Last is the activation of the muscle with top (E), side (F), and all (G) compression. The figure shows compressed faces (blue), faces fixed in the x axis (orange), faces fixed in all axes (red), faces fixed in the z axis (yellow), and faces with traction applied (green). 74

Figure 4-4 Least Square Means of the force by external loading. For the four external transverse loads it is shown that higher external loads result in lower force along the line of action (x axis) of the muscle block. These forces are calculated from a combination of all conditions. Forces were taken on the positive x face in the x direction at 0% (a), 50% (b), and 100% (c) activation. The error bars represent the standard error of the least square means force. 76

Figure 4-5 The Least Square Means of the force for the computational experiments by direction of loading. Data were taken for 0% (a), 50% (b), and 100% (c) activation. External transverse loading from any direction led to lower force compared with no external load. Force reduction is greatest for

compression from all directions. The error bars represent the standard error of the least square means force. 77

Figure 4-6 The Least Square Means of the muscle force for the experiments by amount of load separated for five different initial pennation angles at 0% (a), 50% (b), and 100% (c) activation. The greatest reduction in least squares mean force is shown for computational experiments with pennation angles of 0° and 10°. Higher pennations lead to less reduction in least squares mean force as well as lower least squares mean forces for each amount of external loading. The error bars represent the standard error of the least square means force. 78

Figure 4-7 The Least Square Means of the force for the computational experiments by load separated for initial muscle length at 0% (a), 50% (b), and 100% (c) activation. Force reduction is more pronounced with longer muscle lengths. The error bars represent the standard error of the least square means force..... 79

Figure 4-8 Strain-energy potentials for the computational experiments at 100% activation. The computational experiments are separated by initial muscle length, initial pennation angle, external load, and loading direction. Shown are the volumetric (purple), active (orange), passive (dark blue), and base material (light blue) strain-energy potentials. 83

List of Symbols

f_c	applied force
f	fibre force
α	Pennation angle
K	kernel
I	image region
$\mathcal{H}$	Hessian
$gauss(x, y)$	gaussian function
$\nu_0(s)$	vesselness
λ_2	largest eigenvalue
$\mathcal{R}_B$	geometric ratio
β	threshold value
c	threshold value
$\mathcal{S}$	square root of the sum of the eigenvalues squared
F_{m}	muscle force
$F_{\max}$	maximum isometric force
$\hat{a}(t)$	activation
$\hat{F}_{\mathrm{a}}(\hat{l}_{\mathrm{f}})$	active force-length relationship
$\hat{F}_{\mathrm{p}}(\hat{l}_{\mathrm{f}})$	passive force-length relationship
$\hat{F}_{\mathrm{a}}(\hat{v})$	active force-velocity relationship
l_f	fascicle length
T_m	muscle thickness
Δp	change in pressure
γ	tension
R	radius
E	total strain energy
$U(u, \tilde{J}, \tilde{p})$	total strain energy potential
u	displacement
$\tilde{J}$	dilation
$\tilde{p}$	pressure
U_{int}	internal strain energy potential
U_{ext}	external strain energy potential
F	deformation gradient

$\psi_{\mathrm{vol}}(\tilde{J})$	volumetric strain energy density
$\psi_{\mathrm{iso}}(\bar{b})$	isochoric strain energy density
$\overline{(b)}$	left Cauchy-Green tensor
v	volume
a	boundary area
Ω	system domain
$\partial\Omega$	system boundary
f_b	boundary force
f_t	traction force
κ	bulk modulus
ψ_{muscle}	muscle strain energy density
ψ_{base}	Base material strain energy density
$\sigma_{muscle}(\lambda)$	muscle fibre stress
λ	Along fibre stretch
σ_0	maximum isometric force
$\hat{\sigma}_{active}(\lambda)$	active muscle fibre stress
$\hat{\sigma}_{passive}(\lambda)$	passive muscle fibre stress

Published studies

Research contained in this thesis has been published in the following peer-reviewed journals:

Chapter 2	Ryan, D.S., Stutzig, N., Siebert, T., Wakeling, J.M. (2019) Passive and dynamic muscle architecture during transverse loading for gastrocnemius medialis in man, *J. Biomech.*, 86, pp. 160-166.

Chapter 1.

Introduction

The main goal of this thesis is to study the effect of external transverse loading of skeletal muscle on muscle force production and architecture. This is achieved by performing external transverse loading experiments on the medial gastrocnemius of humans, as well as through a three-dimensional finite element muscle model. Previous research has shown that external transverse loading and restrictions to radial expansion of skeletal muscle reduces muscle performance in rats (Siebert *et al.*, 2014a), frogs (Azizi *et al.*, 2017; Sleboda and Roberts, 2019), and rabbits (de Brito Fontana *et al.*, 2018). These studies have shown that external transverse loading and restrictions to radial expansion can reduce muscle force (Siebert *et al.*, 2014; de Brito Fontana *et al.*, 2018; Sleboda and Roberts, 2019), increase muscle force (Sleboda and Roberts, 2019), and reduce work performed by the muscle (Azizi *et al.*, 2017).

Previous research has shown that external transverse loading affects muscle performance in animal models, however it has not been established if human muscle is affected in a similar manner. The effects of external transverse loading on muscle architecture have not been studied either. We aim to show that force reduction occurs in human muscle as a result of transverse loading. Furthermore, we aim to give a better understanding of the mechanisms involved in force reduction due to external transverse loading by studying variations in muscle length, pennation angle, and loading directions.

In this introduction we present an overview of muscle physiology and the basic mechanisms involved in muscle contraction as they relate to transverse loading. We give a brief description of our interpretation of external transverse load and describe previously performed research studying external transverse loading. Following this we discuss the analysis techniques used throughout this thesis to give a basic understanding of where they come from and how they are applied. We aim to give the reader a basis on which they can interpret the research performed as part of this thesis.

1.1. Muscle Structure and Function

Muscle has the ability to contract and in doing so it is able to generate force. The contraction of skeletal muscle starts in its smallest repeating unit, the sarcomere. The sarcomere is made up of myofilaments that slide past one and other to generate force in a process named the sliding filament theory.

1.1.1. Sarcomere structure

A sarcomere runs from Z disc to Z disc and within these are contained the I band, the A band, and the H zone (Figure 1-1). Within the sarcomere there are three main types of myofilament: actin, myosin, and titin. The I band is a section that contains the Z disc and actin filaments. The A band contains both actin and myosin filaments. The H zone is a section that only contains myosin filaments. These regions are clearly visible in light microscope images, showing up as dark and light bands which gives striated muscle its striped pattern (Huxley and Hanson, 1954; Huxley and Niedergerke, 1954; Fox, 2006). Titin is a large protein that spans the I and A band connecting the myosin filaments to the Z discs. The titin functions as a spring and is partly responsible for the passive elastic properties of the sarcomere (Li *et al.*, 2002; Labeit and Kolmerer, 2014). The other filaments, actin and myosin will be discussed in the following section on the mechanics of sarcomeres.

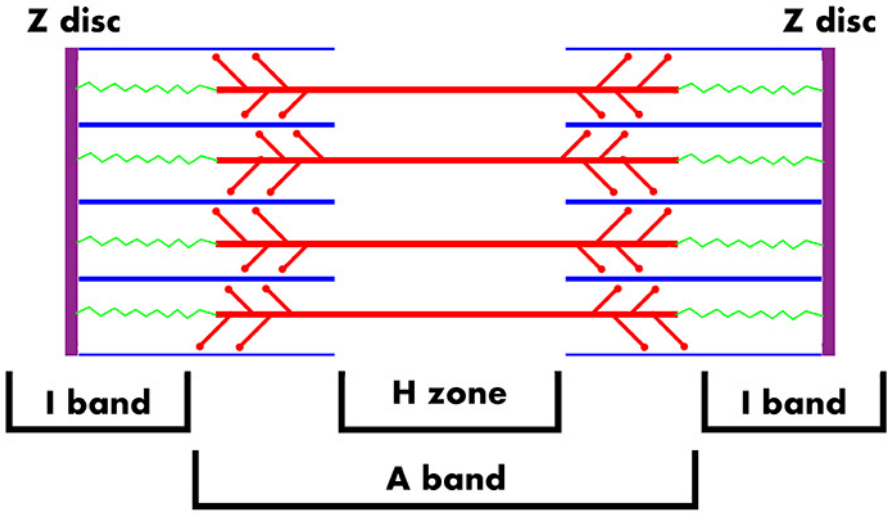

Figure 1-1 **A schematic of a sarcomere. The schematic shows the myosin (red), actin (blue), and titin (green) filaments, along with the Z discs (purple), I bands, A band, and H zone.**

1.1.2. Sliding filament theory

The mechanism of the sarcomere was first published in 1954 by Huxley and Niedergerke (1954) and Huxley and Hanson (1954). Both developed the same theory individually and they were slightly different, however generally they determined the same mechanism was involved. The theory that they developed is now known as the sliding filament theory. The modern interpretation of this theory is as follows. The myosin and actin filaments are interlocked in a hexagonal pattern in such a way that they can slide alongside one and other. Extrusions on the myosin, which consist of an arm and two heads, are able to bind with the actin and form cross-bridges. The molecule adenosine triphosphate (ATP) is able to bind to the head of the myosin which puts the myosin head in a state where it is able to bind with an actin binding site. As the myosin head binds to the actin the ATP is reduced to adenosine diphosphate (ADP) and phosphate (Pi) and as the phosphate is released the myosin head undergoes a structural change. This power stroke of the myosin head pulls the myosin along the actin, after which the ADP is released. The cross-bridge now remains attached until another ATP molecule binds to it and causes it to release and again load the head ready to bind again (Cooke, 1997; Gordon *et al.*, 2000; Fox, 2006). As the heads of the myosin filaments bind, power stroke, and unbind, in a process called cross-bridge cycling, the myosin are able to slide along the actin which causes the sarcomere to shorten. Lengthening of the sarcomeres happens as cross-bridges release and the sarcomere is stretched by an external force.

Sarcomeres are often considered to be one-dimensional actuators. However, for external transverse load to affect the longitudinal force of the sarcomere there has to be some form of three-dimensional interaction connecting transverse and longitudinal forces. Ideas linking the transverse and longitudinal forces often depend on the muscle maintaining a nearly constant volume or being nearly isovolumetric.

1.1.3. Isovolumetric properties

Skeletal muscle as a whole is what is known as a near isovolumetric material. Meaning that muscle remains at nearly a constant volume (Abbott and Baskin, 1962). The first indications that muscle hardly changed volume where in the 17th century, when Jan Swammerdam tried to prove the exact opposite (Cobb, 2002). The near isovolumetric property of muscle is important because it means that a muscle does not

shrink as it shortens. Rather, it will shorten along its line of action and expand in the transverse directions. This is most clearly seen in the bulging of muscle during an active contraction.

1.1.4. Link between longitudinal and transverse forces

One way in which transverse forces can be linked with longitudinal forces is through the structure of the sarcomere. Like whole muscle the sarcomeres maintain a near constant volume (Millman, 1998; Irving *et al.*, 2000). As such when sarcomeres contract the radial distance between actin and myosin filaments (lattice spacing) increases. The change in lattice spacing was shown to have an effect on the force-length relationship of the sarcomere (Williams *et al.*, 2013). The possibility exists that external transverse loading affects lattice spacing and changes the force produced by the sarcomere.

As a muscle contains approximately 80 % water (Van Loocke *et al.*, 2008) it has been suggested that the water acts as a hydraulic gear between the transverse and longitudinal directions (Siebert *et al.*, 2014a). The transverse load compressed the fluid in the muscle in the transverse direction causing it to expand in the longitudinal direction. The expansion of the fluid in the longitudinal direction would act against the contraction of the muscle and cause a reduction in muscle force.

The extracellular matrix surrounding the muscle fibres has also been suggested as a cause for muscle force reduction as a result of external transverse loading. The external transverse load could cause the helical collagen fibres of the extracellular matrix (Bailey *et al.*, 1979; Rowe, 1981; Purslow and Trotter, 1994; Gillies *et al.*, 2011) to reorient to be more in line with the longitudinal direction of the muscle fibre (Siebert *et al.*, 2014b). This could increase the passive forces in longitudinal direction of the muscle fibres and reduce the force the muscle fibres produce.

1.1.5. Force-length

As previously mentioned, muscle force is dependent on the sarcomeres within the muscle. More precisely the structural arrangement of the sarcomeres determines the maximum isometric force of the muscle. Isometric contractions are contractions where

the muscle does not change in length. The maximum isometric force is an important value that is used when discussing the force-length relationship. One of the earliest descriptions of the force-length relationship is by Ramsey and Street (1940). Studies have followed Ramsey and Street (1940) determining the force-length relationship for frog muscle fibres (Gordon *et al.*, 1966; Moss, 1979) and cat soleus muscle (Rack and Westbury, 1969) and has been used when modelling muscle (Zajac, 1989). The relationship describes how the length of a muscle determines the force that it can produce. This curve is often normalized to the maximum isometric force which the muscle is able to produce at its optimum length. The force-length relationship is often described as two curves, the active and passive force-length curves. The active force-length curve describes how much force a contracting sarcomere, fibre, or muscle can produce and results from the cross-bridges that form between the myosin and actin filaments. The active force-length curve consists of an ascending limb and a descending limb, and a peak at optimum length. The passive force-length curve describes the elastic properties that a sarcomere, fibre, or whole muscle has when it gets stretched beyond optimum length and results largely from the protein titin.

External transverse loads could cause the muscle or muscle fibres to lengthen due to being compressed. This together with the resting muscle length at the time of external transverse loading will determine where on the force-length curve the muscle will be working. Lengthening of the muscle or muscle fibres could cause a reduction in the number of cross-bridges that can be formed on a sarcomere level. The lower number of cross-bridges could result in a reduction in the force that is produced.

1.1.6. Muscle fibre pennation

The pennation angle of a muscle is the angle between the longitudinal direction of the muscle fibres, and the line of action of the muscle. External transverse loading can cause reorientation of the pennation angle of pennate muscles either through lengthening the muscle or compressing the thickness of the muscle.

Skeletal muscle differs in fibre orientations from muscle to muscle and can be split into three types, namely parallel, unipennate, and multipennate muscle (Gans and Bock, 1965; Lieber and Fridén, 2000; Eng *et al.*, 2018). A parallel fibred muscle is a muscle where the muscle fibres all run parallel to the line of action of the muscle. In a

pennate muscle the fibres run oblique to the line of action, with all the fibres running in the same direction. For a multipennate muscle the fibres run oblique to the line of action and there are two distinct fibre angles. In parallel fibred muscles the fibres transition into a tendon on either end of the muscle (Elliott, 1965; Benjamin and Ralphs, 2000). The tendon is a stiff structure primarily made of collagen fibres (Heinemeier *et al.*, 2007; Kjær *et al.*, 2009). In pennate and bipennate muscles this is not possible. For a pennate muscle the fibres transition into an aponeurosis, which in turn transitions into a tendon (Magnusson *et al.*, 2003). The aponeurosis is a thin sheet of connective tissue mostly made up of collagen fibres, and like tendon is much stiffer than muscle tissue is (Azizi *et al.*, 2009). A bipennate muscle will have an internal tendon to which each half of the muscle can connect (Brukner and Connell, 2016).

Parallel fibred muscles have fibres, or series of fibres, that run from tendon to tendon and this allows for a large range of motion and high muscle velocities. However, the force depends on the number of parallel muscle fibres that the muscle contains. Each fibre, or series of fibres, in parallel within a muscle adds to the force of the muscle. As such, it is an advantage to have as many muscle fibres in parallel as possible when that muscle needs to produce a high force. However, the more parallel fibres in a muscle the thicker it gets and often times the constraints of the body do not allow for a thick muscle. In situations such as these is where pennate muscles are found. By placing the fibres at an oblique angle, it is possible to fit more fibres in parallel in the same amount of space and as a result get a higher muscle force (Wickiewicz *et al.*, 1983; Powell *et al.*, 1984; Vogel, 2003; Folland and Williams, 2007). It is important to note that these fibres will be shorter and therefore the range of motion and velocity capacity of the muscle are reduced. Also, the fibres no longer contract in the line of action of the muscle and as such the applied force resulting in joint rotation is only a portion of the force produces by the fibres. More precisely the component of force contribution to the applied force is dependent on the cosine of the pennation angle (Equation 1-1) (Epstein and Herzog, 1998),

$$f_c = f\cos(\alpha) \tag{1-1}$$

where f_c is the applied force, f is the total fibre force, and α is the pennation angle.

External transverse loading can reorient the pennation angle which could affect the muscle force. At the same time pennation angles rotate to a higher pennation when a muscle contracts (Narici *et al.*, 1996; Maganaris *et al.*, 1998). The rotation occurs because muscle fibres shorten during contraction and bulge in the transverse direction. To make space for the thicker muscle fibres the pennation angle has to rotate (Randhawa and Wakeling, 2018). The external transverse load can restrict the rotation of the pennation angle which would restrict muscle fibre bulging and also the shortening of the muscle fibres. Limiting the shortening of the muscle fibres could limit the force produced by the muscle fibres.

External transverse loading can affect sarcomeres, muscle lengths, and pennation angles and these have an effect on muscle force production. In this thesis the muscle length and pennation angle will be investigated as possible mechanisms involved in force reduction as a result of transverse loading.

1.2. Transverse loading of muscle

A key concept within this thesis is external transverse loading. We define external transverse loading as an external load that is applied to the muscle perpendicular to the line of action of the muscle. There are a couple of ways in which an external transverse load can occur or be applied on the muscle. The first would be any external load that comes from a source external to the body of the individual and that is being applied onto the body, such as a foreign object pressing against the body. This type of external loading happens for instance when we lean against objects, such as a table or a wall, or when we wear clothing or accessories, such as a backpack. Another type of loading would be from within the body of the individual itself. One scenario in which this happens is when a muscle is trying to bulge during contraction, but it is being restricted from doing so by surrounding tissues or organs, an example of which would be when a muscle runs along a bone. Loading could also occur when muscles are positioned next to one and other. As one muscle contracts and bulges it will push into the muscle lying next to it applying an external load on that muscle.

The maximum isometric force of the medial gastrocnemius of rats was measured for muscle with and without external transverse load (Siebert *et al.*, 2014a; Siebert *et al.*, 2014b). External transverse loads were applied to the medial gastrocnemius using a

weight loaded plunger with weights ranging from 65 to 265 g (13 – 53 kPa). The study showed that maximum isometric force of the muscle was reduced by 4.8 % (65 g) to 12.8 % (265 g) as a result of the external transverse load on the muscle. It was also shown that the lifting work performed by the muscle on the external load was between approximately 1200 and 1800 J m^{-3}. These results were replicated using a Hill-type muscle model that included a gearing ratio between lifting height of a transverse load and muscle length (Siebert *et al.*, 2014b; Siebert *et al.*, 2018). These models showed that the force reduction due to transverse loading could in part be linked to the lifting work performed by the muscle.

The torque capacity of the simultaneous contraction of rabbit quadriceps muscles was compared to the summed torque capacity of the individual contraction of each quadriceps muscle (de Brito Fontana *et al.*, 2018). The summed torque capacity was shown to be 20% higher than that of the simultaneously contracting quadriceps. One suggested cause of the difference in torque capacity was that intermuscular pressure resulted in transverse loading of the muscles. However, more recent work varied intermuscular pressure by varying muscle force and found that the difference between simultaneous and summed contractions did not correspond with changes in intermuscular pressure (de Brito Fontana *et al.*, 2020).

Restrictions to the radial expansion of leopard frog muscle were used to determine whether increased stiffness of the extracellular matrix could limit the mechanical work of shortening muscle (Azizi *et al.*, 2017). The extracellular matrix can increase with age through the accumulation of advanced glycation end products (Kjaer, 2004; Kragstrup *et al.*, 2011). Frog muscle was inserted into polypropylene tubes to simulate the restrictions to radial expansion caused by the stiffening of the extracellular matrix. A maximum isometric force showed a reduction of approximately 4.8% for the constrained condition compared to the unconstrained condition. The mechanical work produced by the muscle in its line of action decreased by approximately 50% for the constrained condition. The extracellular matrix that surrounds muscle fibres consists largely out of collagen fibres (Bailey *et al.*, 1979; Rowe, 1981; Gillies *et al.*, 2011). These collagen fibres wrap around the muscle fibres in a helical pattern and the angle of the helical fibres depends on the length of the muscle (Purslow and Trotter, 1994). A model of a collagen wrapped muscle fibre showed that different helical angles of the collagen fibres limited fibre strain to different degrees (Azizi *et al.*, 2017). Helical angles smaller

than 40° limited fibre strain, whereas helical angles higher than 60° did not limit fibre strain.

Changes in contractile force have also been observed in compression experiments of bullfrog semimembranosus muscle (Sleboda and Roberts, 2019). Muscle was fitted with a pressure cuff to apply compression (35 kPa) and the contractile force was measured for compressed muscle at different muscle lengths. Results of the compression experiments showed that muscle at a normalized length of 1.10 or shorter produced lower forces than uncompressed muscle. Muscle at a normalized length of 1.20 or longer produced higher forces than uncompressed muscle. Physical models consisting of water-filled silicone tubes helically wrapped in Kevlar thread were used to mimic the effect the extracellular matrix had on contractile force changes (Sleboda and Roberts, 2019). The helical angle of the extracellular matrix has been show to change when muscle shortens or lengthens (Purslow and Trotter, 1994). As such tubes with different helical angles were used to represent muscle at different lengths. A longitudinal force decrease was found for tubes representing shorter muscle, whereas a force increase was found for tubes representing longer muscle.

Force reductions have been shown in rats (Siebert *et al.*, 2014a; Siebert *et al.*, 2014b), rabbits (de Brito Fontana *et al.*, 2018, 2020), and frogs (Azizi *et al.*, 2017; Sleboda and Roberts, 2019). The mechanisms involved in the reduction in force caused by transverse loading or constraint to radial expansion has been linked to the work a muscle can produce as well as the structure of the extracellular matrix. The aim of this thesis is, in part, to determine whether force reductions due to transverse loading can be observed in humans.

Transverse loading of muscle in humans happens in several different situations, such as sports (Sperlich *et al.*, 2010; Faulkner *et al.*, 2013; Rennerfelt *et al.*, 2019), medical treatment (Brandjes *et al.*, 1997; Agu *et al.*, 1999; Hara *et al.*, 2019), and sitting (Linder-Ganz *et al.*, 2007). In a variety of sports garments ranging from whole-body compression suits to compression socks pressures have been measured of approximately 2.7 kPa (Sperlich *et al.*, 2010; Faulkner *et al.*, 2013; Rennerfelt *et al.*, 2019). To treat lymphedema compression bandages are applied to the lower limb. For treatment to be successful the applied pressure needs to be approximately 6.7 kPa (Hara *et al.*, 2019). For the treatment of thrombosis compression stockings are

recommended and can apply pressures of approximately 2 kPa (Agu *et al.*, 1999). To study pressure sores from prolonged sitting the pressures were measured in the gluteus muscle. Interestingly, calculated interface pressures (17 kPa), i.e. between the seat and the body, were lower than those calculated in the gluteus muscle (32 kPa: Linder-ganz *et al.*, 2007). Transverse loading experiments on rat and frog muscle used pressures between 10 and 50 kPa (Siebert *et al.*, 2014a; Sleboda and Roberts, 2019) which is comparable to the pressures described here for the transverse loads that occur for humans.

The mechanisms involved in force reduction in transverse loading have been determined to be, in part, because of the work muscle performs (Siebert *et al.*, 2014b; Azizi *et al.*, 2017; Siebert *et al.*, 2018) and the structure of the extracellular matrix (Azizi *et al.*, 2017; Sleboda and Roberts, 2019). It has not been shown whether external transverse loading leads to force reduction in humans. Neither has it been determined how muscle architecture is affected by transverse loading and whether changes in muscle architecture can be linked to the mechanisms involved in force reduction due to transverse loading.

1.3. Experimental quantification of muscle architecture

To quantify muscle architecture under unloaded and loaded conditions, as well as before and during muscle twitches we needed a non-invasive method. For this purpose we chose to use ultrasound imaging.

Previously measurement of muscle architecture of human muscle was done on cadavers (An *et al.*, 1981; Wickiewicz *et al.*, 1983; Brand *et al.*, 1986; Cutts, 1988; Friederich and Brand, 1990). Measurements were made of muscle length, muscle volume, fibre length, fibre pennation angle, and sarcomere length. A problem with measurements taken from cadavers is that the muscles often come from older individuals and have undergone fixation (Fukunaga *et al.*, 1992). More recently muscle architecture has been studied using either ultrasound (Kawakami *et al.*, 1993; Narici *et al.*, 1996; Maganaris *et al.*, 1998; Lichtwark *et al.*, 2007; Rana *et al.*, 2009; Randhawa and Wakeling, 2018) or MRI (Damon *et al.*, 2002; Sinha *et al.*, 2006; Lansdown *et al.*, 2007; Bolsterlee *et al.*, 2015).

1.3.1. Ultrasound Imaging

Ultrasound sonography is the use of sound to visualize tissues within the body. Ultrasound was derived from the sonar techniques used during World War I, and the first ultrasound images were produced in the 1950s (Pillen *et al.*, 2008; Moore and Copel, 2011). Ultrasound sonography works through the use of piezoelectric crystals. The crystals have the ability to produce and receive soundwaves by applying a current to them. The sound produced is in the ultrasound range which are sound frequencies above 20 kHz (Moore and Copel, 2011). Most ultrasound equipment used today works in the range of 5 to 20 MHz (Pillen *et al.*, 2008). Ultrasound travels well through fluids and as such travels well through the body. Soundwaves are emitted from the transducer which has a series of piezoelectric crystals lined up within it. As the soundwaves travel through the body, they encounter tissues of different acoustic impedance. Acoustic impedance is determined by the tissue density and the velocity at which sound travels through it (Pillen *et al.*, 2008). Traveling through a tissue part of the sound is reflected as an echo, and part of it continues to travel through the tissue. Differences in acoustic impedance result in different amounts of reflection. The reflections of sound are received by the piezoelectric crystals and based on the travel time of the signal a current is produced that determines the brightness of the part of the image where the signal was received from. Higher frequencies will give an image with more detail, however higher frequencies travel less well through tissues and therefore limit the scanning depth (Pillen *et al.*, 2008).

Ultrasound sonography is a technique often used because it is non-invasive and delivers real-time, dynamic images of the regions being scanned. It is often compared with magnetic resonance imaging (MRI), which is also a non-invasive method of studying tissues within the body. Although MRI gives more detailed images than those obtained through ultrasound, the long acquisition time of the images doesn't allow for imaging of dynamic events such as fast muscle contractions. Therefore, when studying muscle contractions ultrasound sonography is a good technique to acquire data.

A range of different muscle characteristics can be quantified from ultrasound images, such as muscle thickness, pennation angle and fascicle length (Figure 1-2)(Narici *et al.*, 1996; Maganaris *et al.*, 1998). Furthermore, it is possible to determine fascicle width strain by using a Fourier transform (Wakeling and Randhawa, 2014) and

fascicle curvatures using fascicle tracking (Namburete *et al.*, 2011). Muscle thickness is measured because it indicates the deformation caused by the external transverse load. Similarly, the fascicle width strain is measured to determine how it is affected by external transverse loading. Fascicle length can be used to determine force-length properties and pennation angle can be used to determine the difference between fascicle force and the force in the line-of-action of the muscle. Fascicle length and pennation angle have also been used to drive muscle models (O'Neill *et al.*, 2013; Hutchinson *et al.*, 2015; Dick *et al.*, 2017).

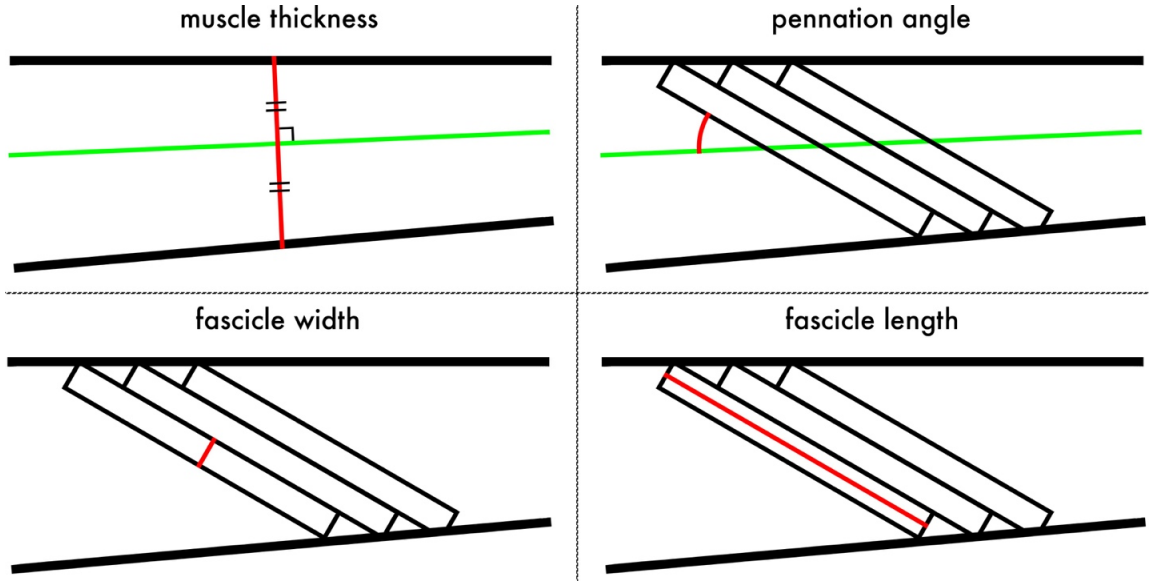

Figure 1-2 Definitions for the different architecture elements as they are used throughout this thesis. Shown are the definitions for muscle thickness, pennation angle, fascicle width, and fascicle length.

Image data that have been collected from the use of ultrasound sonography can be quantitatively assessed to determine what happens as a result of external transverse loading. To get a more objective evaluation of the data it is good practise to quantify the muscle architecture. This can be achieved by manually measuring the desired architecture elements; however, this becomes cumbersome when a large amount of data are collected and need to be analysed. Furthermore, architecture elements within the images might not be clearly measurable due to noise or unwanted elements in the images. For these reasons we implement digital image processing techniques to filter the data and automatically process it. The following section will describe and discuss the imaging techniques used to analyse the external transverse loading experiments.

1.3.2. Automated tracking of muscle architecture

Several methods have been described for automatically tracking muscle architecture such as fascicle orientation (Zhou and Zheng, 2008; Rana *et al.*, 2009), fascicle length (Miyoshi *et al.*, 2009; Cronin *et al.*, 2011), and fascicle and aponeuroses displacements (Zhao and Zhang, 2011; Darby *et al.*, 2012) and have been shown to give accurate results of these measures. Certain automated trackers (Cunningham, 2015; Hodson-Tole and Lai, 2019) were used on the data obtained for this thesis. However, the large deformations of the muscle in a short period of time that occur during muscle twitches caused the trackers to fail. Not all automated trackers work with the use of sequential images. Certain trackers evaluate every frame as a stand-alone image in which the muscle architecture is determined (Zhou and Zheng, 2008; Rana *et al.*, 2009). Whereas others use information from one frame to determine the muscle architecture in the following frame (Miyoshi *et al.*, 2009; Cronin *et al.*, 2011; Zhao and Zhang, 2011; Darby *et al.*, 2012; Hodson-Tole and Lai, 2019). Methods that work on individual frames seem to work better on the ultrasound data that we collected. The large displacement of features from frame to frame in our data cause the correlations to fail that are used in the methods that use sequential images. The methods described here were put together for the analysis of our data to overcome these challenges in tracking muscle architecture.

1.3.3. Digital Image Processing

Digital image processing is used frequently in science (Soeller and Cannell, 1999; Schindelin *et al.*, 2009; Ternifi *et al.*, 2020) to manipulate images in such a manner that they become useful to the user for their chosen purposes. A digital image is no more than a large matrix of values where each position, or pixel, has one (greyscale) or three (colour) values position. Like any set of numbers, we are able to manipulate these numbers and calculate useful values. There is the possibility to change brightness and colours, to highlight important elements, remove elements that are interfering with the image, measure elements within the image, and myriad of other techniques.

For the goals of this thesis we focus on highlighting architectural elements within our ultrasound data that we need to quantify which is done using several techniques.

Image convolution

Image convolution is part of several of the techniques used throughout this thesis. Therefore, a brief description is given on the process of image convolution.

Through image convolution it is possible to apply many filters to an image to break down elements, blur them, or detect and highlight them through techniques known as erosions, gaussian blurs, and edge detection, respectively (Shen and Sethi, 1996; Ryu and Nishimura, 2009). Convolution can be expressed as an integral (Equation 1-2), which is approximated by a summation (Equation 1-3) (Fialka and Čadík, 2006; Podlozhnyuk, 2007).

$$g(y_j) = \int_{\Omega} f(x)k(x, y_j)dx \tag{1-2}$$

$$N_N \sum_{i=1}^{N} f(x_i)k(x_i, y_j)w_j \tag{1-3}$$

The process of convolution involves the use of a kernel, or matrix of numbers, of which the values are multiplied to the values of a region of interest of the image. Those values are summed and divided by the number of pixels in the kernel, and the resulting value becomes the pixel value in the filtered image. The region of interest of the image is the same size as the kernel and is taken at every pixel of the original image. For example, we have a 3 x 3 kernel named K (Equation 1-4A), and we choose a random pixel from our original image and take a 3 x 3 region surrounding that pixel named I (Equation 1-4B). Each corresponding value of the kernel is multiplied with the same value of the region of the image and then summed up (Equation 1-5) and divided by 9 (Equation 1-6). That value will give the pixel value for the new image at the exact coordinates of the pixel chosen in the original image. Repeating this for every pixel of the original image yields a new filtered image, which in the case of the example would be a blurred image. Edge effects do occur as it is not possible to take a sufficient sized region from the image. This is partly solved for by taking the available region of the image and padding it so the size of the region matches the size of the kernel.

$$K = \begin{matrix} 0.5 & 0.5 & 0.5 \\ 0.5 & 1 & 0.5 \\ 0.5 & 0.5 & 0.5 \end{matrix} (A); \qquad I = \begin{matrix} 64 & 83 & 53 \\ 59 & 92 & 49 \\ 61 & 89 & 55 \end{matrix} (B) \tag{1-4}$$

$$(0.5 * 64) + (0.5 * 83) + (0.5 * 53) + (0.5 * 59) +$$

$$(1 * 92) + (0.5 * 49) + (0.5 * 61) + (0.5 * 89) + (0.5 * 55) = 348.5 \quad (1\text{-}5)$$

$$\frac{348.5}{9} \approx 39 \quad (1\text{-}6)$$

Frangi filter

In ultrasound images there is a degree of noise as well as small, blob-like sections of either fascicles or blood vessels that obscure the image. Using the Frangi filter we are able to remove these obscuring elements and get a clearer depiction of the fascicles throughout the muscle.

Using imaging techniques such as x-ray imaging, it can be difficult to obtain an accurate and clear representation of the vasculature within the body. This is mainly due to the range of size differences in the vessels and the overlap of organs. To accommodate this problem Frangi *et al.* (1998) published their development of a multiscale vessel enhancement filter. The principle is based on the eigenvalues of the Hessian, where the Hessian is obtained from the convolution of second order derivatives of a gaussian function over the image at a series of scales.

A version of the multiscale vessel enhancement filter was developed to distinguish the muscle fascicles in ultrasound images taken of human muscle. The filter enhances any vessel-like structures, such as fascicles, and reduces any blob-like structures which are unlikely to represent fascicles.

Given an image of x by y pixels, for each pixel we have to obtain the Hessian matrix. The Hessian matrix is a matrix built up of second order partial derivatives (Equation 1-7),

$$\mathcal{H} = \begin{bmatrix} \partial^2 g(x,y)/\partial x^2 & \partial^2 g(x,y)/\partial x \partial y \\ \partial^2 g(x,y)/\partial y \partial x & \partial^2 g(x,y)/\partial y^2 \end{bmatrix} \quad (1\text{-}7)$$

where $\mathcal{H}$ is the Hessian, and g are the image data. Four kernels are constructed, each representing a second order partial derivative of the gaussian function (Equation 1-8).

Convolving the image data with each of these kernels results in the second order partial derivatives of the image data at each pixel.

$$gauss(x,y) = a\, e^{-\frac{(x-x_0)\cos\theta - (y-y_0)\sin\theta}{2{\sigma_x}^2} + \frac{(x-x_0)\sin\theta + (y-y_0)\cos\theta}{2{\sigma_y}^2}} \tag{1-8}$$

This is also where the scaling of the filter is applied. The process of obtaining the Hessian at every pixel is repeated several times with gaussian kernels of different sizes depending on the range of scaling that is being applied.

From the Hessian we can calculate two eigenvalues. These eigenvalues represent the magnitude of the axes of the ellipse that makes up our fascicle. For our fascicle to be vessel-like ideally, we need our smallest eigenvalue to be close to zero, and our larger eigenvalue needs to be far greater than the other. The eigenvalues in turn are used to calculate a vesselness measure (Equation 1-9),

$$v_0(s) = \begin{cases} 0, \ \lambda_2 > 0 \\ e^{-\frac{\mathcal{R}_B^2}{2\beta^2}}\left(1 - e^{-\frac{\mathcal{S}^2}{2c^2}}\right) \end{cases} \tag{1-9}$$

where $v_0(s)$ is the vesselness, λ_2 is the largest eigenvalue, $\mathcal{R}_B$ is a geometric ratio, β and c are threshold values, and $\mathcal{S}$ is the square root of the sum of the eigenvalues squared. Through this we get a single value at each pixel of the given image for every level of scaling that we have used. The scaling that gives the highest vesselness measure at a given pixel is the pixel value used for the final image. The final image is a grayscale image in which the vessels of our original image are amplified.

Hough transform

Manual digitization of muscle fascicles can be a time-consuming process. For our data we use the Hough transform to produce lines that represent the trajectory of fascicle segments. We calculate the angle of each line and use the mean of the angles relative to the line-of-action of the muscle to determine the mean pennation angle for each frame of the ultrasound data.

The Hough transform was patented in 1962 by P.V.C. Hough. It was initially used to determine trajectories of particles in a bubble chamber. The Hough transform converts data from a binary image into a parameter space where a local peak detection can be

used to determine patterns within that image (Illingworth and Kittler, 1988). Although the Hough transform can be used to detect many shapes, here we will focus on the detection of lines within an image. Consider a given space in x and y. Within this space we assume a series of points that lie on a straight line. For a straight line we can use the equation, $y = ax + b$, where a is the slope of the line and b determines the intercept with the y axis. At each given point we can draw a series of lines with varying values of a and b which can then be represented in an a and b parameter space as a line. When this is done for all the given points, we are given a series of intersecting lines in (a, b) space. The point where the lines intersect gives us values of a and b represent the slope and intercept of a line that passes through all the given points in the (x, y) space. A problem occurs with lines that approach vertical where a becomes infinitely large. For this reason it was proposed by Duda and Hart (1972) to use the line representation $\rho = x\cos(\theta) + y\,sin(\theta)$. Here (ρ, θ) space is used to find a local peak that indicates the ρ and θ values that give a line that passes through all given points. Previous research has implemented a method similar to the one described here using the Hough transform and they were able to show their method was reliable compared to manual tracking (Zhou and Zheng, 2008).

Fourier transform

We use the Fourier transform to determine the changes in fascicle width. The transverse bulging of fascicles might prove to be important when transversely loading a muscle.

Through the use of the Fourier series it is possible to reconstruct almost a periodic signal. Using the Fourier transformation, it is possible to deconstruct periodic signals to analyze components within the function. Recorded signals are often noisy or are a mixture of several signals. It is therefore useful to extract specific components from the signal to analyze them. The Fourier Transformation has been used to analyze, for example, vibrations, sound, light, and to perform digital image processing (Butz, 2006). Often the signal that is recorded is not a continuous signal but rather measured in intervals, which is especially the case with digital signals. To analyze the non-continuous signals we are able to use the discrete Fourier transformation (James, 2011).

The Fourier transform was used to determine the frequencies of the striation pattern in the filtered images from the ultrasound data to obtain the strain in fascicle

width. As explained previously, within the ultrasound image different elements are represented by different brightness's. As the signal travels through parallel muscle fascicles it passes the connective layer surrounding the fascicle, which is dense and shows as bright pixels, and the muscle fibres, which are mainly made of water and so show as dark pixels. This repeats itself for each fascicle and the result is a pattern of light and dark bands throughout the muscle. Applying the Frangi filter to the image will amplify this pattern even more. The light and dark pattern is a waveform and therefore has a wavelength. By calculating the spatial frequency of the pattern using a 2D discrete Fourier transform we can obtain this wavelength as $wavelength = \frac{1}{frequency}$ (Wakeling and Randhawa, 2014).

Fascicles within the image are not laid out in perfect rows, therefore when the ultrasound takes a slice through the muscle it will pass through the middle of some fascicles where it will only graze others. As a result of this the image that is obtained does not show an equally spaced striated pattern. Therefore, the wavelength that is measured is not a true representation of the width of the fascicle. The Fourier transform determines a distribution of frequencies from the ultrasound data. From this distribution the representative frequency is determined using the moment of frequency (Wakeling and Randhawa, 2014). Changes to the distribution of frequencies provide a wavelength that can be associated to changes in fascicle width giving us an indication on the strains in width of the fascicles as they either bulge or shrink.

Fascicle curvature

Studies on muscle architecture have often made the assumption that fascicles run in straight lines through the muscle (Zhou and Zheng, 2008; Miyoshi *et al.*, 2009; Rana *et al.*, 2009; Cronin *et al.*, 2011; Zhao and Zhang, 2011). For the purpose of calculating the fascicle length throughout this thesis we assume fascicles to be straight. However, research indicates that fascicle trajectories could be curved (Kawakami *et al.*, 1998; Maganaris *et al.*, 2002; Muramatsu *et al.*, 2002; Wang *et al.*, 2009; Stark and Schilling, 2010; Namburete *et al.*, 2011; Darby *et al.*, 2013). It is possible that fascicle lengths are underestimated when assuming straight fascicle trajectories. Accurate fascicle lengths are important when determining the force-length relationship or when the data is used to drive muscle models. The determination of pennation angles could also be different if fascicle curvature is accounted for. More accurate measurement of

pennation angles could improve calculations of gearing ratios of muscle or improve muscle models.

Aside from accurate fascicle length and pennation angle measurements the fascicle curvature is of interest because of its connection to intramuscular pressure (Hill, 1948; Sejersted *et al.*, 1984; van Leeuwen and Spoor, 1992). Furthermore, changes intramuscular pressure has been linked to changes in joint torque (Sylvest and Hvid, 1959; Baumann *et al.*, 1979; Sejersted *et al.*, 1984; Aratow *et al.*, 1993; Ateş *et al.*, 2018). A direct link between fascicle curvature and joint torque has also been shown (Rana *et al.*, 2014). Joint torque depends on muscle force and external transverse loading affects muscle force. We aim to show that there is a link between fascicle curvature and external transverse loading.

1.4. Computational simulations of muscle force

It is possible change certain muscle architecture parameters in physical experiments. However, changing one parameter often leads to a change in other parameters. Using computational experiments we are able to independently vary muscle architecture parameters in order to determine their effects on muscle force reduction due to transverse loading.

The data from experiments tell us many things about what happens to transverse loaded muscle. Aside from performing more variations of the loading experiments to gain a better understanding of the mechanism involved we can choose to simulate the experiments using a computer model. An advantage of running computer models is that it is possible to vary large number of elements independent of one and other. By doing so it is possible to learn what the role is that each element plays. To better understand the mechanisms of force reduction in muscle under external transverse loading we are able to vary loading parameters such as amount of load and the direction of loading. Furthermore, we are able to perform these loadings on muscles with varying muscle architecture, such as different pennation angles and different muscle lengths. The following section will discuss the basics of muscle modelling and describe the type of model using in this thesis.

The first introduction of the finite element method was in 1943 by Courant, who introduced the approximation of numerical solutions to a torsion problem related to columns using triangular subdomains (Williamson, 1980; Logan, 2007). In the late 1940s, with the rise of jet engines, aircraft engineers started using finite element modelling to solve for the large loads on airplane frames (Hutton, 2004).

The method is used to solve boundary value problems for complicated geometries, loadings, and material properties. It is a numerical method that approximates the solution of, for example, displacements, heat transfer, and fluid flows in a certain structure. It is used when exact, analytical methods cannot be applied due to the complexity of the problem. Rather than solve the solution for the whole structure, solutions are found for subsections known as finite elements. The solutions from the finite elements are combined to give the approximate solution to the whole structure. With the use of subsections and interpolations it becomes possible to get a solution for any given point of the structure (Hutton, 2004; Logan, 2007).

Finding an exact solution to describe the contraction of a muscle would be near impossible. The shape of a muscle and the deformations that happen during contraction are too complex to use an exact, analytical method. Therefore, an approximate numerical solution has to be found.

In biomechanics finite element modelling has been used to solve many complex problems. The method has been applied to determine ventricular stresses and deformations of the heart (Nielsen *et al.*, 1991), forces throughout the shoulder joint (van der Helm, 1994), stresses in the foot during stance (Gefen *et al.*, 2000), the moment arms of hip muscles (Blemker and Delp, 2005), the effects of intramuscular fat on muscle contractions (Rahemi *et al.*, 2015), and history effects in skeletal muscle (Seydewitz *et al.*, 2019).

Much work has been done in the area of continuum mechanics to model skeletal muscle using finite element modelling. Many models work by using strain energy equations (Gielen *et al.*, 2000; Johansson *et al.*, 2000; Yucesoy *et al.*, 2002; Jenkyn *et al.*, 2002; Teran *et al.*, 2003; Blemker and Delp, 2005; Blemker *et al.*, 2005; Röhrle and Pullan, 2007; Rehorn and Blemker, 2010; Rahemi *et al.*, 2014, 2015) although others use equations of stresses (Kojic, Mijailovic and Zdravkovic, 1998; Oomens *et al.*, 2003).

Another difference between models is that some choose to use fibre properties as is done in Hill-type models (Johansson *et al.*, 2000; Blemker and Delp, 2005) whereas others are based off of the Huxley model (Gielen *et al.*, 2000; Oomens *et al.*, 2003). Recent work has used continuum mechanics models to study Duchenne muscular dystrophy (Stefanati *et al.*, 2020) and the electromechanical delay in muscle (Schmid *et al.*, 2019). We chose to base our modelling work on the model used by Rahemi *et al.* (2015). The reasons for this where that this model incorporates base material properties that represent non-contractile tissues in the muscle such as the extracellular matrix, blood vessels and nerves. Only one other model was found that implemented such a base material (Yucesoy *et al.*, 2002). The second reason was that the model by Rahemi *et al.* (2015) allows for the implementation of external transverse loads in order for us to perform muscle compression experiments.

The external transverse loading of muscle has been modelled previously using a Hill-type muscle model (Siebert *et al.*, 2018) and three-dimensional geometries (Siebert *et al.*, 2012). The Hill-type muscle model by Siebert *et al.* (2018) was a two-dimensional model and could therefore not account for three-dimensional shape changes of the muscle. The model used by Siebert *et al.* (2012) did not include muscle forces but rather calculated shape changes from changes occurring in all dimensions. As such neither of these models were suited to give us a full solution to our problem.

The model run for this project is a quasi-static model of a fibre-reinforced, non-linearly-elastic transversely isotropic composite biomaterial. The main components of the model are the muscle fibres which have active and passive force-length properties. The active and passive muscle fibre properties are similar to those used in many Hill-type muscle models.

There are two classic types of muscle model, the Huxley model and the Hill models. The Huxley model is based on the work of A.F. Huxley and models the cross-bridge interaction of the actin and myosin filaments. The Hill model is a result of the work by A.V. Hill and uses the velocity dependent characteristic of muscle on muscle force and included later were the passive and active force-length properties (Hill, 1938; Ramsey and Street, 1940; Epstein and Herzog, 1998).

$$F_{\mathrm{m}} = F_{\max}\left[\hat{a}(t)\,\hat{F}_{\mathrm{a}}\left(\hat{l}_{\mathrm{f}}\right)\hat{F}_{\mathrm{a}}(\hat{v}) + \hat{F}_{\mathrm{p}}\left(\hat{l}_{\mathrm{f}}\right)\right]\cos\alpha \tag{1-11}$$

where muscle force (F_{m}) is calculated from maximum isometric force ($F_{\max}$), activation ($\hat{a}(t)$), active and passive force-length properties ($\hat{F}_{\mathrm{a}}(\hat{l}_{\mathrm{f}})\ and\ \hat{F}_{\mathrm{p}}(\hat{l}_{\mathrm{f}})$), force-velocity properties ($\hat{F}_{\mathrm{a}}(\hat{v})$), and fibre pennation angle (α). The Hill-type muscle model has been widely used in the field of biomechanics to model muscle forces related to human jumping (Pandy *et al.*, 1990), walking (Anderson and Pandy, 2001; Lichtwark and Wilson, 2008), and lower limb movement (Lloyd and Besier, 2003; Arnold *et al.*, 2010). Furthermore, it has been used to model muscle functions in animals such as the rat gastrocnemius (Ettema and Huijing, 1994), walking in cats (Sandercock and Heckman, 1997), and rabbit hindlimb (Winters *et al.*, 2011). It was also used to study force enhancement and force depression effects caused by titin (Rode *et al.*, 2009).

The computational experiments that were run were of isometric contractions and as such the force-velocity properties of muscle were not included. Included in the model were the passive force-length properties of the base material that represents the non-fibre tissues within the muscle such as blood vessels, nerves, and connective tissues.

Using a modified version of the model by Rahemi *et al.* (2015) allows us to obtain a detailed solution for a transversely loaded three-dimensional muscle model. We have chosen to simplify the problem by using a cuboid geometry to represent our muscle. The strain-energy density patterns in an isolated block of muscle were shown to be similar to those of a block of muscle within an MRI-derived geometry (Wakeling *et al.*, 2020). Therefore, we expect the block of muscle to be representative of whole muscle. Within this geometry the model works to calculate the critical points of the strain energies to produce the pressure, dilation, and displacement of the muscle.

1.5. Specific Aims

Although much research gets done on isolated muscle, in real world situations muscle is never found without surrounding tissues and often times interacts with objects that are in close vicinity. Muscles are grouped together with other muscles, there are bones that they run along, and organs that lie next to them. As for the objects in our surroundings, there are the clothes we wear, things we carry, and objects we touch or bump in to. Even taking away all those factors we would still have to consider that muscle is encapsulated by connective tissue, namely the fascia. Essentially, muscle is never able to contract freely. As such it is important to determine how external loads and

restrictions influence the way that muscle functions. Going by the knowledge provided by previous research we know that in rats external loading of the muscle reduces maximum muscle force (Siebert *et al.*, 2014), and that in rabbits muscles produce more force when they contract individually of one and other rather than simultaneously (de Brito Fontana *et al.*, 2018). Therefore, we have set a series of specific aims that we wish to address in this thesis.

Aim 1: Determine the effects of external transverse loading on maximum twitch muscle force during contraction in the medial gastrocnemius in humans. Our goal is to replicate the results found in rats where external transverse loading causes a decrease in maximum muscle force and that the decrease in muscle force is determined by the amount of external loading. This aim is addressed in chapter 2.

Aim 2: Study the muscle architecture (muscle thickness, pennation angle, fascicle width, and fascicle length) using ultrasound sonography to determine if and how it is affected by external loading. The goal is to show what changes occur in muscle and fascicle properties as the muscle is transversely loaded, and to discuss how these changes relate to any possible reductions in maximum twitch muscle force during contraction. This aim is addressed in chapter 2.

Aim 3: To alter the external loading method and muscle length to determine if this has an effect on the force reduction and muscle architecture changes caused by external transverse loading. The intent is to gain a better understanding of the mechanisms involved by changing the experimental design. This aim is addressed in chapter 3.

Aim 4: Independently vary loading direction, pennation angle, and muscle length to determine how they relate to the mechanisms involved in the reduction in muscle force as a result of external transverse loading. Using physical experiments this is not possible, therefore we use a computational framework using a finite element method. The model is qualitatively validated by replicating previously performed physical experiments. This aim will be addressed in chapter 4.

Portions of this thesis have been published or are in the process of being published elsewhere. Portions of Chapter 2 have been published in the *Journal of Biomechanics* (Chapter 2; Ryan *et al.*, 2019). The contents of Chapter 3 and Chapter 4 are being prepared to be submitted for publication.

Chapter 2.

Passive and dynamic muscle architecture during transverse loading for gastrocnemius medialis in man

2.1. Introduction

During muscle contractions, muscle architecture undergoes transient changes (Narici *et al.*, 1996; Maganaris *et al.*, 1998), and such changes have been shown to be influenced by external compression generated by compression bandages (Wakeling *et al.*, 2013). Unidirectional transverse loading of rat muscle causes a decrease in muscle force during contraction (Siebert *et al.*, 2014a; Siebert *et al.*, 2016), however, the mechanisms involved are not fully understood. This study aimed to characterise the changes in architecture that occur with transverse loading, and its relation to reductions in muscle force.

Many studies into the behaviour of muscle contraction have been done in isolated muscle or muscle fibres (Hill, 1938; Gordon *et al.*, 1966). However, external compression from either adjacent muscles and tissues, or loads external to the body can change the contractile behaviour of muscle (Reinhardt *et al.*, 2016; Wick *et al.*, 2018; de Brito Fontana *et al.*, 2018). For instance, the medial and lateral gastrocnemius and soleus muscles of the triceps surae contract synergistically to perform ankle plantarflexion. Although these muscles are activated separately, they are in apposition and so bulging of one of these muscles may lead to compression in the others: muscles undergo very limited volume changes during contraction (Abbott and Baskin, 1962; Baskin and Paolini, 1967) and are thus nearly isovolumetric and as a result will bulge when they contract. The bulging of one muscle into another will result in transverse loads on these muscles (Reinhardt *et al.*, 2016). Furthermore, tight packing of muscles in muscle packages leads to transverse forces in between muscles influencing muscle shape and architecture (Wick *et al.*, 2018). This is not the only way in which muscles can undergo transverse loading. With many of our muscles having a superficial placement in our body, our surroundings are also able to cause transverse loads on our muscles, for instance in our gluteal muscles when we sit.

Magnetic resonance imaging (MRI) is able to provide detailed images of muscle shape, position, and volume in vivo, however due to the long acquisition times this method is most suitable for passive and prolonged low-level contractions (Kawakami *et al.*, 1995; Finni *et al.*, 2003; Lansdown *et al.*, 2007; Infantolino *et al.*, 2012; Schenk *et al.*, 2013; Bolsterlee *et al.*, 2015). The imaging of muscle architecture is possible in passive and contracting muscle using ultrasound, with negligible acquisition times (Herbert *et al.*, 1995; Narici *et al.*, 1996; Maganaris *et al.*, 1998; Rana and Wakeling, 2011; Randhawa and Wakeling, 2013; Wakeling and Randhawa, 2014), and changes in muscle thickness, pennation angle, fascicle length, and fascicle thickness have been measured.

When transverse loads are applied to a muscle, they can change the muscle architecture and forces developed by the muscle belly. In isolated rat muscle (Siebert *et al.*, 2014a), the force production in the longitudinal direction decreased as transverse load was increased. In humans, compression bandages applied to the leg reduced the muscle thickness and pennation angle and resulted in longer fascicles during contraction (Wakeling *et al.*, 2013). In leopard frogs, rigid tubes that prevented transverse expansion of the muscle resulted in reduced external work done during contraction (Azizi *et al.*, 2017).

It is important to understand how transverse and longitudinal forces can be linked to each other because it has been shown that changes in the former result in changes in the latter. An important feature of muscle to consider is that muscle is made up of around 80% water (Van Loocke *et al.*, 2008). The combination of a near isovolumetric muscle filled with fluid allows for pressure changes in the muscle. These changes can have a big influence on the forces throughout the muscle and influence the shape of the muscle. To study the significance of intramuscular fluid, fluid volumes were manipulated in bullfrog muscle and a sleeve fitted bladder (Sleboda and Roberts, 2017). Increases in fluid volume showed an increase in passive force in both muscle and bladder. This showed that internal fluid and muscle structure interact to influence muscle shape changes. As fibres contract, their longitudinal forces act to shorten them. The pressure changes within the fibre translate shortening to transverse expansion. In pennate muscle this transverse expansion will result in rotation of the fascicles to a higher pennation angle. Thus, observing the fibre deformations due to transverse loading provides an opportunity to examine the mechanisms that link transverse and longitudinal forces and deformations.

Previous studies have shown that transverse loads reduce muscle force in isolated single muscle experiments. The aim of this study was to determine the changes in muscle thickness, pennation angle, fascicle thickness, and fascicle length of the medial gastrocnemius in humans resulting from transverse load and how they relate to force reduction. We hypothesize that transverse loading will cause a significant flattening of the both passive and active muscle and this results in changes in muscle thickness, pennation angle, fascicle thickness, and fascicle length. Furthermore, greater changes in muscle thickness, pennation angle, fascicle thickness, and fascicle length will be seen with greater transverse loads.

2.2. Materials and Methods

Twenty-nine healthy young adults participated in this study (age 25 ± 5 yrs, body height 181.0 ± 7.4 cm, body mass 76.5 ± 9.4 kg). All participants gave informed consent before taking part in the study. The study was conducted in accordance to the latest declaration of Helsinki. Ethical approval for the study was received from Simon Fraser University, Canada.

Before testing, participants were asked to warm up by running on a treadmill for 5 minutes, perform 3 sets of 10 repetitions of calf raises and 10 calf jumps. Participants lay prone on a platform with their right foot flat on the force plate with toes pointing straight down (Figure 2-1). Two self-adhesive electrodes were placed on the lower leg: the anode was fixed in the popliteal fossa and the cathode about 2 cm proximal to the patella.

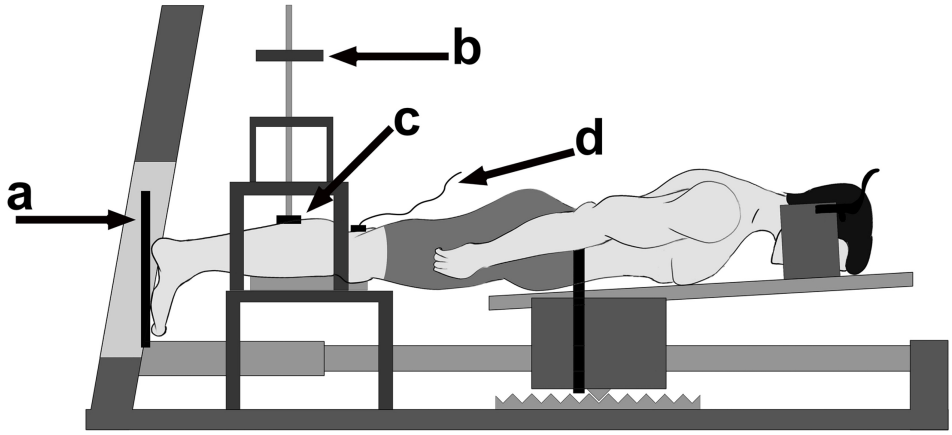

Figure 2-1 **Schematic of the experimental design. Showing the position of the force plate (a) and the point at which load was added (b). The point of contact between the gastrocnemius and the transversal load is at the same position that the ultrasound probe was positioned (c). The calf muscles of the participants were stimulated in the popliteal fossa with a current stimulator (d).**

Electrical stimuli were elicited in the posterior tibial nerve, to evoke maximal force twitches in the triceps surae muscles of the right leg using a constant current stimulator (DS7AH Digitimer, Herfordshire, UK). To find maximum twitch force (MTF), the current was slowly ramped up, starting at 5 mA, until twitch force as measured at the force plate plateaued. Stimuli were administered as double-twitches (i.e., 2 consecutive stimuli with an interstimuli interval of 10 ms).

An unloaded set of pretest and posttest twitches were delivered. A force plate (Type 9260 AA3, Kistler Instrumente AG, Winterthur, Switzerland) was used to measure MTF (Figure 2-1a). If the posttest forces were within 5% of the pretest forces we assumed no changes to the experimental design occurred and that fatigue was minimal during testing, and the collected data were taken to be valid. No ultrasound data were collected during the unloaded trials because the ultrasound probe and the attached equipment already placed 0.92 kg of load on the muscle and so the measured forces would not have reflected unconstrained twitch forces.

Three trials with five twitches per trial were conducted for each participant, with transverse loads of 2, 4.5, and 10 kg presented in a random order. Transverse loading was achieved by placing a rod in line with gravity inside a frame to maintain its vertical

alignment. A plate was positioned at the upper end of the rod (Figure 2-1b) and was loaded with weights to get the desired transverse load. The lower end of the rod was affixed to a block (34 x 100 mm) (Figure 2-1c) that was used to transfer the transverse load from the rod to the muscle.

A linear ultrasound probe (Echoblaster 128, Telemed, Lithuania) was placed on the right medial gastrocnemius (MG) in line with the transverse load by placing the probe inside the block on the lower end of the rod. The probe and transverse load were positioned medial to the midline of the lower leg. The subject was slightly rotated using supports so that the vertical probe compressed rather than displaced the MG, imaged the muscle belly close to its optimal location (Bolsterlee *et al.*, 2016) and was aligned with the fascicles parallel to the scanning plane. This gave continuous, quantitative data on muscle architecture throughout muscle twitches. Ultrasound videos (604 x 515 pixels; 80 Hz) were collected from the ultrasound system, providing a 65 mm field of view with a 50 mm scanning depth. The superficial and deep aponeuroses of the MG were manually traced. A second order polynomial was fitted to the traces and displaced by 10 pixels either down (superficial) or up (deep). This allowed a region of interest for the muscle belly to be isolated. A straight midline between the aponeuroses was taken as the line of action of the muscle. The muscle thickness was the mean distance between the aponeuroses in the direction perpendicular to the midline of the muscle.

A multi-scale vessel enhancement filter (Frangi *et al.*, 1998) was applied to the ultrasound images to enhance fascicles with high vesselness, and supressed blob-like elements (Rana *et al.*, 2009). We then used a Hough transform to determine the mean pennation angle of the fascicles: after filtering the image was binarized to produce a black and white image. For each morphological component in the binarized image we applied the Hough transform to determine the best fit line. From each of these lines we then determined the angle relative to the x-axis. As our pennation ran from top left to bottom right only negative angles were representative of fascicles and positive angles were discarded. Similarly, any angles smaller than 5° were discarded as they most likely represented blood vessels running through the muscle. The final pennation angle was calculated by taking the mean angle of all lines relative to mean position of the aponeuroses, which was assumed to be the line of action of the muscle.

A 2D-Discrete Fourier transform was applied to the filtered region of interest to find the transverse wavelength across the muscle fascicles (Wakeling and Randhawa, 2014). Stripes in the ultrasound images are considered to lie in the same direction as the muscle fascicles. As the fascicles dilate, the spacing of these stripes gets wider; thus their transverse wavelength is proportional to the fascicle width. Fascicle lengths were approximated by (Equation 2-1)

$$l_f = \frac{T_m}{\sin \alpha} \quad (2\text{-}1)$$

where l_f is fascicle length, T_m is muscle thickness, and α is pennation angle.

Pennation angle, muscle belly thickness, muscle fascicle thickness, and fascicle length were quantified for the initial testing state (100 ms before each muscle twitch), and for the value of either the pennation angle, muscle thickness, fascicle thickness, or fascicle length that showed the largest deviation from the initial state during each twitch. All data are presented as mean ± standard deviations (Table 1). The data were tested using a one-way ANOVA for repeated measures, with a post-hoc Bonferroni test, to see if significant differences existed between the different loading trials with each condition compared to the other two. Tests were considered significant when $p < 0.05$. All statistical analyses were performed using IBM SPSS Statistics for macOS (Version 25 IBM Corp., Armonk, NY).

2.3. Results

Electrical stimulation caused the MG to twitch, peaking after about 60 ms, and this caused a transient increase in force on the force plate (Figure 2-3G). The ultrasound images showed that during each twitch the muscle fascicles underwent transient shortening, coupled with a transient increase in thickness and pennation angle; the muscle belly also increased in thickness during each twitch.

Mean MTF for the unloaded pretests and posttests showed no significant differences between each other (Figure 2-2). MTF decreased with increased transverse loading. The 2, 4.5, and 10 kg trials showed twitch forces of 147.4 ± 7.5, 141.8 ± 7.4, and 136.1 ± 7.2 N, respectively. Compared to unloaded values this equates to decreases of 9, 13, and 16%, respectively. The twitch forces for the loaded trials were

significantly different from the pretest and the posttest values, and all loaded trials were found to be significantly different from each other (Figure 2-2).

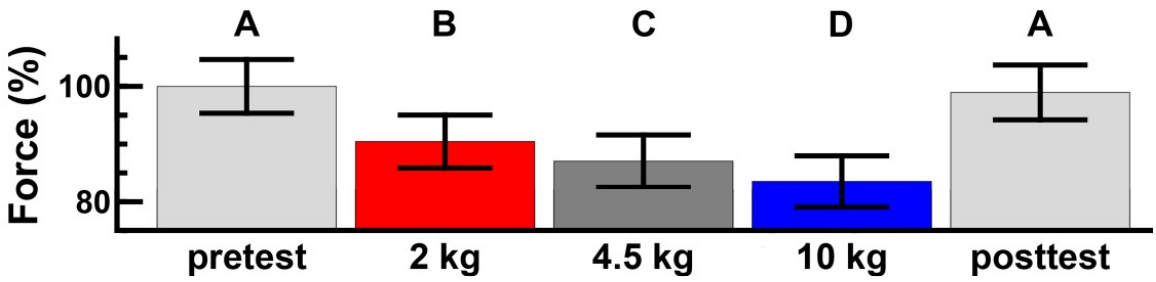

Figure 2-2 **Mean maximum twitch forces (MTF; mean ± SE), for each trial, given as percentage of pretest twitch force. Statistics showed no significant differences between pretest and posttest force. The forces for each loaded trial were significantly different from one and other as well as from the pre- and posttest. Means with different letters are significantly different ($p < 0.001$).**

Table 2-1 **The values (mean ± SE) for each trial of the measured muscle architecture. The values are given for muscle at rest (passive), at peak active contraction (active), and the change that have occurred. Significant differences between trials are given († - sign. differences between 2 kg and 4.5 kg, ‡ - sign. differences between 4.5 kg and 10 kg, + - sign. differences between 2 kg and 10 kg). The transverse wavelength corresponds to fascicle thickness.**

	2kg	4.5kg	10kg	significance
pennation angle (°)	n = 155	n = 149	n = 152	
passive	11.9 ± 3.3	11.0 ± 3.2	10.3 ± 2.9	†,+
active	18.3 ± 3.1	16.7 ± 3.6	14.2 ± 3.3	†,+,‡
change	6.3 ± 2.4	5.8 ± 2.1	3.9 ± 2.2	†,+,‡
muscle thickness (mm)	n = 159	n = 156	n = 153	
passive	13.4 ± 3.4	12.7 ± 3.6	12.2 ±3.6	†,+
active	18.9 ± 5.7	18.0 ± 5.5	15.8 ± 4.6	†,+,‡
change	5.5 ± 3.2	5.2 ± 2.9	3.7 ± 1.8	+,‡
transverse wavelength (mm)	n = 157	n = 156	n = 153	
passive	1.2 ± 0.07	1.2 ± 0.07	1.2 ± 0.07	
active	1.5 ± 0.4	1.3 ± 0.1	1.3 ± 0.2	†,+
change	0.3 ± 0.4	0.1 ± 0.1	0.1 ± 0.1	†,+
fascicle length (mm)	n = 156	n = 149	n = 152	
passive	65.4 ± 12.1	68.1 ± 13.6	71.9 ± 36.7	
active	52.2 ± 5.5	56.3 ± 4.9	58.1 ± 7.0	†,+,‡
change	-13.2 ± 12.1	-11.8 ± 12.7	-13.8 ± 32.0	

When the transverse loads were applied to the muscle the initial muscle thickness and pennation angle both decreased with this decrease being greater at higher loads. As the muscle contracted with the applied loads there were reduced increases in pennation angle (Figure 2-3A), muscle thickness (Figure 2-3C), and fascicle thickness (Figure 2-3E) during each twitch with increasing load. There was no significant effect of the transverse load on the initial fascicle length (Figure 2-4) or thickness (Figure 2-3E,F). Trials with the highest transverse load (10 kg) showed the smallest increases in muscle thickness (Figure 2-3D) and pennation angle (Figure 2-3B) during each twitch. The extent and significance of these effects is shown in Table 2-1. A representation of the individual measured values is shown in figure 2-5 for the three main measurements (muscle thickness (Figure 2-5A), pennation angle (Figure 2-5B), and wavelength (Figure 2-5C)).

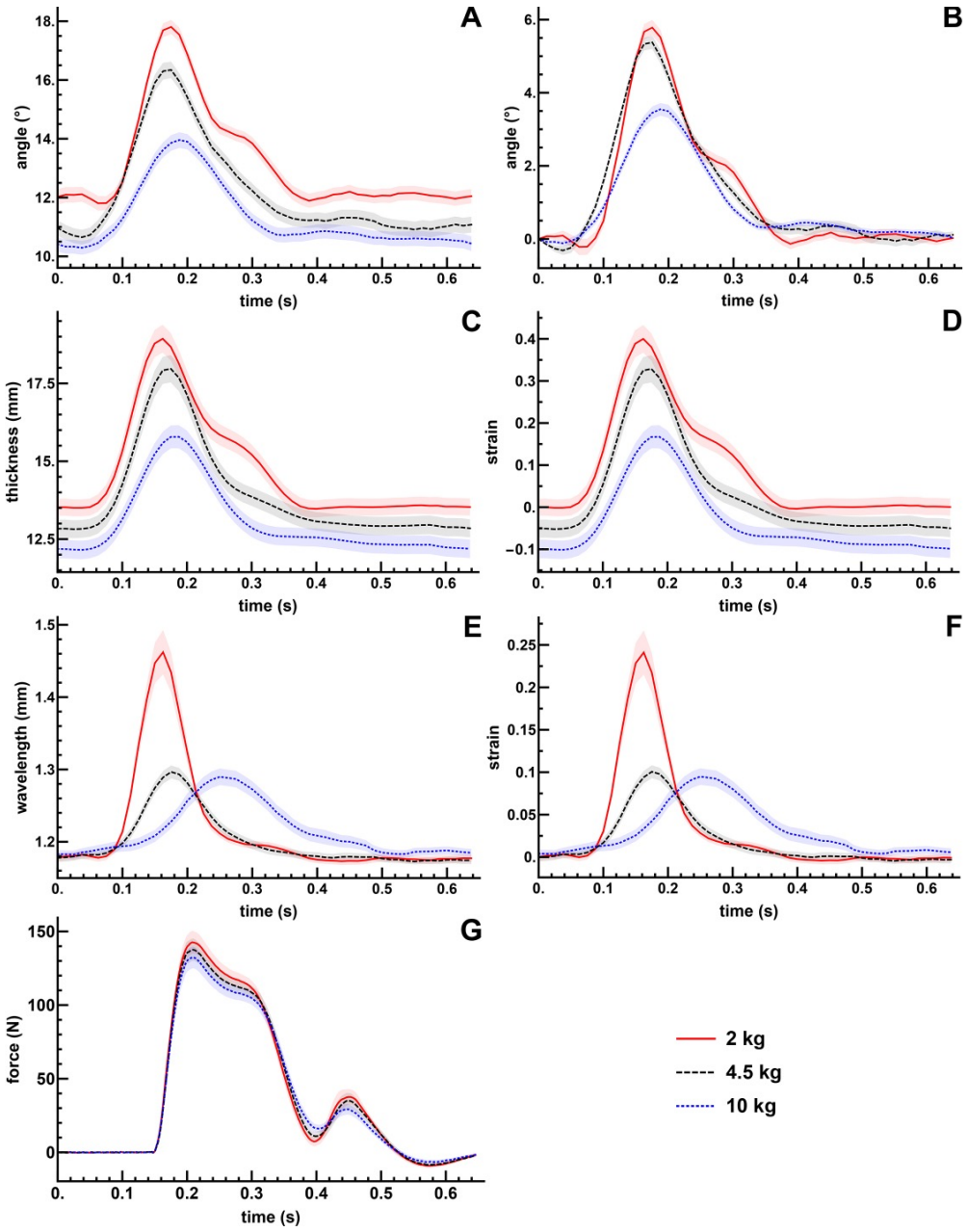

Figure 2-3 **Changes in muscle architecture induced by transverse muscle loading. Absolute values for pennation angle (A), muscle thickness (C), and transverse wavelength (E) as well as corresponding changes in pennation angle (B) and strains for muscle thickness (D) and transverse wavelength (F). Twitch force is presented in (G). Note that, the transverse strain of wavelengths corresponds to the transverse strain of the fascicles . The graphs show the mean of all participants with standard errors for the 2 (red), 4.5 (black), and 10 kg (blue) trials. Muscle thickness and transverse wavelength changes were scaled to the 2 kg trials. Higher transverse loads show lower absolute values both for passive values and during contraction. The changes in transverse wavelength were interpreted as fascicle thickness strains.**

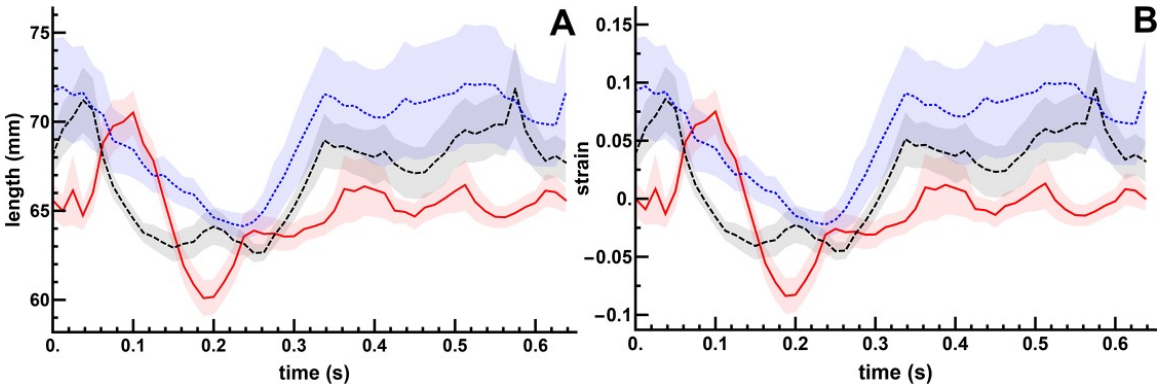

Figure 2-4 **Fascicle lengths (A) and fascicle length changes (B) during contraction for the 2 (red), 4.5 (black), and 10 kg (blue) trials (mean ± SE). The changes were scaled to the 2 kg trials. Fascicle length was calculated as a function of pennation angle and muscle thickness.**

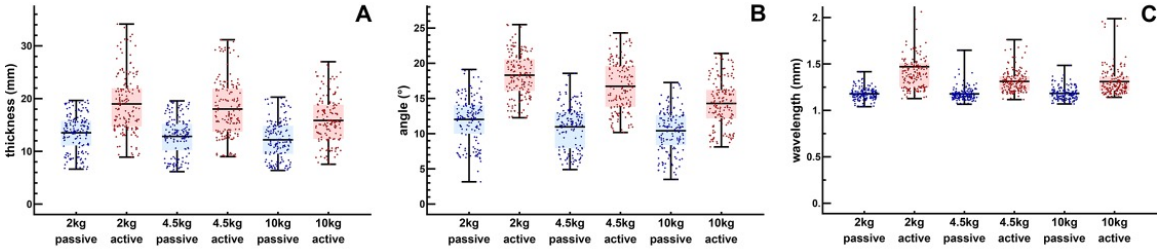

Figure 2-5 **Measured values for muscle thickness (A), pennation angle (B), and wavelength (C) for individual measurements. The values are given for muscle at rest (blue), and at peak active contraction (red). The box plots show the mean with 25 and 75 % quantiles with the whiskers showing the minimum and maximum values.**

2.4. Discussion

Transverse loading has an observable effect on muscle deformation and contraction dynamics. Reduced increases in muscle thickness (Figure 2-3C, D) showed that the transverse loading restricted the muscle from bulging under the applied load during contraction. Likewise, the transverse load limited the increases in the pennation angle (Figure 2-3A, B). These findings were mirrored at the fascicle level where the smallest transverse expansion concurred with the greatest transverse load (Figure 2-3E, F).

2.4.1. Force reduction

Plantarflexion force was measured for twitches at MTF. As a result of transverse loading MTF decreased and increases in transverse load resulted in a greater decrease (Figure 2-3G). These findings are consistent with studies done on rat gastrocnemius muscle (Siebert *et al.*, 2014a) where maximum isometric contractions showed a decrease in force between 4.8% and 12.8% for lowest to highest transverse load, respectively. Comparatively, our study found decreases in MTF between 9% and 16% for lowest to highest transverse load, respectively. Both studies match up well, albeit that our study found higher decreases in force. Although different contraction types were used (supramaximal stimulation vs. double-twitch stimulation), the durations of contraction were similar (300 ms in rat; 250 ms in man). Furthermore, the transverse pressures applied were of similar magnitude (1.3 N cm^{-2} to 5.3 N cm^{-2} in rat; 0.6 Ncm^{-2} to 2.9 N cm^{-2} in man).

2.4.2. Muscle deformation

Due to volumetric constraints muscle fascicles expand in girth when they shorten in length, however transverse deformations in a contracting muscle can be anisotropic (Rahemi *et al.*, 2014; Randhawa and Wakeling, 2018), in part due to asymmetries in the stress through the muscle that would be affected by the transverse loads applied in this study. Furthermore, the local deformations in the muscle belly within the field of view of the ultrasound image should not be expected to be representative to all regions of the muscle or to all directions. To create space for the fascicles to expand they need to rotate to a higher pennation angle (Herbert *et al.*, 1995). Rotation to a higher pennation angle can result in an increase in muscle thickness, depending on the amount of fascicle shortening. This explanation is consistent with the increases in muscle thickness that were measured in this study. The transverse load has a large component in line with fascicle thickness, and even more so as higher loads decrease pennation angles. Therefore, it is probable that transverse load restricts the expansion in fascicle thickness, with higher loads imposing greater restrictions. The restriction in muscle thickness expansion will lead to smaller changes in pennation angle, as is shown in this study. In turn, muscle thickness will also be restricted in how much it can change, which is also shown in this study.

2.4.3. Fascicle pennation and length

When transverse load was applied to the passive muscle the pennation angle decreased to between 10.5 and 12.1 degrees (Figure 2-3A). These pennation angles are less than those reported for the unloaded MG (17.3 to 22.3 degrees) (Narici *et al.*, 1996; Maganaris *et al.*, 1998), and so the reduced pennation angle in the initial inactive state here is consistent with reductions in pennation angle due to transverse load. Pennation angles can increase by 18-20 degrees during a maximal isometric contraction for the MG (Narici *et al.*, 1996; Maganaris *et al.*, 1998). However, this study utilized twitches that would not reach a full activation state and so we would expect more modest increases in pennation angle: and the increases in pennation angle of 4 to 6 degrees are in accordance with this. The initial fascicle lengths for the loaded states in this study (mean of 68 mm) were longer than resting fascicle lengths from previous studies of 45 mm (Maganaris *et al.*, 1998; knee angle of 90 degrees), and 57 mm (Narici *et al.*, 1996; extended knee), suggesting that the transverse load caused a lengthening of the fascicles (Table 2-1) in addition to a reduction in the pennation angle.

We suggest that it is unlikely that the changes to fascicle length and pennation angle are responsible for the decreases in the muscle twitch force with transverse loading *per se*. The transverse load causes the pennation angle to decrease and the fascicles to lengthen. The decreases in pennation angle would increase the component of (longitudinal) fascicle force in the line of action in the muscle, and this would actually counter any decreases in muscle twitch force. The increases in fascicle length would extend the fascicles down the descending limb of their force-length relationship for their initial states (Maganaris, 2003; Kawakami and Fukunaga, 2006); so the muscle twitches would consequently shorten the fascicles to be closer to their optimal length, this would tend to increase the muscle force and thus counter the reductions resulting from the transverse load. Instead, it is possible that the reductions in muscle force are due to transverse mechanisms working within the muscle.

2.4.4. Intramuscular pressure

Intramuscular pressure within muscle increases during contraction and has been reported in the range of 100 – 300 mm Hg in frog gastrocnemius (Hill, 1948), and similar pressures should be found in muscles across size ranges provided they share similar

shape and intrinsic strength (Hill, 1948). Indeed, intramuscular pressures, at maximum voluntary contraction, of 200 mm Hg and 225 mm Hg have been reported for the tibialis anterior and soleus in man, respectively (Aratow *et al.*, 1993; Ateş *et al.*, 2018). Based on the contact area of the indenter, the pressures exerted by the transverse load in this study ranged from 43-218 mm Hg, and so span the range of expected intramuscular pressures. There would thus be sufficient intramuscular pressure generated during the contraction to lift the transverse load, and this is seen by the increases in muscle thickness during the twitches. The lifting heights of the loads were 15.2, 16.3, and 14.1 mm, for the 2, 4.5, and 10 kg loads respectively. Therefore, the lifting work performed by the muscle would be approximately 1224, 2953, and 5676 J m^{-3} for the 2, 4.5, and 10 kg loads respectively. These were higher than measured in rat studies (Siebert *et al.*, 2014a) which were measured between approximately 1204 and 1801 J m^{-3}. This difference was due to the loads (0.065 – 0.265 kg) and lifting heights (0.61 – 1.69 mm) being lower than in the rat study compared to the current study.

2.4.5. Muscle models

A combination of experimental and modelling work has shown a link between longitudinal and transverse forces during muscle contraction (Siebert *et al.*, 2014b; Siebert *et al.*, 2018). A Hill-type model was adapted to include an external mass, and a spring-damper component (Siebert *et al.*, 2014b). The external mass represented the transverse load on the muscle, and the spring-damper was used to represent the viscoelastic properties of the muscle tissue. An energy balance was used to link the work of the contractile component and energy in the series elastic component with the work done through the lifting of the mass and the deformation of the spring-damper. By doing so the model was able to replicate reductions in muscle force and increases in muscle thickness found in both previous observations (Siebert *et al.*, 2014a) and our study. These ideas parallel a recent model of dynamic muscle contractions in which the energy state within the muscle is made up of kinetic, volumetric, base material, and contractile components (Ross *et al.*, 2018). Transverse deformation of the muscle results in strain energy within the base material and this base material and the volumetric components (from the intramuscular fluid) redistribute the forces across all three-dimensions. Thus, transverse work done against the volumetric and base material

components and to lift the transverse load result in a reduction of the work that can be done in the line-of-action of the muscle belly.

2.4.6. Fascicle length calculation

The subject rotation and ultrasound probe placement were set to provide the clearest views of the fascicles within the muscle belly. Probe misalignments cause only minor errors in the estimation of pennation angle for the MG (Rana *et al.*, 2013), however, the compression from the probe resulted in lower pennation and longer fascicle lengths than in unloaded muscle (Narici *et al.*, 1996; Maganaris *et al.*, 1998). These lower pennations increase the extent to which fascicles extend beyond the scanned images, and so their length must be obtained by extrapolation and are more sensitive to errors. Nonetheless, changes in fascicle length were observed during the twitches and between compressive loads, however the additional variability in the length measurements contributed to the lack of significant differences being found for the fascicle lengths between conditions.

2.4.7. Limitations

The nerve stimulation excited several muscles in the lower leg. A maximal stimulus intensity was selected that achieved maximum twitch torque, where higher intensities resulted in decreased torque due to co-contractions. The co-contractions were observed during stimulation; however, they were not quantified. More accurate results could possibly be obtained if the medial gastrocnemius was individually stimulated.

As several muscles were excited by the nerve stimulation the measured force was a combination of the forces from all the muscles excited. It was not possible to determine the part of the measured force that was produced by the medial gastrocnemius. Furthermore, the force was measured from the ankle torque and it was not possible to determine muscle force as moment arms of the muscles and of the foot were not measured.

This study applied pressure and reported the architectural changes in one localized region of the lower leg, the MG; however, adjacent muscles that were not

tested may impinge on and influence each other and the net joint torque (de Brito Fontana *et al.*, 2018).

The positioning of the probe resulted in loading of the muscle. To not interfere with the unloaded measurements of the force we chose to not measure ultrasound data from the unloaded trials. For future studies it would be valuable to find a manner in which ultrasound can be measured without loading of the muscle.

Collection of the ultrasound data for the fascicles is possible because the fascicles run parallel to the ultrasound scanning plane. As pennation angle increases as a result of muscle activation the fascicles become more perpendicular to the probe surface. As the fascicle become more perpendicular to the probe the signal reflected by the fascicles becomes less. There is the possibility that this could cause the ultrasound data to decrease in accuracy as the muscle activates. These possible inaccuracies could then have an effect on the measured fascicle thickness and fascicle length. For our loaded trials this would have minor effects as the pennation angles are small. The effect would be greater when measuring unloaded muscle as pennation angles are higher at nearly 40° for maximum voluntary contractions (Narici *et al.*, 1996).

2.4.8. Conclusion

In this study, we have shown that transverse loading has an effect on human MG contraction. We have shown that greater transverse loads result in lower contraction force, as well as changes in muscle architecture. However, architectural changes cannot completely explain muscle force reduction and it seems that intramuscular pressure and internal work play a significant role in muscle shape and force production. Thus, analysis of intramuscular pressure in relation to muscle architecture might lead to a better understanding of the effects of transverse loading and muscle forces in general.

Chapter 3.

The effect of multidirectional loading on contractions of the medial gastrocnemius

3.1. Introduction

Muscle force is affected by compression applied to the muscle. Research has shown that applying transverse loads to the gastrocnemius in rats will lead to a reduction in muscle force of nearly 13% (Siebert *et al.*, 2014a). More recently it was shown that transverse loads have a similar effect on the human gastrocnemius where a 16% force reduction was measured at higher loads (Chapter 2; Ryan *et al.*, 2019; Stutzig *et al.*, 2019). Siebert *et al.* (2018) showed that multidirectional loading caused reductions in twitch force, but these reductions were less than for the unidirectional transverse loads. In vitro compression of bullfrog semimembranosus muscle showed changes in muscle force which were dependent on the length of the muscle (Sleboda and Roberts, 2019).

Muscle exists as a part of a whole organism, and as such interacts with surrounding structures such as organs, bones, skin, and other muscle. In the lower leg of humans we find the tibia and fibula bones and thirteen muscles (Fukunaga *et al.*, 1992). As such, any transverse bulging of a given muscle is going to cause it to press against either bones, other muscles, or both. These structures form barriers that impede the deformation of muscle as it contracts and relaxes. Muscle deforms in three dimensions during contraction. It contracts along its long axis, but due to the isovolumetric nature of muscle, it will bulge in the transverse directions as well. Azizi *et al.* (2017) constrained the transverse bulging of frog muscle using polypropylene tubes. This restriction to bulging caused a decrease of 50% in the power that the muscle was able to output during contraction. In rabbit muscle (de Brito Fontana *et al.*, 2018) showed that muscle force was lower when the quadriceps muscles contracted as a bundle than the summation of their individual forces if they had contracted in isolation from each other.

Muscle contraction leads to changes in muscle architecture (Narici *et al.*, 1996; Maganaris *et al.*, 1998; Wakeling and Randhawa, 2014). Recent research has shown

muscle architecture changes are affected by transverse muscle loading (Chapter 2; Wakeling *et al.*, 2013; Ryan *et al.*, 2019). Muscle thickness, pennation angle, and fascicle thickness increased with muscle contraction and increased less with higher transverse loads applied to the muscle. However, it is not known if the changes in muscle architecture lead to a change to the muscle force reduction when transversely loaded.

It has been hypothesized that there is anisotropy between the thickness and width of a muscle (Azizi *et al.*, 2008; Holt *et al.*, 2016). Recent research has shown asymmetries in the bulging of muscle fascicles (Randhawa and Wakeling, 2018) and in rat muscle (Konow *et al.*, 2020). Similar asymmetries in bulging could also result from asymmetries in stress distribution. As such differences in loading design could affect muscle architecture in different ways. Siebert *et al.* (2018) showed that multidirectional sling loading resulted in lower force reductions than unidirectional loading (Chapter 2; Ryan *et al.*, 2019; Stutzig *et al.*, 2019). Still undetermined is whether changing from unidirectional loading to multidirectional loading will have an effect on muscle architecture.

The changes in muscle force due to transverse loading are dependent on the resting length of the muscle (Sleboda and Roberts, 2019). Muscle lengths at normalized lengths between 0.9 and 1.1 showed a decrease in muscle force when compressed. The greatest reduction in muscle force was approximately 12%. Muscle length of 1.2 showed an increase in muscle force when compressed, with an increase of approximately 3%. These changes in muscle force due to compression at different muscle lengths were linked to the helical fibre properties of the extracellular matrix. Experiments on silicone tubes wrapped in Kevlar fibre showed similar results to the bullfrog muscle experiments (Sleboda and Roberts, 2019). Larger helical angles led to reductions in force, whereas smaller angles led to increases in force. The helical angles represented the extracellular matrix at different muscle lengths because the angle of the collagen fibres in the matrix reorients as the muscle changes length.

There is an indication that transverse muscle loading leads to a change in fascicle length (Chapter 2; Ryan *et al.*, 2019) and past research has shown that fibre force is in part determined by the length of the fibre (Ramsey and Street, 1940). Being a bi-articulate muscle (Hodson-Tole *et al.*, 2016) the length of the medial gastrocnemius is

determined by the angle of the ankle as well as the angle of the knee (Fukunaga *et al.*, 1996, 1997; Narici *et al.*, 1996; Herbert *et al.*, 2002). This leads to a wide range of muscle lengths that the medial gastrocnemius can take on, with the result that it works over a range of the force-length relationship, both at rest and during activation (Maganaris, 2003; Kawakami and Fukunaga, 2006). For the current study participants are measured with their knees bent at a 90° angle in contrast to previous studies where knees were kept fully extended (Chapter 2; Siebert *et al.*, 2018; Ryan *et al.*, 2019; Stutzig *et al.*, 2019). As a result of knee angle change the whole muscle-tendon unit changes in length (Herbert *et al.*, 2002). The medial gastrocnemius is shorter at a 90° knee angle than it is with the knee extended, though a large amount of the change in length is attributed to tendon lengthening rather than fascicle lengthening (Herbert *et al.*, 2002). Furthermore, the torque produced by the medial gastrocnemius was shown to be lower at flexed knee angles than at extended knee angles (Cresswell *et al.*, 1995; Maganaris, 2003). As such the knee position of the participants needs to be taken into account when comparing force measurements with previous research on *in vivo* muscle force reductions measured in humans.

Fascicle curvatures have been observed in the vastus medialis (Sejersted *et al.*, 1984) and triceps surae (Kawakami *et al.* 1998; Maganaris *et al.* 1998), and quantified in the medial gastrocnemius (Namburete *et al.*, 2011; Darby *et al.*, 2013) and the triceps surae (Muramatsu *et al.*, 2002; Rana *et al.*, 2014). The triceps surae showed an increase in fascicle curvature with higher ankle torque (Rana *et al.,* 2014). Muscle fibre curvature is related to intramuscular pressure (Hill, 1948), and intramuscular pressure increases with increases in joint torque (Sylvest and Hvid, 1959; Baumann *et al.*, 1979; Sejersted *et al.*, 1984; Aratow *et al.*, 1993; Ateş *et al.*, 2018). According to the law of Laplace (Equation 3-1), the change in pressure, Δp, depends on two factors according to the following equation,

$$\Delta p = \frac{2\gamma}{R} \tag{3-1}$$

where γ is tension and R is the radius of the curvature of the fibre (Sejersted *et al.*, 1984; van Leeuwen and Spoor, 1992). External loading was shown to be linked to intramuscular pressure, as an increase in intramuscular pressure of approximately 24 mmHg was found by applying compression stockings (Rennerfelt *et al.*, 2019). This series of relationships leads us to question whether transverse loading affects fibre

curvature and if differences can be seen in fibre curvature between loaded and unloaded muscle contractions.

As multidirectional loading resulted in less force reduction than unidirectional loading we hypothesize that muscle architecture will change but do so to a lesser degree than happened in our previous study with unidirectional loading (Chapter 2; Ryan *et al.*, 2019). The shorter resting length of the muscle due to a change in knee angle will alter the effects of external transverse loading. We hypothesize that the shorter length of the muscle will make it less susceptible to force reduction and architecture changes. Furthermore, we hypothesize that fascicle curvatures will increase with muscle activation and external transverse loading will change fascicle curvature.

3.2. Material and Methods

20 young adults were recruited (sex: 3 female / 17male, age: 26.1 ± 5.0 years, height: 180 ± 6 cm, weight: 77.0 ± 10.1, BMI: 23.7 ± 2.6, physical activity per week: 6.0 ± 4.5 hours). All participants gave informed consent before taking part in the study and the study was approved by the Office of Research Ethics at Simon Fraser and Stuttgart Universities.

A custom chair was constructed that allowed participants to sit upright with their back fully supported (Figure 3-1). Bars were fixed over the knees to prevent the lower leg from moving upwards and in front of the shins to prevent the lower leg from moving forward during contraction. The knee and ankle angles were held at 90° angles. The right foot was placed on a force plate (AMTI OR-6, Watertown, USA) (Figure 3-1A) to determine twitch force throughout the trials. We took the measured force as a representation of the muscle twitch force of the medial gastrocnemius. However, in actuality the measured force was a summation of multiple muscles contracting and the assumption was made that muscle moment arms stay constant throughout contraction. An electrode was placed in the popliteal fossa, with the second electrode positioned over the front of the knee, to stimulate the popliteal nerve (Figure 3-1E) and elicit a contraction from the calf muscles (DS7AH Digitimer, Herfordshire, UK). A latex sling (420 x 150 mm) (Figure 3-1C) was wrapped around the calf at the height of the gastrocnemii and attached to a cable and pulley system. The sling was kept in place for all trials, and during weighted trials either 5 kg or 10 kg weights were attached to the

pulley system (Figure 3-1B). A linear ultrasound probe (Echoblaster 128, Telemed, Lithuania) (Figure 3-1D) was positioned superficial to the sling to scan through to the medial gastrocnemius, providing a 65 mm field of view with a 50 mm scanning depth (604 x 515 pixels; 80 Hz). The ultrasound probe was centered on the medial gastrocnemius in both the anterior-posterior and medial-lateral directions. The long axis of the probe was lined up with the long axis of the muscle. The probe surface was kept as parallel as possible with the surface of the muscle so that complete fascicles appeared in the scanning plane.

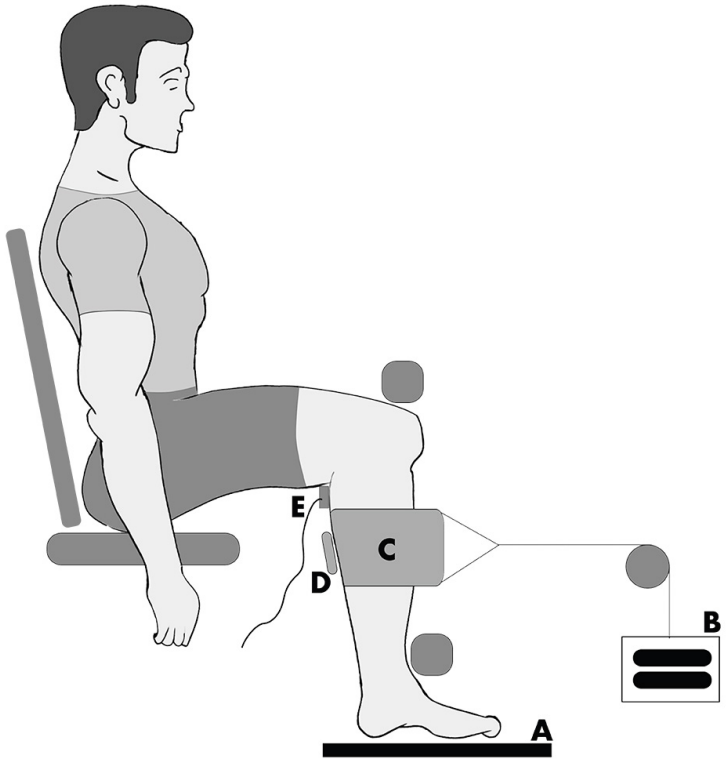

Figure 3-1 Experimental design for the collection of force data and ultrasound data. Participants were seated in a custom designed chair with their right foot placed on a force plate (A). Through the use of a pully system weights (B) loaded the sling (C) which was wrapped around the calf to apply transverse loads to the muscle. Ultrasound images (D) were taken of the medial gastrocnemius, and the muscle was stimulated using an electrode (E) in the popliteal nerve.

The participants performed a warm-up that consisted of 10 calf raises, 3 sets of skipping rope (20 skips per set), and 10 repetitions of walking a set of stairs. Participants were then seated and secured in the measurement chair, and the stimulation electrodes

were placed. The stimulation current was increased by 1 mA increments until the measured twitch force showed a plateau. The stimulation current at the start of the plateau region was used throughout the trials. The stimulation current was determined for unloaded muscle. It was assumed that nerve position within the leg did not change between unloaded and loaded conditions.

The study consisted of four trials: pretest, posttest, and two loaded trials. Pre- and posttest had no load applied to the sling. 5 kg and 10 kg weights loaded the sling for the loaded trials and were applied in a random order. Twitch forces and ultrasound data were collected for three twitches for each trial.

The maximum twitch force between the pre- and posttest were compared to determine reliability of the performed trials. The set of trials was deemed unreliable when differences between the maximum twitch force between pre- and posttest were greater than 5%, as something within the set-up might have changed to cause the difference in force. Unreliable trials were removed from the data set.

The ultrasound data (Figure 3-2) were analysed for a series of frames centred around the maximum twitch force in four steps following our previous procedures (Chapter 2; Ryan *et al.*, 2019): manual digitization, multiscale vessel enhancement filtering (Frangi *et al.*, 1998), Hough line detection (Hough, 1962; Duda and Hart, 1972; Illingworth and Kittler, 1988), and Fourier transformation (Wakeling and Randhawa, 2014). These steps allowed us to quantify the muscle thickness, pennation angle, and the spacing of the fascicular stripes that we term the fascicle thickness. Fascicle lengths were estimated by dividing muscle thickness by the sine of the pennation angle. All raw data were filtered using a Gaussian filter before analysis.

The elicited muscle twitches cause the leg of the participant to jerk. Although the leg is fixed, not all movement of the leg can be prevented. The positioning of the ultrasound probe is crucial to the reliability of the measurements and therefore any movement caused by the twitch could result in measurement differences within a subject. After analysis of the data it was apparent that the fascicle length measurements did not return to their pre-twitch value within the 0.5 second window that the data were analysed. Possibly the 0.5 second analysis period was not sufficiently long to show fascicle lengths returning to initial values. Therefore, the baseline variability analysis was

performed. To asses reliability of the apparatus and ultrasound data collected we calculated the baseline variability as the difference between the end values of a given architectural measure resulting from a muscle twitch with the start values immediately before the following muscle twitch measured. These calculations were done between the first and second, and second and third measured muscle twitches. The period between consecutive twitches was approximately 10 seconds. The baseline variability with 1, 2, or 3 standard deviations added were set as a threshold to determine whether changes in muscle architecture were greater than this baseline variability. This method was adapted from the computer determination of onset for EMG (Di Fabio, 1987; Hodges and Bui, 1996; Stokes *et al.*, 2000; Allison, 2003).

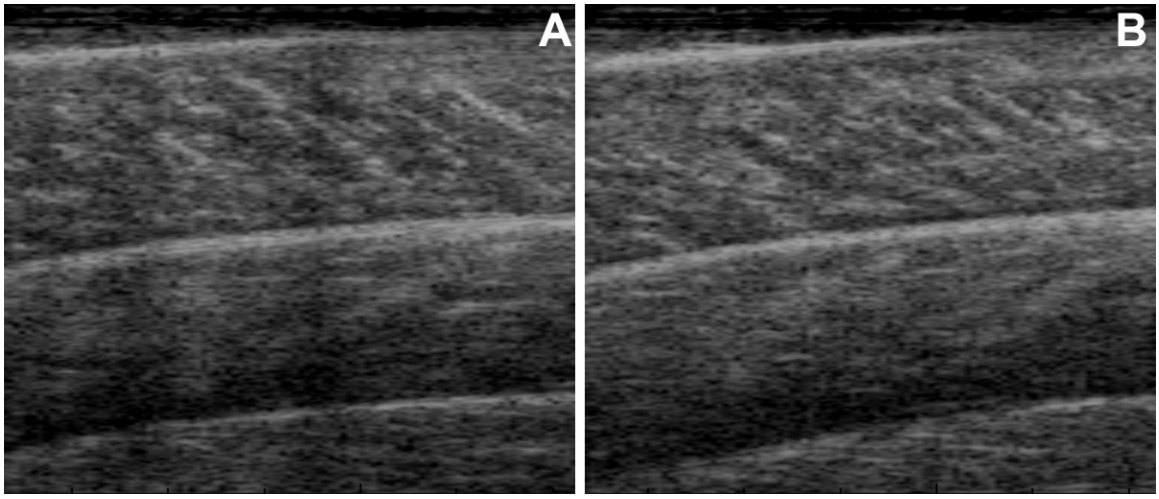

Figure 3-2 Ultrasound example data of the medial gastrocnemius. Ultrasound images for the passive unloaded pretest (A) and the passive 10kg loaded (B) measurements.

In each frame of the ultrasound data the aponeuroses were manually segmented using a custom written Mathematica code (Wolfram Mathematica 11, Oxfordshire, UK). The muscle thickness was calculated as the mean distance between the aponeuroses. The positions were also used to isolate the gastrocnemius muscle in each frame. Frames in which the muscle was isolated had the multiscale vessel enhancement filter applied to them using scales 1, 2, and 3 (Frangi *et al.*, 1998; Rana *et al.*, 2009; Namburete *et al.*, 2011). Hough line detection was applied to the filtered gastrocnemius regions (Hough, 1962). The filtered image was binarized to produce a black and white image. For each morphological component in the binarized image we applied the Hough transform to determine the best fit line. From each of these lines we then determined the angle relative to the x-axis (long axis of the image). As the fascicles ran from top left to

bottom right of each image only negative angles were representative of fascicles and positive angles were discarded. Similarly, any angles smaller than 5° were discarded as they most likely represented blood vessels running through the muscle. The final pennation angle was calculated by taking the mean angle of all lines relative to the mean position of the aponeuroses, which was assumed to be the line of action of the muscle.

For each isolated and enhanced frame the wavelength of the fascicles in the muscle belly was determined using a 2D-Discrete Fourier transform (Wakeling and Randhawa, 2014; Chapter 2; Ryan *et al.*, 2019). The transform was applied to find the transverse wavelength across the muscle fascicles. Stripes in the ultrasound images were considered to lie in the same direction as the muscle fascicles. As the fascicles dilated, the spacing of these stripes got wider; thus their transverse wavelength was proportional to the fascicle width.

The method to quantify the fascicle curvature from ultrasound data was based on Namburete *et al.* (2011). The initial step was to determine the fascicle orientation at every pixel for a given image taken from the ultrasound data. Previously described methods using the Hough transformation were not suitable for this task, as it only provided orientations at positions in the image where fascicles were clearly visible. To get the orientation at every pixel we performed a convolution using an anisotropic wavelet kernel (Rana et al, 2009). The wavelet used was highly directional in shape and could therefore be constructed with an orientation to it. A set of these wavelets was constructed with angles ranging from 90° to -90°. The given image was convolved with each wavelet, and the wavelet that produced the highest convolution value at a given pixel was determined to represent the fascicle orientation at that pixel. The trajectories of the fascicles were calculated using the Fibre Assignment by Continuous Tracking method (Mori and van Zijl, 2002; Jiang *et al.*, 2006). The method started with selecting a pixel within the image as the seed point. At this seed point the orientation was determined and a step was taken following a vector whose orientation was that of the seed point and had a fixed magnitude. Following the vector, we obtained a second pixel within the image. At this pixel the process was repeated. Starting from the seed point this process was done forwards and backwards a given number of times after which we obtained a segment of the fascicle trajectory running through our seed point. The fascicle tracking was done for every pixel in the image (Figure 3-3). Using the points of the fascicle segment two parametric functions were obtained by interpolating a third

order polynomial through the x and y values of the coordinates and used to solve the Frenet-Serret formulas which calculated a curvature value. Curvature was calculated for any pixel that allowed a segment of the fascicle to be tracked. From each seed points 10 steps of 25 pixels each were taken (5 in each direction) to determine fascicle trajectories. Weighted mean angles were calculated at each step. For each frame the root mean square of the curvatures was calculated. This was done to adjust for opposing curvatures that could occur if fascicles are S-shaped.

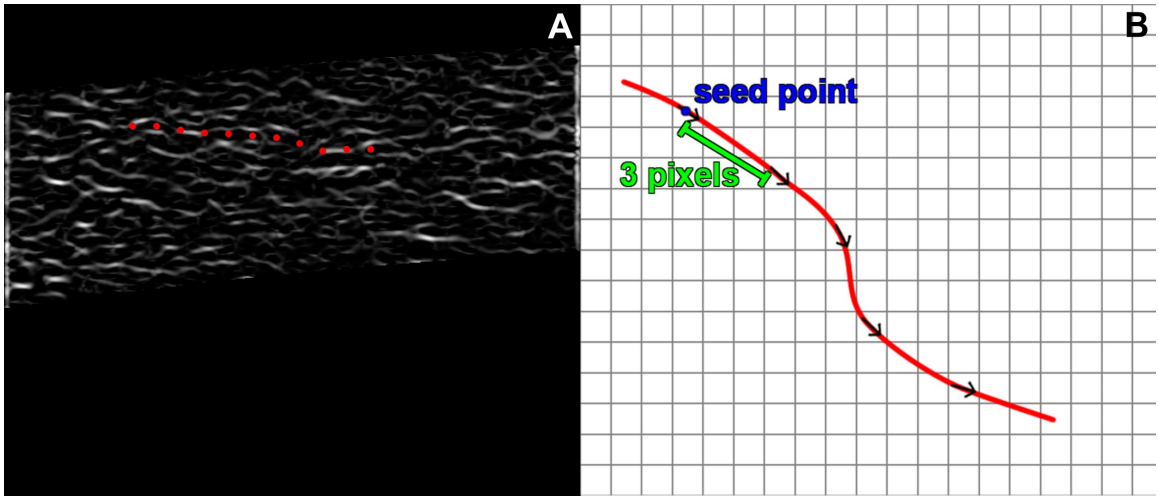

Figure 3-3 Images illustrating fascicle trajectory calculation. Example of a fascicle trajectory calculated along 11 points (A). Schematic of a fascicle trajectory calculation with a 3 pixel jump distance and 4 jumps along the trajectory.

The pennation angle, muscle thickness, fascicle thickness, and fascicle length were determined for passive loaded muscle before muscle activation. This was done for all four trials. Statistical analyses were performed to determine significant differences between the passive states of the four trials for all muscle architecture measurements. This analysis was performed to determine the effects of external transverse loading on passive resting muscle. The maximum, for pennation angle and muscle thickness, and the minimum, for fascicle thickness and fascicle length, were determined for a 0.5 s window around each muscle twitch. These maxima and minima were determined for all four trials. This allowed us to determine the change that occurred in a measurement as a result of muscle activation. Comparing the change between unloaded and loaded trials, as well as between the two loaded trials, could tell us whether muscle architecture is affected by external transverse loading. Statistical analyses for all architecture measurements were performed to determine significant differences between either the

maxima or minima of the four trials. The root mean square of the fascicle curvature for passive loaded muscle before muscle activation, as well as the root mean square of the fascicle curvature at maximum twitch force were determined. Significant differences between the four trials were determined for both the passive curvatures as well as the active curvature. All the statistical differences were calculated using a one-way repeated measures ANOVA in IBM SPSS Statistics (Version 25 IBM Corp., Armonk, NY). Subjects were considered random and twitches between individuals were considered to be independent of one and other. Differences between trials were determined with a post-hoc Bonferroni test. Tests were considered significant when $p < 0.05$.

For all five muscle architecture measurements, as well as all four trials, the value for passive loaded muscle and either maximum or minimum were compared to one and other to determine if muscle architecture significantly changed with muscle activation. Significant differences were calculated using independent samples t-tests. Tests were considered significant when $p < 0.001$.

A smaller p value was used for the t-tests compared to the one-way repeated measures ANOVAs. This was done to allow for the Bonferroni correction because a large number of t-tests that were used compared to the lower number of repeated measures ANOVAs.

3.3. Results

Excitation of the popliteal nerve resulted in twitch contractions of the triceps surae muscles. This was shown by the transient increase in force (Figure 3-4I) measured from the foot. During each twitch the muscle increased in thickness (Figure 3-4C, D), pennation rotated to a greater angle (Figure 3-4A, B), and fascicle thickness decreased (Figure 3-4E, F, Figure 3-5).

Neither the 5 kg, nor the 10 kg transverse loads resulted in a reduction in twitch force compared to the unloaded pre- and posttest trials (Figure 3-4I). There was also little effect of the transverse load on the muscle architecture. For the resting state before each twitch, the transverse load resulted in a significant decrease in the pennation angle (Figure 3-4A,B) and the muscle thickness (Figure 3-4C,D), but not in the fascicle length or transverse wavelength (Figure 3-4C-H; Table 3-3). The peak thickness reached

during the twitch was significantly lower in the loaded contractions (Figure 3-4C,D), but there was no significant effect of the transverse load on the peak pennation, fascicle length or transverse wavelength (Figure 3-4A,B, E-H; Table 3-3).

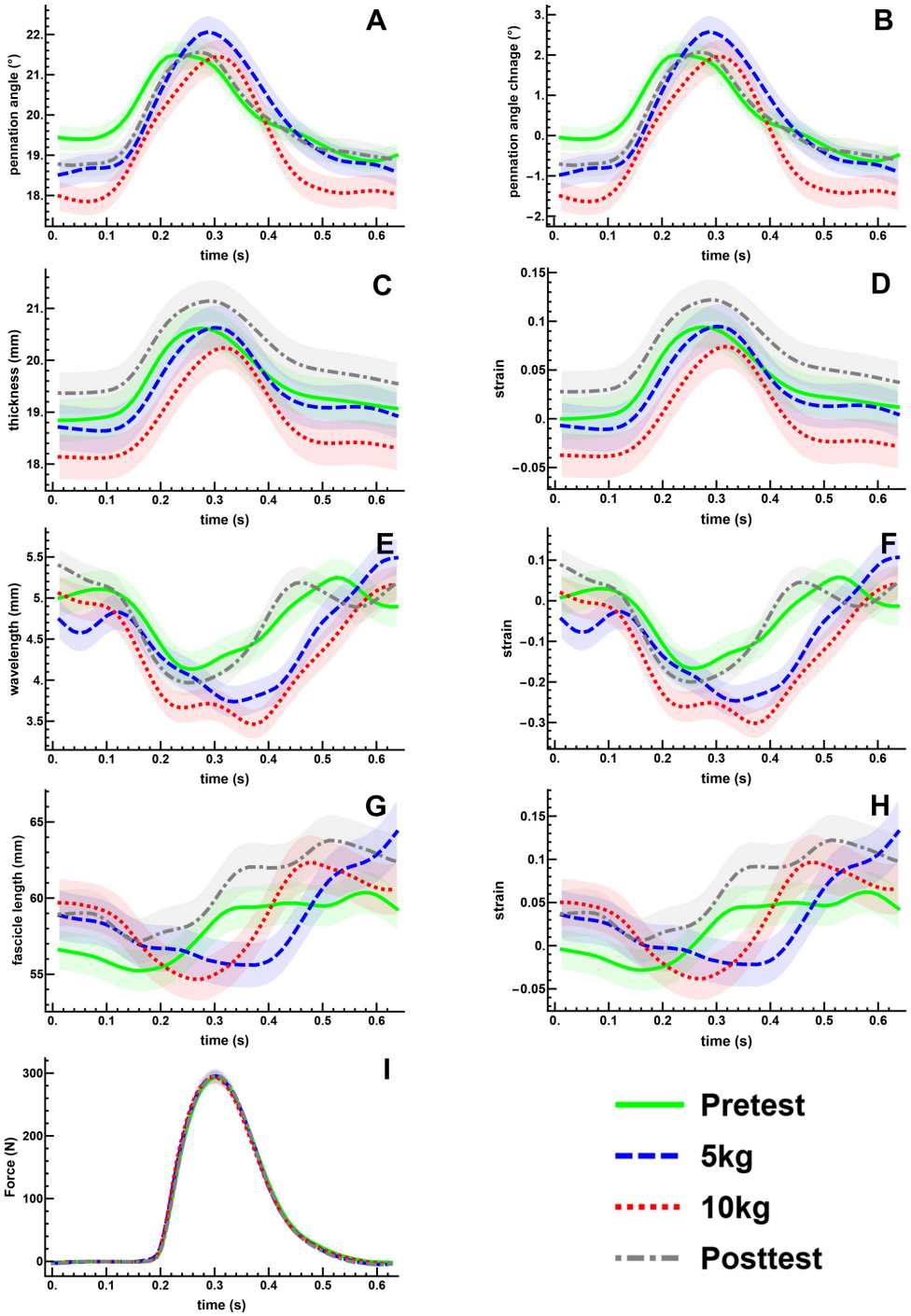

Figure 3-4 **The mean changes in muscle architecture and force measured during muscle twitches. The mean and standard error for all measured twitches are plotted for the pre- (green, solid) and posttest (gray, dot-dashed), and the 5 kg (blue, dashed) and 10 kg (red, dotted) loaded trials. Transient increases are shown for the pennation angle (A,B) and muscle thickness (C,D). The transverse wavelength (E,F) and fascicle length (G,H) show transient decreases. The measured twitch force (I) shows an increase with muscle activation.**

Muscle thickness and pennation angle significantly increased between the passive and active states of each twitch, whereas fascicle wavelength and fascicle length values did not differ significantly (Figure 3-5). As such it can be said that muscle thickness and pennation angle changed with muscle activation, but fascicle thickness and fascicle length remained unchanged with muscle activation.

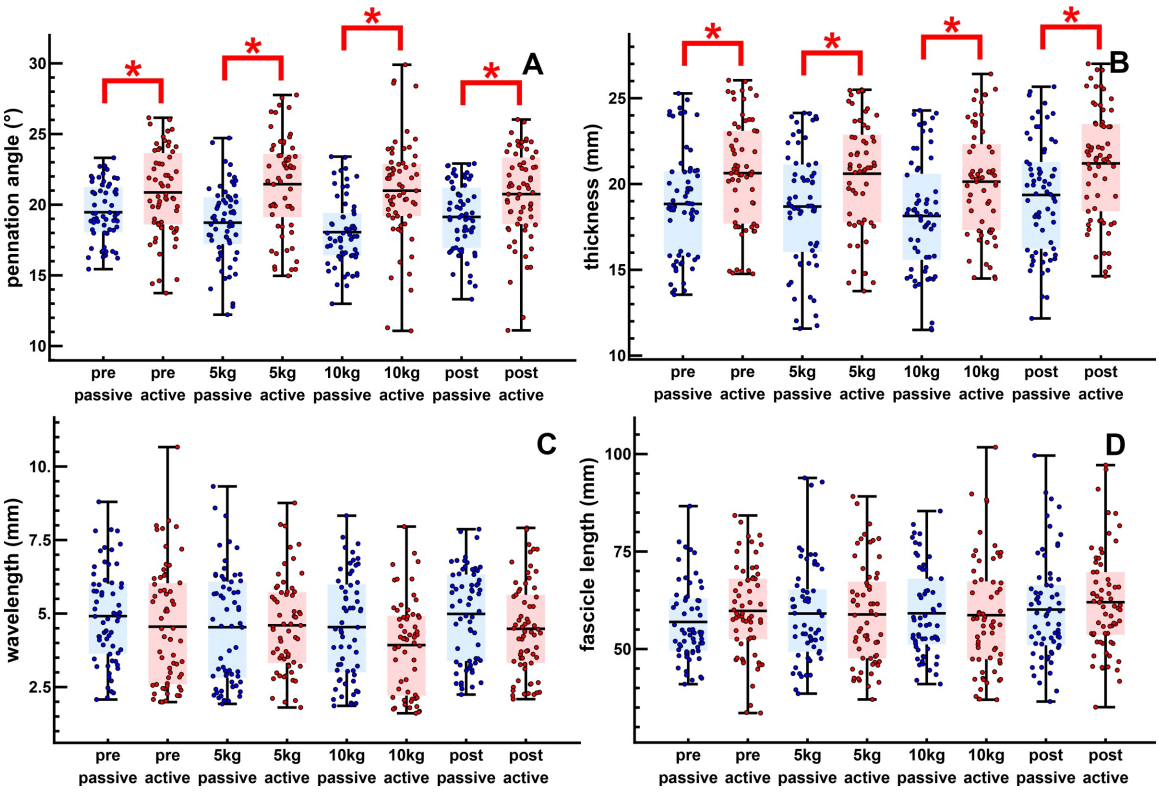

Figure 3-5 The passive loaded and peak active loaded values for all twitches. Passive (blue) and active (red) values are shown for the pennation angle (A), muscle thickness (B), transverse wavelength (C), and fascicle length (D). The dots show individual twitches with the boxes showing the mean and span from the 0.25 to the 0.75 quantile. Significant differences are shown between passive and active states (*, p < 0.001).

To determine whether the change in muscle architecture was discernible from the baseline variability between twitches we compared the change in muscle architecture with the mean of the resting variation plus 1, 2, and 3 times the standard deviation of the resting variation (Table 3-1). At a threshold of the mean plus 1 standard

deviation all changes were higher than the threshold. At a threshold of the mean plus 2 standard deviations pennation angle and muscle thickness changes were higher than the threshold, changes in fascicle thickness and fascicle length were not. For a threshold of the mean plus 3 standard deviations only the changes in muscle thickness were higher than the threshold.

Table 3-1 **Calculations of the baseline variation between the end and beginning of consecutive twitches compared to the change in muscle architecture. The mean measured change in muscle architecture was compared to thresholds of the baseline variation at the mean plus 1, 2, and 3 times the standard deviation. Comparisons were made for all trials for the pennation angle, muscle thickness, fascicle thickness, and fascicle length. The table indicates changes higher than the threshold (green, clear) and lower than the threshold (red, shaded).**

		baseline variation				measured change
	trial	mean ± SD	mean + 1 SD	mean + 2 SD	mean + 3 SD	Mean ± SD
pennation angle (°)	pre	0.98 ± 0.72	1.70	2.41	3.13	2.73 ± 1.44
	post	1.06 ± 0.87	1.93	2.80	3.67	3.18 ± 1.37
	5	1.06 ± 0.86	1.93	2.79	3.65	3.84 ± 1.40
	10	1.14 ± 0.79	1.93	2.71	3.50	3.77 ± 1.48
muscle thickness (mm)	pre	0.33 ± 0.25	0.58	0.83	1.08	1.83 ± 0.72
	post	0.29 ± 0.20	0.50	0.70	0.91	1.84 ± 0.66
	5	0.39 ±0.29	0.68	0.98	1.27	2.04 ± 0.94
	10	0.29 ± 0.21	0.49	0.70	0.91	2.20 ± 1.39
fascicle thickness (mm)	pre	0.72 ± 0.61	1.33	1.94	2.55	1.37 ± 0.67
	post	0.76 ± 0.63	1.39	2.02	2.65	1.71 ± 0.93
	5	0.69 ± 0.67	1.36	2.03	2.70	1.88 ± 1.00
	10	0.61 ± 0.61	1.21	1.82	2.43	2.03 ± 1.21
fascicle length (mm)	pre	3.28 ± 2.53	5.81	8.34	10.86	6.97 ± 2.87
	post	3.26 ± 2.78	6.04	8.81	11.59	8.60 ± 4.01
	5	3.70 ± 3.06	6.76	9.82	12.88	8.39 ± 3.94
	10	3.56 ± 3.01	6.57	9.59	12.60	8.62 ± 5.50

Transverse loading of the medial gastrocnemius caused the fascicle curvature to decrease in their resting state (Figure 3-6, Table 3-2), flattening out the fascicles by compressing them. During the muscle twitches the fascicle curvatures increased slightly, however these increases were not statistically significance.

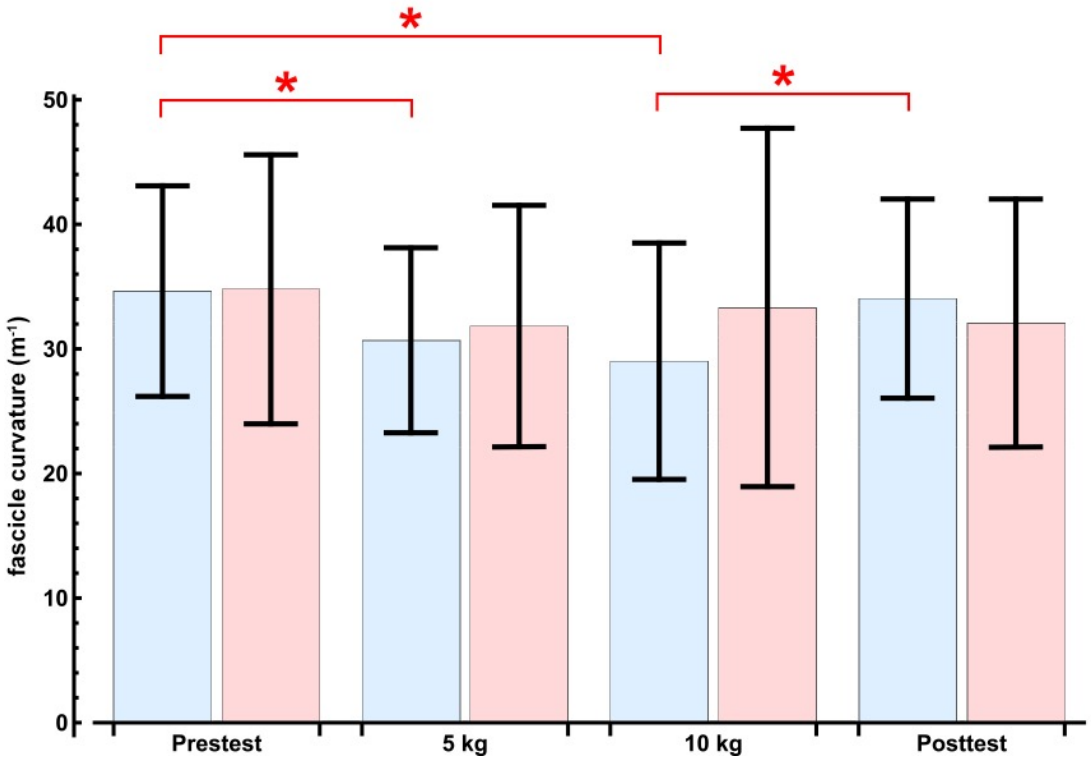

Figure 3-6 **Mean resting passive (blue) and peak active (red) curvatures measured for all trials. The error bars indicate the standard deviations. The loaded trials show lower curvatures than the unloaded trials, and for the loaded trials the peak active curvature is higher than the resting passive curvature. Significances between trials are shown (*, $p<0.05$).**

Table 3-2 **Curvatures for the four trials at resting passive and peak active states. Comparisons of the curvatures are made between the four trials at both passive resting and peak active state. Data show the mean and standard deviation of all twitches. Significances are indicated between pretest and 5 kg (*), pretest and 10 kg (†), pretest and posttest (|), 5 kg and 10 kg (±), 5 kg and posttest (‡), and 10 kg and posttest (+).**

		mean ± SD	Significance
curvature (m^{-1})			
passive	pretest	34.8 ± 8.5	*, †, +
	5 kg	30.7 ± 7.4	
	10 kg	29.0 ± 9.5	
	posttest	34.0 ± 7.9	
active	pretest	35.1 ± 10.8	
	5 kg	31.8 ± 9.7	
	10 kg	33.3 ± 14.4	
	posttest	32.8 ± 9.9	

Significant differences were mainly found for the pennation angle and muscle thickness (Table 3-3). Passively loaded muscle showed significant differences between the pretest and loaded trials for pennation angle and between the posttest and the loaded trials for the muscle thickness. The change from passive to actively loaded muscle was significantly different for the pretest and loaded trials for the pennation angle. Changes for muscle thickness were not significant although actively loaded muscle showed differences between the posttest and the loaded trials. Changes between the pretest and loaded trials were significant between the pretest and the loaded trials. For fascicle length the changes were different between the pretest and posttest. This would suggest fascicle length measurements were not reliable.

Table 3-3 Comparisons of the muscle architecture measurements between the four trials at passive resting state, peak active state, and the change between passive and active. Means and standard deviations are given for the pennation angles, muscle thicknesses, transverse wavelengths, and fascicle lengths. Significances are indicated between pretest and 5 kg (*), pretest and 10 kg (†), pretest and posttest (|), 5 kg and 10 kg (±), 5 kg and posttest (‡), and 10 kg and posttest (+).

	pretest	5kg	10kg	posttest	significance
pennation angle (°)					
passive	19.4 ± 2.0	18.7 ± 2.7	18.1 ± 2.4	19.2 ± 2.4	*,†,+,±
active	20.9 ± 2.1	21.5 ± 3.4	21.0 ± 3.7	20.7 ± 3.3	
change	2.7 ± 1.5	3.8 ± 1.4	3.8 ± 1.5	3.1 ± 1.4	*,†,‡
muscle thickness (mm)					
passive	18.9 ± 3.2	18.7 ± 3.5	18.1 ± 3.3	19.1 ± 3.2	†,‡,+,±
active	20.7 ± 3.2	20.6 ± 3.3	20.1 ± 3.1	21.0 ± 3.2	†,‡,+,±
change	1.8 ± 0.7	2.0 ± 0.9	2.2 ± 1.4	1.9 ± 0.7	
transverse wavelength (mm)					
passive	4.9 ± 1.6	4.5 ± 1.9	4.5 ± 1.8	5.0 ± 1.5	
active	4.6 ± 2.0	4.6 ± 1.6	3.9 ± 1.6	4.5 ± 1.6	±
change	1.4 ± 0.7	1.9 ± 1.0	2.0 ± 1.2	1.7 ± 0.9	*,†
fascicle length (mm)					
passive	57.2 ± 10.2	59.1 ± 12.6	59.2 ± 11.3	59.2 ± 12.6	†
active	60.0 ± 11.9	58.9 ± 13.0	58.7 ± 14.5	61.8 ± 13.2	
change	7.0 ± 2.9	8.4 ± 3.9	8.6 ± 5.5	8.6 ± 3.8	|

The lifting heights of the weights were measured during each twitch for all the trials. The mean lifting heights for the unloaded pre- and posttest were 5.04 ± 1.52 mm and 5.15 ± 1.59 mm respectively. For the 5 kg trials the mean lifting height was 12.38 ± 3.42 mm and for the 10 kg trials the mean was 15.89 ± 4.05 mm. The mean lifting heights of all four trials were compared using a one-way repeated measures ANOVA. No significant differences were found between the mean lifting height of the pre- and posttest. The unloaded trials were significantly different from the loaded trials, and the mean lifting heights of the 5 kg and 10 kg trials were significantly different ($p < 0.05$).

The lifting work of the muscle was estimated for the 5 kg and 10 kg loaded trials. Lifting work was estimated at 2476 and 6360 J m^{-3} for the 5 and 10 kg trials respectively. Muscle volume was assumed to be 243.7 cm^3 (Fukunaga *et al.*, 1992).

3.4. Discussion

In this study we found no change in twitch force when the human gastrocnemius muscle was transversely loaded with a compression sling. This finding was different from previous studies where decreases in force due to muscle loading have been reported in rat (Siebert *et al.*, 2014a) and human studies (Siebert *et al.*, 2018; Ryan *et al.*, 2019; Stutzig *et al.*, 2019). A major difference in this current study was that the muscle was held at a shorter length: in this study the mean fascicle length was 60 mm, compared to our previous length of 70 mm (Chapter 2; Ryan *et al.* 2019). However, recent studies have shown that compression-related reductions in muscle force may be exacerbated at shorter muscle lengths (Sleboda and Roberts, 2019), and thus the differences in our study may be due to a complex interaction of different factors during contraction: length, pennation angle and direction of loading.

3.4.1. Muscle length compared to the force-length relationship

In the endomysium the collagen fibres were shown to have an average angle of 59° which got lower in lengthened muscle (34°) and higher in shortened muscle (73°) (Purslow and Trotter, 1994). Physical muscle models showed that a helical fibre arrangement with a low angle reacted to compression by shortening, whereas with a high angle compression caused lengthening (Sleboda and Roberts, 2019). According to our data (Table 3-3) transverse loading of passive muscle showed no changes in fascicle length. Although fascicle length measurements were disputable, the assumption is that in our current experiment the fascicles were working over the same range of the force-length relationship for both unloaded and loaded muscle. As a result, we would expect no change in muscle force, which is what the current results showed. In previous studies (Chapter 2; Ryan *et al.*, 2019; Stutzig *et al.*, 2019) muscle was kept at a longer length. In longer muscle transverse loading would lead to shortening of the fascicles, assuming that the helical angle of the extracellular matrix was lower than 59°. This would explain the force reduction as the fascicles would be working lower on the ascending

limb of the force-length relationship when active (Kawakami and Fukunaga, 2006). However, fascicle length was not measured for unloaded conditions in previous studies. Fascicle length was shown to increase with higher transverse load which would suggest transverse loading at longer muscle lengths does not lead to shortening but rather to lengthening of the fascicles.

3.4.2. Knee angle related to muscle force

Cresswell *et al.* (1995) found that plantar flexor torque was lower when the knee was flexed compared to the knee being extended. With the knee flexed at 60° plantar flexor torque was 60% of the torque found with the knee fully extended. There is the possibility that force reduction due to transverse loading is diminished because the gastrocnemii were unable to deliver the full torque that they would be able to deliver when the knee was fully extended. However, it should be mentioned that measured twitch forces were greater in the current study compared to studies performed previously (Chapter 2; Ryan *et al.*, 2019; Stutzig *et al.*, 2019). Stimulation currents were higher in our current study (170mA) than those used previously (30mA) (Chapter 2; Ryan *et al.*, 2019; Stutzig *et al.*, 2019). At higher stimulation currents especially the soleus would produce a higher force as it would not be affected by knee angle. The possibility remains that because the gastrocnemii are producing a lower force due to knee angle they were less affected by transverse loading which could contribute to the lack of force reduction found in this study.

3.4.3. Pennation angle of transversely loaded muscle

Assuming fascicle lengths were shorter we would expect greater pennations. Shortening of fascicles leads to bulging in the transverse directions due to their isovolumetric characteristics (Abbott and Baskin, 1962; Baskin and Paolini, 1967) which would result in increases in pennation angle (Randhawa and Wakeling, 2018). This was reflected in the pennation angle measurements of the current study which were close to 20° compared to previous studies (Chapter 2; Ryan *et al.*, 2019; Stutzig *et al.*, 2019) were pennation angles were closer to 10°. It should be noted that lower pennation angles would not only be due to longer fascicle lengths but likely also due to gravity compression the muscle because participants were lying down for the previous study (Chapter 2). Muscle with a pennation angle lower than 15° tends to thicken with muscle

activation whereas muscle with a pennation angle higher than 15° tends to get thinner with muscle activation (Wakeling 2020). In the previous studies (Chapter 2; Ryan *et al.*, 2019; Stutzig *et al.*, 2019) muscle would tend to get thicker because of the lower pennation angle, which was shown in the muscle thickness measurements. This tendency to expand against the direction of the transverse load could contribute to the reduction in twitch force that was measured. In our current study the muscle would tend to get thinner because of the higher pennation angle. This would cause it to not expand against the transverse load and would not contribute to any force reductions. However, the muscle thickness measurements of the current study showed an increase in thickness with muscle activation which goes against supporting this argument, albeit this increase in thickness was less (2 mm) than in previous studies (5 mm: Chapter 2; Ryan *et al.*, 2019; Stutzig *et al.*, 2019).

3.4.4. Anisotropic deformation

Anisotropic deformations of the muscle and muscle fascicles as a result of muscle activation have been shown in previous research (Randhawa and Wakeling, 2018; Konow *et al.*, 2020). Therefore, anisotropy because of transverse loading could also occur. The unidirectional block loading used in previous studies (Chapter 2; Ryan *et al.*, 2019) would result in decreases in fascicle thickness and increases in the width of the fascicles. Deformation from sling loading would be more symmetrical as there was loading in both the thickness and width directions of the fascicles. Differences in fascicle deformations could have an effect on pennation angle changes and muscle thickness changes and therefore contribute to force reductions due to transverse loading.

3.4.5. Fascicle curvature

Our method of curvature calculation was based off of the method described by Namburete *et al.* (2011). They presented curvatures measured between approximately 10 and 16 m^{-1} which are comparable, albeit lower, than the curvatures that were measured in this study (30 - 35 m^{-1}). The conditions under which the curvatures were measured were different between the two studies. Namburete *et al.* (2011) measured participants seated in a dynamometer with their ankle at 75° relative to the tibia. This ankle angle would result in the medial gastrocnemius being stretched more when compared to the 90° ankle angle used in this study. Stretching of the muscle could result

in stretching of the fascicles which would cause the curvature to be reduced. However, ankle angle did not greatly impact fascicle curvature during measurements of three-dimensional curvatures by Rana *et al.* (2014). Furthermore, to calculate curvatures Namburete *et al.* (2011) used three points when tracking fibres, whereas 10 points were tracked along the fibre in this study. It is important to note that a curvature lower than 16 m^{-1} was expected because maximum twitch force was used rather than maximum voluntary contractions as was done by Namburete *et al.* (2011). The curvatures measured by Rana *et al.* (2014) were even smaller (4.15 – 4.08 m^{-1}) than those measured by Namburete *et al.* (2011). They measured curvatures at the same ankle angle as was reported here, however knee angle was not fully extended (135°) so the muscle would be shorter and thus a higher curvature would be expected. They also used three points when tracking fibres. Another difference in method was that the fascicle trajectories were fitted to a second order polynomial, whereas in this study they were fitted to a third order polynomial. The reason for choosing a third order polynomial was to allow for S-shaped curvatures of the fascicles.

Fascicle curvatures found in this study ranged from approximately 30 to 35 m^{-1} for passive and active muscle, respectively. This corresponds to a radius of 33.3 and 28.6 mm for passive and active, respectively. Fascicle lengths were measured at approximately 59 mm. An approximate radius of 30 mm compared to a length of 59 mm means fibres would have a very high curvature, which does not agree with observation of the images taken from the ultrasound. Estimation from the ultrasound images shows nearly no curvature. Therefore, it is likely that the current method for curvature calculation overestimated fascicle curvature. Other studies have measured curvature for passive and active muscle between 0.4 and 5.5 m^{-1}, respectively (Muramatsu *et al.*, 2002; Rana *et al.*, 2014). It is possible that because of the number of points tracked along each fibre the mean measured curvature is different between studies. If fibres are S-shaped than curvatures in the middle of the muscle belly would be close to zero. Tracking three points along the fibre would capture these low curvatures. This would lower the mean curvature calculated for the muscle. By tracking five points in either direction of the seed point it is possible that the low curvatures in the middle of the muscle belly are missed. The tracked points would extend into the curvature of the fibre close to the aponeuroses which would overestimate the curvatures of the middle of the muscle belly. This would result in a higher mean curvature for the muscle.

3.4.6. Limitations

For the unidirectional loaded study 10 kg load was used on a smaller surface area compared to the multidirectional loading, therefore a higher pressure was applied. It was expected that there were greater deformations of the muscle in the unidirectionally loaded experiments due to higher pressures. This was supported by the fact the greater changes in resting pennation and muscle thickness were measured when unidirectional loading was applied (Chapter 2; Ryan *et al.*, 2019) compared to multidirectional loading. Although we had greater deformations of the muscle architecture due to higher pressure, it should not affect force reduction. Force reduction in the muscles line-of-action was shown to be independent of local transverse pressure and dependent on local transverse force (Siebert *et al.*, 2016). Furthermore, the load applied by the sling would not solely be on the medial gastrocnemius but shared between the medial and lateral gastrocnemius and the rest of the lower leg. As such the 10 kg load of the unidirectional block loading is not fully comparable to the 10 kg load of the multidirectional sling loading. Use of a higher load or a redesign of the multidirectional loading could show increased effect of transverse loading.

The absence of higher levels of loading was one of the limitations in this study. The loads were chosen according to loads used in previous studies, however, the differences in the experimental design could have altered the load needed to show significant effects of loading on the muscle. A reason to not include more loaded trials was due to the electrical stimulation of the participants. In regard to ethics it was chosen to keep the trials to a minimum because of the discomfort of the electrical stimulation experienced by the participants.

Another limitation was that participants could only be measured in a seated position when using the current experimental design. Ideally, we would have taken measurements of participants standing as well as seated. However, within the current design ankle rotation was prevented by locking the legs in place by placing a fixed bar on top of the knees. If participants stood there would be no such method within the current design to prevent ankle rotation. A change in design to allow measurements of varying muscle lengths would be interesting for future studies.

The reliability of the ultrasound remains an issue. This is not specific to this study but rather to ultrasound measurements in general as changes in the positioning of the ultrasound probe can lead to errors (Bolsterlee *et al.*, 2016). Our analysis of the baseline variability from consecutive twitches would suggest that the changes in muscle architecture that were measured are reliable within a threshold of one standard deviation. However, the reliability of the fascicle length remains an issue. The fascicles seem to shorten during contraction and upon relaxation of the muscle the fascicles lengthen beyond the resting length they had before contraction. This would not make sense when measuring from one twitch to the next as the fascicles would have to shorten more during the following twitch to compensate for the longer fascicles. The added shortening is not shown in the results. The measured resting state variation for the fascicle lengths and the change in length between fascicle lengths before muscle activation and after activation are both approximately 4 mm. This would suggest an upwards drift in fascicle length between consecutive twitches. This seems unlikely as fascicle length would be approximately 8 mm longer for the third measured twitch compared to the first measured twitch. A possibility is that the shorting of the fascicles back to resting length happened in the period beyond the analysed section of data of one twitch and the start of the data from the following twitch. As the baseline variability is approximately 4 mm between consecutive twitches it is possible that fascicle length returned to its original resting length in the time between twitches that was not analysed.

The electrical stimulus was applied to the tibial nerve to elicit muscle twitches. Stimulating the tibial nerve affects the medial and lateral gastrocnemius as well as the soleus. Due to the 90° angle of the knee the force of the medial gastrocnemius is reduced in comparison to having the knee fully extended (Cresswell *et al*., 1995). It is possible that the majority of the force measured is produced by the soleus. The external transverse load was mainly applied to the medial and lateral gastrocnemius. Therefore, it could be possible that any force reductions caused to the medial and lateral gastrocnemius are too small to measure in comparison to the force produced by the soleus.

3.4.7. Conclusion

In conclusion, previous studies showed that external transverse loading of the medial gastrocnemius reduced muscle force. However, using an alternative design for the measurements we observed no reduction in force. This is likely due to a shorter muscle length and higher pennation angles as a result of participants being seated with their knee flexed 90°.

Fascicle curvatures were measured, and results indicate that external transverse loading resulted in lower fascicle curvatures in passively loaded muscle. For transversely loaded muscle the curvature seemed to increase with muscle activation, but no statistical difference was found.

Chapter 4.

External transverse loading of muscle using the finite element method

4.1. Introduction

External transverse loading has been studied in rats (Siebert *et al.*, 2014a), bullfrogs (Sleboda and Roberts, 2019), rabbits (de Brito Fontana *et al.*, 2018), and humans (Chapter 2; Chapter 3; Siebert *et al.*, 2018; Ryan *et al.*, 2019; Stutzig *et al.*, 2019). These studies showed that external transverse loading caused a decrease in muscle force. External transverse loading also caused a change in internal muscle architecture (Chapters 2-3; Ryan *et al.*, 2019).(Chapter 2; Ryan *et al.*, 2019). One model has studied the mechanism of force reduction by modelling the muscle with a gearing ratio between the muscle force, transverse load, lifting height of the load, and the longitudinal shortening of the muscle (Siebert *et al.*, 2018). Another study used a muscle model to link the properties of the helical arranged extracellular matrix to the reductions in force (Sleboda and Roberts, 2019). The mechanisms involved in force reduction as a result of external transverse loading have not been studied in regard to muscle architecture. In this study we aim to investigate these mechanisms using three-dimensional finite element modelling of muscle.

To study the mechanisms of force reduction a framework is needed that accounts for the contractile forces in the line-of-action of a muscle, applies transverse loads to a muscle, accounts for the transverse deformations caused by external loading, and related the transverse to the line-of-action forces and deformations.

Physical modelling of muscle was done using water filled silicone tubes, representing muscle, helically wrapped with thread, representing the extracellular matrix (Sleboda and Roberts, 2019). The helical angle of the thread was used as a representation of the length of a muscle. They showed that compression of the tubes caused a change in force, and that the change in force was dependent on the helical angle of the thread. Computational models have also been used to study transverse loading of muscle (Siebert *et al.*, 2018). The Hill-type muscle model was adapted to

include a geometric lever mechanism to model external transverse loading on muscle in a two-dimensional model and was able to replicate results from previous experiments in rats (Siebert *et al.*, 2014a). Though these models were able to show force reduction due to transverse loading they did not consider the internal muscle architecture. Previous research has shown that muscle architecture is an important factor in the development of muscle force, and changes in muscle thickness, pennation angle, and fascicle thickness are decreased as a result of transverse loading. Therefore, internal muscle architecture could be part of the mechanisms involved in force reduction.

The Hill-type muscle model is often used in research to calculate line-of-action force (Sandercock and Heckman, 1997; Wakeling *et al.*, 2012; Lee *et al.*, 2013; Dick *et al.*, 2017). It is a one-dimensional model that takes into account force-length properties (Ramsey and Street, 1940), force-velocity properties (Hill, 1938; Katz, 1939), activation (Zajac, 1989; Lichtwark and Wilson, 2005), and pennation angle (Zajac, 1989; Li *et al.*, 2009; Gerus *et al.*, 2015) and is used to predict muscle force varying over time. Being one-dimensional Hill-type muscle models are unable to represent muscle shape changes and distributions of force and energy in the transverse directions of the muscle. Also missing from the Hill-type muscle model is that it is not able to take into account the environment of the muscle: muscle is surrounded by bone, organs, and other muscles which can lead to transverse loading of the muscle which in turn affects muscle force (Chapter 2; Chapter 3; Siebert *et al.*, 2014a; de Brito Fontana *et al.*, 2018; Ryan *et al.*, 2019; Sleboda and Roberts, 2019; Stutzig *et al.*, 2019). Non-contractile components are not taken into account in the Hill-type model either, other than the series and parallel elastic components. For example, the extracellular matrix, blood vessels, and nerves are part of the muscle but are not considered to affect muscle contraction.

Three-dimensional finite element models have been used for various studies to do calculations on muscle mechanics, where the models account for transverse tissue deformations, and link these 3D deformations to forces in the Hill-type contractile elements. Studies have been done to determine heart deformations (Nielsen *et al.*, 1991) and moment arms in hip muscle (Blemker and Delp, 2005). More recently calculations were performed to study force enhancement and force depression in skeletal muscle which is caused by lengthening and shortening, respectively, of the muscle before contraction (Seydewitz *et al.*, 2019). An often used method to model muscle in finite element models is through the use of strain energy equations (Gielen *et*

al., 2000; Johansson *et al.*, 2000; Jenkyn *et al.*, 2002; Yucesoy *et al.*, 2002; Teran *et al.*, 2003; Blemker and Delp, 2005; Rahemi *et al.*, 2015). These models are able to calculate line-of-action forces, three-dimensional deformation of the muscle, and energy distributions. The properties of the non-contractile elements of the muscle were included in to previous models (Yucesoy *et al.*, 2002; Rahemi *et al.*, 2015). The inclusion of the non-contractile properties and the ability to apply external transverse loads made us adapt the model by Rahemi *et al.* (2015) for our transverse loading study.

The goal of the current project is to study the mechanisms of muscle force reduction as a result of external transverse loading by using a finite element model of muscle. The model allows us to independently vary loading direction, initial pennation angle, and initial muscle length which would not be possible in physical experiments. The model also gives the strain energy potentials which can add to the understanding of force reduction due to transverse loading. Furthermore, we aim to replicate previous experimental findings on the effects of transverse loading on the human calf muscle that were performed in chapter 2 and by Ryan *et al.* (2019) and Stutzig *et al.* (2019) and experiments relating to chapter 3 of this thesis.

4.2. Methods

The model used to simulate the muscle external loading experiments is a quasi-static three-dimensional finite element model based on the mechanics of fibre-reinforced, non-linearly-elastic transversely isotropic composite biomaterial. The basis for the model was obtained from the Deal.II finite element library (Bangerth *et al.*, 2007; Arndt *et al.*, 2017). This is an open source software library built for the C++ coding language. Tutorial *step-44* is a non-linear mechanics problem using the three-field formulation to solve a model for near incompressible and compressible materials (Pelteret and McBride, 2012).

We calculate the stationary points (either maximum or minimum) of the strain energy potential, where the total strain energy potential is the sum of the internal and external potential energies U_{int} and U_{ext}, respectively:

$$U(u, \tilde{J}, \tilde{p}) = U_{int} + U_{ext}. \tag{4-2}$$

Here u is the displacement, $\tilde{J}$ is the dilation, and $\tilde{p}$ is the internal pressure. The left Cauchy-Green tensor is given by $\bar{b} = FF^T$, where F is the deformation gradient. v and a are the volume and boundary area, respectively. The systems domain and boundary are given by Ω and $\partial\Omega$, respectively, and f_b is the boundary force and f_t is the traction force. In the computational experiments Ω will be represented by cuboid geometries with different pennation angles and different strains (Figure 4-1). We will compute equation 4-2 on these reference geometries.

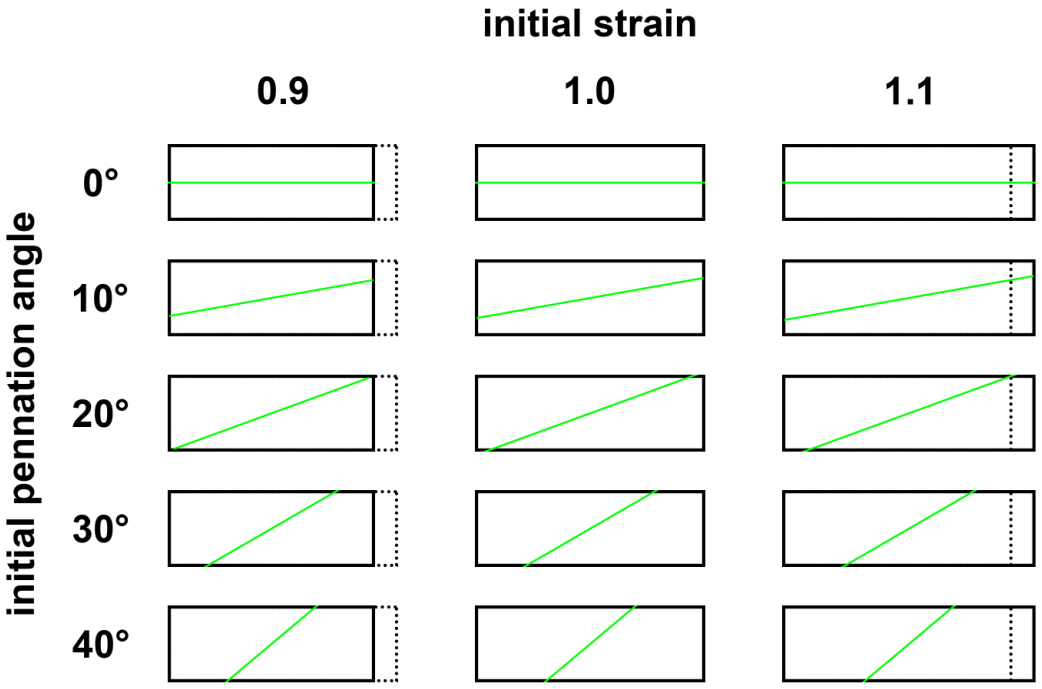

Figure 4-1 Schematic of the cubes on which the model will be computed. The cubes vary in initial pennation angle and initial strain.

Separated into parts, the internal strain energy potential is given by

$$U_{int} = \int_{\Omega} \psi_{\text{vol}}(\tilde{J}) + \tilde{p}(J(u) - \tilde{J})dv + \psi_{\text{iso}}\big(\bar{b}(u)\big)dv, \tag{4-3}$$

and the external strain energy potential is given by

$$U_{ext} = -\int_{\Omega} f_b \cdot u dv - \int_{\partial\Omega} f_t \cdot u da. \tag{4-4}$$

The volumetric ($\psi_{\mathrm{vol}}(\tilde{J})$, Equation 4-6) and isochoric ($\psi_{\mathrm{iso}}(\bar{b})$, Equation 4-7) strain energy densities, also shown in equation 4-2, make up the total internal strain energy density:

$$\psi = \psi_{\mathrm{vol}}(\tilde{J}) + \psi_{\mathrm{iso}}(\bar{b}), \tag{4-5}$$

where the volumetric strain energy density is dependent on the dilation ($\tilde{J}$) and the bulk modulus (κ). In this model we use the form

$$\psi_{\mathrm{vol}}(\tilde{J}) = \frac{\kappa}{4}(\tilde{J}^2 - 1 - 2\log(\tilde{J})). \tag{4-6}$$

The isochoric strain energy density is dependent on the left Cauchy-Green tensor ($\bar{b}$). It is in turn dependent on the strain energy densities of the muscle (ψ_{muscle}) and the base material (ψ_{base}):

$$\psi_{iso} = \psi_{muscle} + \psi_{base}. \tag{4-7}$$

The base material strain energy density is calculated using the Yeoh model (Yeoh, 1993):

$$\psi_{base} = \sum_{i=1}^{3} c_i (I_1 - 3)^i, c_1 = 0.199\ \mathrm{Pa}, c_2 = 0.366\ \mathrm{Pa}, c_3 = 0.0\ \mathrm{Pa}. \tag{4-8}$$

The muscle strain energy density is calculated from the muscle fibre stress ($\sigma_{muscle}(\lambda)$) and the along fibre stretch (λ):

$$\lambda \frac{\delta \psi_{muscle}(\lambda)}{\delta \lambda} = \sigma_{muscle}(\lambda). \tag{4-9}$$

In turn the muscle fibre stress is determined by the maximum isometric stress (σ_0), the active fibre stress ($\hat{\sigma}_{active}(\lambda)$) and the passive fibre stress ($\hat{\sigma}_{passive}(\lambda)$):

$$\sigma_{muscle}(\lambda) = \sigma_0(\hat{\sigma}_{active}(\lambda) + \hat{\sigma}_{passive}(\lambda)), \tag{4-10}$$

where the active fibre stress is defined as

$$\hat{\sigma}_{active}(\lambda) = \begin{cases} 0.0, & \lambda < 0.4, \\ 0.64\sin(1.29\lambda + 0.63) \\ +0.33\sin(5.31\lambda - 4.52) \\ +0.33\sin(6.74\lambda + 1.69) \\ +0.02\sin(19.82\lambda - 7.39) \\ +0.14\sin(8.04\lambda + 2.54) \\ +0.002\sin(32.24\lambda - 6.45) \\ +0.01\sin(22.12\lambda - 2.64), & 0.4 \leq \lambda \leq 1.75, \\ 0.0, & 1.75 < \lambda, \end{cases} \tag{4-11}$$

and the passive fibre stress is given by

$$\hat{\sigma}_{passive}(\lambda) = \begin{cases} 0.0, & 0 \leq \lambda < 1, \\ 2.35(\lambda - 1)^2 + 0.0(\lambda - 1) + 0.0, & 1 < \lambda \leq 1.25, \\ 3.44(\lambda - 1.25)^2 + 1.18(\lambda - 1.25) + 0.15, & 1.25 < \lambda \leq 1.5, \\ 0.43(\lambda - 1.5)^2 + 2.90(\lambda - 1.5) + 0.66, & 1.5 < \lambda \leq 1.65, \\ 3.02(\lambda - 1.65) + 1.1, & 1.65 < \lambda. \end{cases} \tag{4-12}$$

The information and equations above are adapted from Pelteret and McBride (2012) and Rahemi (2015)

To calculate the stationary points of the strain energy potential the following steps are taken. Integrating equation 4-2 for the three variables displacement, dilation, and pressure $(u, \tilde{J}, \tilde{p})$ gives us the three-field formulation (Equations 4-13, 4-14, 4-15) including the boundary conditions (Equations 4-16, 4-17).

$$\frac{\partial U}{\partial u} = 0 \Rightarrow -div\sigma(\nabla u) - f_b = 0, \tag{4-13}$$

holds inside of Ω.

$$\frac{\partial U}{\partial p} = 0 \Rightarrow J(u) - \tilde{J} = 0, \tag{4-14}$$

holds inside of Ω.

$$\frac{\partial U}{\partial \tilde{J}} = 0 \Rightarrow \tilde{p} - \frac{d\psi_{vol}}{d\tilde{J}} = 0, \tag{4-15}$$

holds inside of Ω.

$$u = 0, \tag{4-16}$$

holds on parts of the boundary.

$$\sigma(\nabla u)\mathrm{n} = f_t, \tag{4-17}$$

holds on the remainder of the boundary.

Equation 4-17 can be used to describe traction on the geometry and we can change f_t to apply external loading to the geometry.

We multiply by equations 4-13, 4-14, and 4-15 by a vector field w and scalar fields H and q, respectively, and integrate the results over Ω, which gives us the weak formulations (Equations 4-18, 4-19, 4-20).

$$\int_\Omega \sigma(\nabla u) : (\nabla w) = \int_\Omega f_b \cdot w + \int_{\partial\Omega} f_t \cdot w, \tag{4-18}$$

$$\int_\Omega (J(u) - \tilde{J})H = 0, \tag{4-19}$$

$$\int_\Omega \left(\tilde{p} - \frac{dE_{vol}}{d\tilde{J}}\right) q = 0. \tag{4-20}$$

The weak formulations are combined which results in equation 4-21.

$$A(\eta, \xi) - \int_\Omega f_b \cdot w - \int_{\partial\Omega} f_t \cdot w = 0, \tag{4-21}$$

where $\eta = [u, \tilde{J}, \tilde{p}]$ and $\xi = [w, H, q]$.

Following this we rename equation 4-21 to $[\mathcal{R}(\eta), \xi]$ (Equation 4-22), which give us our nonlinear equation.

$$[\mathcal{R}(\eta), \xi] \equiv A(\eta, \xi) - \int_\Omega f_b \cdot w - \int_{\partial\Omega} f_t \cdot w = 0. \tag{4-22}$$

To solve the nonlinear equation we suppose that $\hat{\eta}$ solved the equation, and we suppose the η is close to $\hat{\eta}$. This way we can linearize $\mathcal{R}$ near $\hat{\eta}$ using Taylor's theorem (Equation 4-23).

$$\mathcal{R}(\eta) \approx \mathcal{R}(\hat{\eta}) + \left(\tilde{J}\mathcal{R}(\hat{\eta})\right)(\hat{\eta} - \eta). \tag{4-23}$$

What we want to find is where $[\mathcal{R}(\eta), \xi] = 0$, combined with our linear function gives equation 4-24.

$$[\mathcal{R}(\eta), \xi] \approx \left[\mathcal{R}(\hat{\eta}) + \left(\tilde{J}\mathcal{R}(\hat{\eta})\right)(\hat{\eta} - \eta), \xi\right] = 0. \tag{4-24}$$

To solve this linear equation an equation of matrices is produced (equation 4-25).

$$\begin{bmatrix} A_{\hat{u}} & B_1^* & 0 \\ B_1 & 0 & B_2^* \\ 0 & B_2 & -C_{\hat{J}} \end{bmatrix} \begin{bmatrix} u \\ \tilde{p} \\ \tilde{J} \end{bmatrix} = \begin{bmatrix} F_{\hat{u}} \\ F_{\hat{p}} \\ F_{\hat{J}} \end{bmatrix}. \tag{4-25}$$

Solving equation 4-25 solves for the difference $(\hat{\eta} - \eta)$, after which η can be obtained by taking $\eta = \hat{\eta} + (\hat{\eta} - \eta)$. Each time the linear solver is run, η is updated until η reaches the maximum allowed iterations, or the solution falls within the prescribed tolerances.

The near incompressibility of the model makes it a good basis to convert it for use as a muscle model. Initial adaptations to the *step-44* model were incorporated into the model by Rahemi (2015) and Rahemi *et al.* (2015). They were able to add several characteristics relating to muscle mechanics to the model. Active and passive muscle fibre properties were included using the active and passive force-length relationships. Added to the model were also base material properties. These base material properties represent the elastic properties of non-fibre tissues that are present in the muscle, such as connective tissues, blood vessels, and nerves.

Adaptations to the model were made to update the active (Figure 4-2) and passive (Figure 4-2) force-length relationships (Equations 4-11, 4-12) by fitting polynomials to data from rabbit muscle (Winters *et al.*, 2011). The Yeoh model (Yeoh, 1993) for the base material properties was updated using across-fibre loaded data (Mohammadkhah *et al.*, 2016). Across-fibre loaded data was used to eliminate any fibre properties which only act in the along fibre direction (Wakeling *et al.*, 2020). Another novel addition to the model was to add the external transverse loads to the boundary conditions of the muscle model. Finally, post processing routines were written to extract force and energy data from the computation of the model.

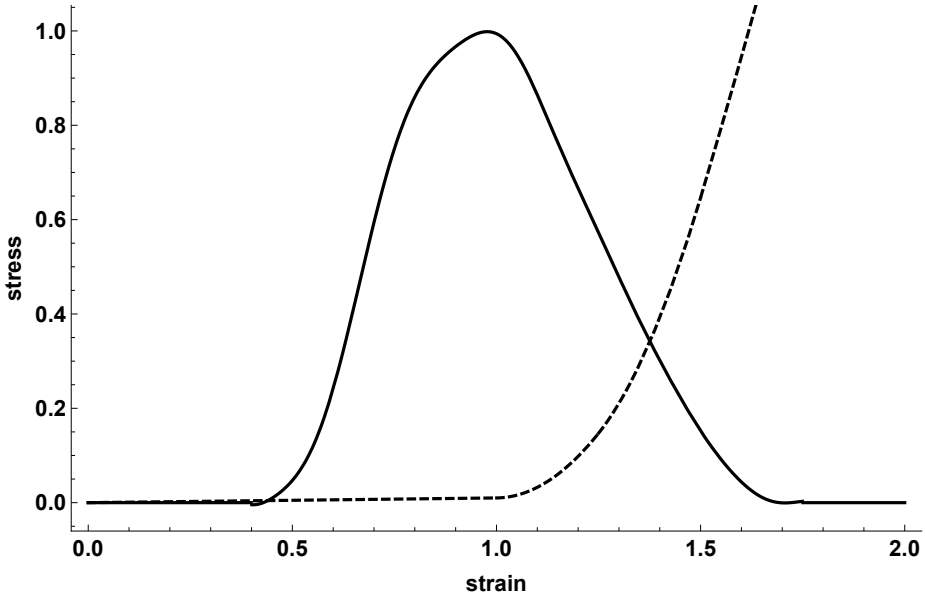

Figure 4-2 Force-length relationship of the muscle fibres as they are used in the finite element model. Shown are the active force-length properties (solid) and the passive force-length properties (dashed).

Compression experiments were performed on blocks of muscle (30 x 10 x 10 mm). All muscles were activated to 100% in steps of 10%. Results were obtained from 240 in silica experiments made up of combinations of four variables. Transverse loads were applied to the muscle using four configurations, loading from the top, from the sides, and from both the top and sides simultaneously. Muscles without loading applied were also run. Intensity levels for the load included 0, 5, 15, and 30 kPa. This series of loads was chosen to match the computational experiments with previous experiments (Chapter 2; Ryan *et al.*, 2019; Stutzig *et al.*, 2019; Chapter 3). To determine the effects of muscle lengths the muscle blocks were either kept at resting length or either shortened or lengthened to strains of 0.9 or 1.10, respectively. Muscles of five different pennations were used with pennation varying from 0° to 40° in 10° increments.

Concrete steps that we take to achieve our solution are the creation of the mesh, setting up the boundary conditions, the setup of the quadrature points, and running the solvers (Pelteret and McBride, 2012). We create the mesh in such a way that the centre of the mesh lies at the origin (0, 0, 0). We determine along each axis what we want the dimensions to be, and by refining our mesh we set the number of cells that the mesh will contain. On the generated mesh we set up the boundaries of our system by assigning boundary IDs to the outer faces of the outer cells. Each boundary ID will determine the boundary condition that will be applied using either traction free, Dirichlet or Neumann

boundary conditions. Boundaries that are left traction free will be able to move in any direction. The boundaries with Dirichlet conditions will be fixed in either the x, y, or z dimensions, or a combination of the three. The Neumann condition are boundaries on which a traction is applied. In our case we use two types boundaries, over several faces, with Neumann conditions, one which we use to set the length of the muscle, and one which is used to apply the compression. Specific conditions for each stage of the model are shown in figure 4-3. Initially the geometry is set up with the -x face fixed in all axes, the -z face fixed in the z axis, and the +x face has traction applied (Figure 4-3A). For top compression, during the compression step the -x face is fixed in the x axis, the -z face is fixed in all axis, and the +z face has compression applied (Figure 4-3B). During activation the -x and +x faces are fixed in the x axis, the -z face is fixed in all axes, and the +z has compression applied (Figure 4-3E). For side compression, during the compression step the -x face is fixed in the x axis, the -z face is fixed in all axes, and the -y and +y faces have compression applied (Figure 4-3C). During activation the -x and + x faces are fixed in the x axis, the -z face is fixed in all axes, and the -y and +y faces have compression applied (Figure 4-3F). For all compression, during the compression step the -x face is fixed in the x axis, the -z is fixed in all axes, and the -y, +y, and +z faces have compression applied (Figure 4-3D). During activation the -x and +x faces are fixed in the x axis, the -z face is fixed in all axes, and the -y, +y, +z faces have compression applied (Figure 4-3G).

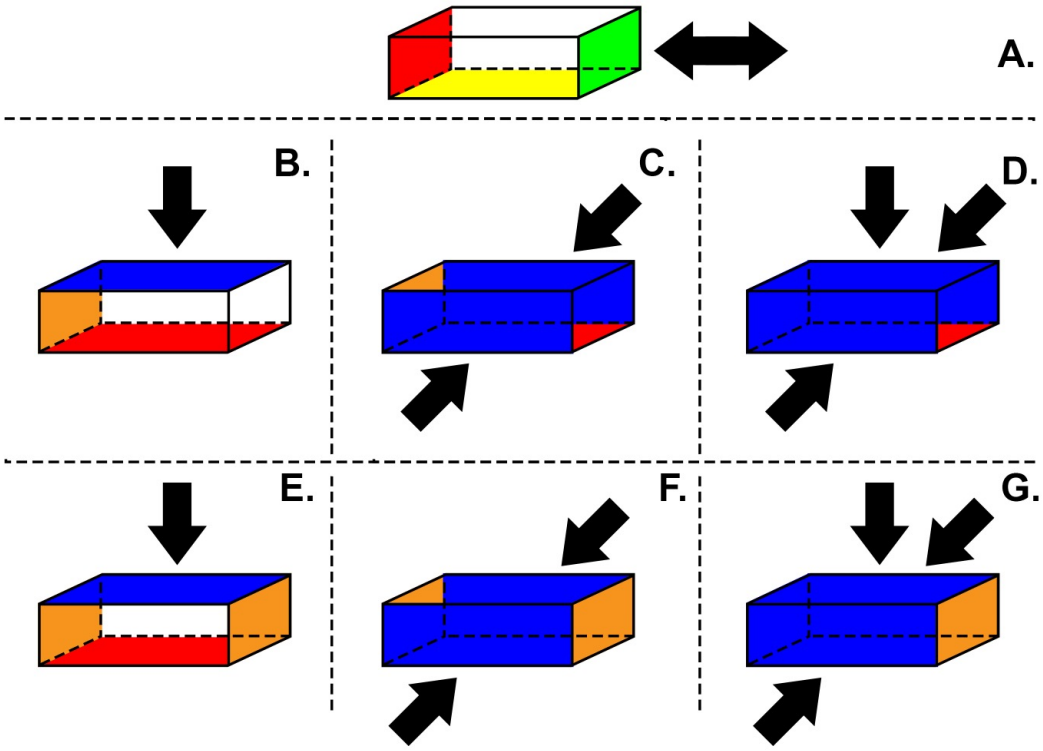

Figure 4-3 **Initially the model is set to lengthen or shorten the muscle (A). Following is the compression of the muscle with top (B), side (C), and all (D) compression. Last is the activation of the muscle with top (E), side (F), and all (G) compression. The figure shows compressed faces (blue), faces fixed in the x axis (orange), faces fixed in all axes (red), faces fixed in the z axis (yellow), and faces with traction applied (green).**

The following step is to set up the quadrature points. These are the points within each cell at which the functions are computed for our computational experiments. The model will then use the nonlinear Newton method to determine the solution at each timestep. For each Newton iteration we go through a series of steps. To start we assemble the system's right-hand side matrix. Following this the errors are determined, and the errors determine if the iteration has converged. If the step has not converged assembling the system's tangent matrix takes place. The next step is to make the boundary constraints that we have set previously. Static condensation is performed to reduce the system to a displacement-only system. The displacement is solved for using the resulting system. Having the displacement allows for post processing to obtain the dilation and the pressure. With the displacement, dilatation, and pressure calculated the data for each quadrature point are updated. After this the next Newton iteration takes place, which continues to happen until the system converges or criteria for stopping the

solver are met. The process is repeated for each timestep and at each timestep we extract the data that we use to analyse the loading and contraction of the muscle model. The data that are extracted are the stresses throughout the computational experiments, the forces on each of the faces, the active and passive fibre energies and base material energy, the fibre orientations at each quadrature point, the displacement of each quadrature point, the internal pressure within the muscle, and the volume of the muscle.

To adjust for the use of many different variations while running the computational experiments all results are given in main effects plots using the least square means. The least square mean gives the mean estimated from a linear model and adjusts for covariates (Oehlert, 2010). Covariates used were the loading direction, initial muscle length, and initial pennation angle. Main effects plots were calculated using JMP 14 (SAS Institute Inc., Cary, NC, 1989-2019). For the main effects plots higher least square means relate to higher mean muscle forces. The greater the slope of the graphs shown in the main effects plots indicate a greater reduction in muscle force.

To compare the results obtained from the computational experiments with previous research we highlight several individual computational experiments (Table 4-1, 4-2, 4-3, 4-4). To compare to experiments performed in chapter 3 we look at computational experiments with a 20° initial pennation angle and an initial muscle length of 0.9. Computational experiments with an initial pennation angle of 10° and an initial length of 1.1 were used to compare with experiments run in chapter 2 and by Ryan *et al.* (2019) and Stutzig *et al.* (2019). For top loading and all direction loading a compression of 15 and 5 kPa were chosen, respectively. This was done because the chosen load was applied to all chosen surfaces, which means that for loading from all directions each of the three surfaces had 5 kPa applied. The top loaded computational experiments had 15 kPa applied to a single surface. Therefore, a comparison between 5 and 15 kPa for the all direction loading and top loading, respectively, gives a more accurate comparison between computational experiments.

4.3. Results

The mean unloaded force was calculated as 1.2 N, 10.8 N, 18.5 N, for 0%, 50%, and 100% activation respectively, along the line of action (x-axis) of the muscle taking into account all variations (direction, initial pennation, initial length). The percentages in

force reduction are the force reduction relative to the mean unloaded force for each level of activation. The computational experiments showed that external loading lead to a lower mean muscle force compared to unloaded muscle (Figure 4-4). At 0% activation the data showed force reductions of 0.06 (4.8%), 0.18 (14.6%), 0.33 (27.8%) N for the 5, 15, and 30 kPa loads, respectively. At 50% activation the data showed force reductions of 0.06 (0.5%), 0.19 (1.8%), 0.41 (3.8%) N for the 5, 15, and 30 kPa loads, respectively. At 100% activation the data showed force reductions of 0.06 (0.3%), 0.21 (1.1%), 0.45 (2.5%) N for the 5, 15, and 30 kPa loads respectively. In the 0% activation (Figure 4-3a4a) the least squares means show negative forces which corresponds to the lengthening of the muscle due to transverse loading. At the 50% (Figure 4-3b4b) and 100% (Figure 4-3c4c) activation the least squares means are positive in value indicating forces in the shortening direction of the muscle.

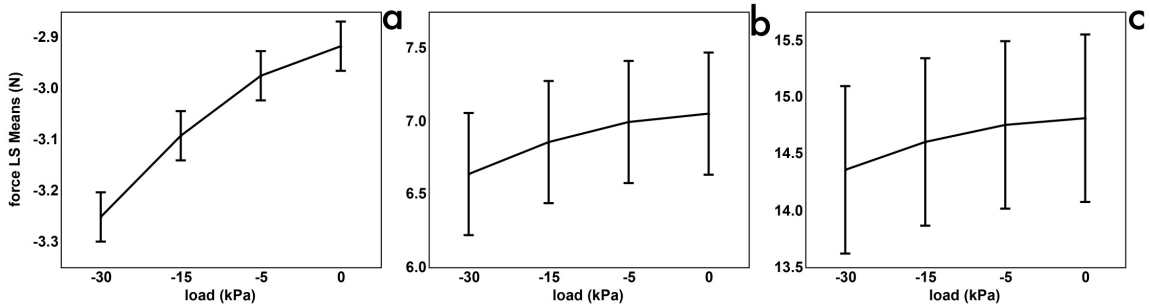

Figure 4-4 Least Square Means of the force by external loading. For the four external transverse loads it is shown that higher external loads result in lower force along the line of action (x axis) of the muscle block. These forces are calculated from a combination of all conditions. Forces were taken on the positive x face in the x direction at 0% (a), 50% (b), and 100% (c) activation. The error bars represent the standard error of the least square means force.

External transverse loading was applied using four different configurations, from the top, the sides, from all directions, and with no external loading applied (see Figure 4-3). The lowest mean muscle force was found for external loading from all directions when compared to no external loading (Figure 4-5). Loading from the top and side also showed lower mean maximum muscle force compared to no loading but higher force than loading from all directions. As before the percentages in force reduction are the force reduction relative to the mean unloaded force at each activation level. Force reductions at 0% activation were calculated at 0.27 (22.8%), 0.10 (8.6%), and 0.19

(15.9%) N for loading from all directions, from the sides, and from the top, respectively. At 50% activation they were calculated at 0.33 (3.1%), 0.18 (1.7%), and 0.15 (1.4%) N for loading from all directions, from the sides, and from the top, respectively. At 100% activation they were calculated at 0.36 (2.0%), 0.20 (1.1%), and 0.16 (0.9%) N for loading from all directions, from the sides, and from the top respectively.

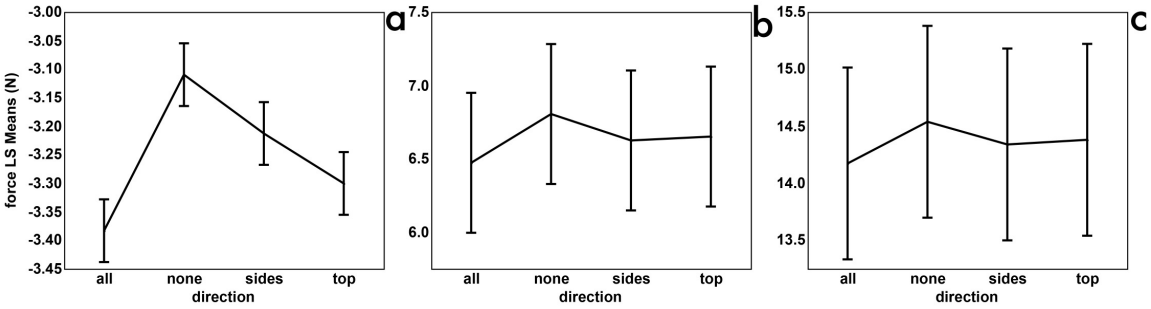

Figure 4-5 The Least Square Means of the force for the computational experiments by direction of loading. Data were taken for 0% (a), 50% (b), and 100% (c) activation. External transverse loading from any direction led to lower force compared with no external load. Force reduction is greatest for compression from all directions. The error bars represent the standard error of the least square means force.

For the comparison of the experiments with different initial pennation angles we show that experiments with lower initial pennation angles have higher mean muscle forces, except for the 10° and 20° when activation is 0% and the 10° at the other activation levels. A greater initial pennation angle leads to less reduction in mean muscle force for increases with external load (Figure 4-6). The greatest reductions in mean force were found for computational experiments with pennation angles for 0° and 10° and an initial pennation angle of 40° showed a reduction at 0% activation but an increase in force at activations of 50% and 100%. As before the percentages in force reduction are the force reduction relative to the mean unloaded force at each activation level. The reductions in force at maximum load and 0% activation were approximately 0.36 (29.8%), 0.35 (29.0%), 0.33 (27.8%), 0.33 (27.5%) N, and 0.30 (25.2%) N for pennations of 0°, 10°, 20°, 30°, and 40° respectively. The reductions at maximum load and 50% activation were 0.65 (6.0%), 0.62 (5.8%), 0.52 (4.8%), and 0.32 (3.0%) N for 0°, 10°, 20°, 30°, and 40° respectively. At 40° pennation force increased by 0.05 (0.5%) N. Reductions for maximum load at 100% activation were 0.86 (4.6%), 0.81 (4.4%), 0.63

(3.4%), and 0.29 (1.5%) N for 0°, 10°, 20°, 30°, and 40° respectively, and at 40° force increased by 0.31 (1.7%) N.

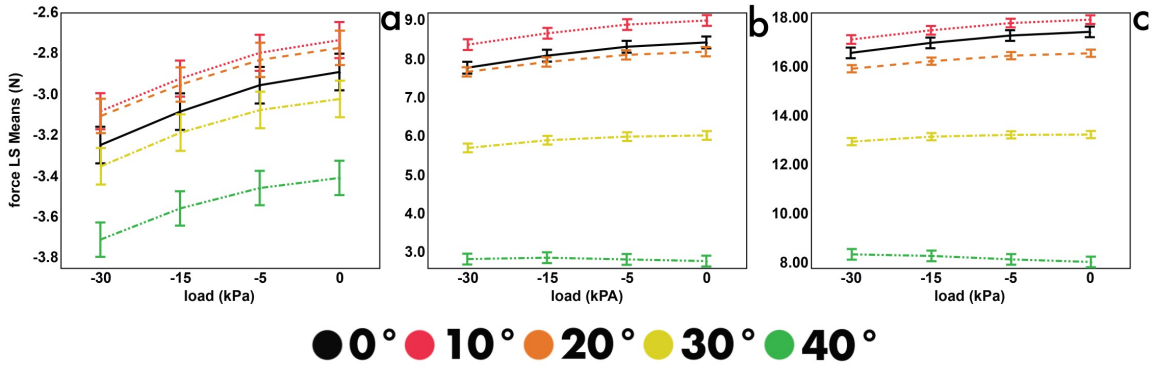

Figure 4-6 **The Least Square Means of the muscle force for the experiments by amount of load separated for five different initial pennation angles at 0% (a), 50% (b), and 100% (c) activation. The greatest reduction in least squares mean force is shown for computational experiments with pennation angles of 0° and 10°. Higher pennations lead to less reduction in least squares mean force as well as lower least squares mean forces for each amount of external loading. The error bars represent the standard error of the least square means force.**

Comparing the least square means of the force for the three initial muscle lengths we show that at 0% activation shorter muscle showed higher force reductions. At 50% activation shorter muscle showed the least amount of force reduction with the greatest reduction seen at a strain of 1.0. For 100% activation it showed that the higher the initial length the greater the reduction in force (Figure 4-7). As before the percentages in force reduction are the force reduction relative to the mean unloaded force at each activation level. For the maximum loaded conditions at 0% activation the computational experiments showed a reduction in muscle force of approximately 0.46 (38.5%), 0.32 (26.8%), and 0.22 (18.2%) N for the initial lengths of 0.9, 1.0, and 1.1 respectively. At 50% activation they showed a reduction of approximately 0.26 (2.4%), 0.50 (4.7%), and 0.48 (4.5%) N respectively. At 100% activation they showed a reduction of approximately 0.17 (0.9%), 0.59 (3.2%), and 0.61 (3.3%) N respectively. The maximum muscle force is shown to be higher for computational experiments with longer initial muscle lengths, except for the 1.0 strain at 100% activation.

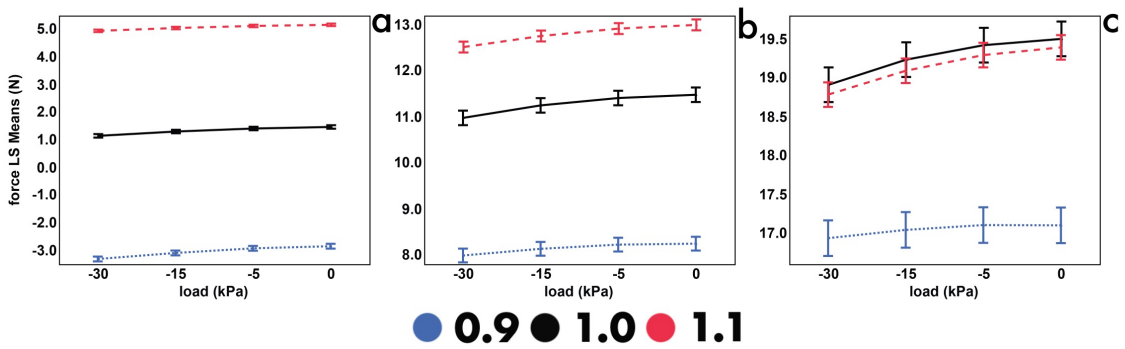

Figure 4-7 **The Least Square Means of the force for the computational experiments by load separated for initial muscle length at 0% (a), 50% (b), and 100% (c) activation. Force reduction is more pronounced with longer muscle lengths. The error bars represent the standard error of the least square means force.**

For the forces the example computational experiments show a reduction in force for computational experiments with transverse loading compared to those without transverse loading between the uncompressed and fully activated conditions (Table 4-2). Here top loading shows a greater reduction in force than loading from all directions. Also, the 10° pennation computational experiments showed a greater reduction in force than the 20° pennation computational experiments. For all example computational experiments transverse loading in passive muscle resulted in an increase in muscle length (Table 4-3). For the 20° pennation computational experiments the thickness is shown to decrease as a result of transverse loading and similarly thickness decreased due to activation. For the 10° pennation computational experiments the only change in thickness was a decrease in thickness as a result of transverse loading for the top loaded computational experiments (Table 4-3). A decrease in pennation was shown for all example computational experiments both as a result of transverse loading as well as activation (Table 4-4). Internal pressures are shown to be lower for computational experiments with transverse loading compared to those without transverse loading. Furthermore, the computational experiments with 10° pennation and a length of 1.1 showed higher internal pressures than the computational experiments with 20° pennation and 0.9 initial length (Table 4-4).

Table 4-1 **Details on the example computational experiments. Each computational experiment varies in initial pennation angle, initial muscle length, loading direction, and loading intensity.**

model examples	1	2	3	4	5	6
initial pennation angle (°)	20	20	20	10	10	10
initial muscle strain	0.9	0.9	0.9	1.1	1.1	1.1
loading direction	top	all	none	top	all	none
loading (kPa)	-15	-5	0	-15	-5	0

Table 4-2 **The forces calculated for the example computational experiments. Shown are the values at the unloaded, loaded, and maximum active state of each computational experiment. Given are the change in force between the unloaded and loaded state, as well as between the loaded and maximum active state and unloaded and maximum active state. The percentage force reduction between the unloaded and maximum active state is also given.**

	force (N)					
	1	2	3	4	5	6
unloaded	-4.52	-4.50	-4.49	3.98	3.99	4.00
loaded	-4.76	-4.62	-4.49	3.85	3.92	4.00
change	-0.24	-0.11	0.00	-0.13	-0.06	0.00
maximum active state	16.23	16.36	16.49	20.64	20.81	21.08
change loaded - act.	20.98	20.98	20.98	16.80	16.89	17.08
change unloaded - act.	20.74	20.86	20.98	16.67	16.82	17.08
% force reduction	1.12	0.56	0.00	2.42	1.50	0.00

Table 4-3 **The length, thickness, and width for the example computational experiments. Shown are the values at the unloaded, loaded, and maximum active state. Also shown are the change between the unloaded and loaded state, as well as between the loaded and maximum active state.**

	length (mm)					
	1	2	3	4	5	6
unloaded	24.79	24.79	24.81	35.68	35.69	35.71
loaded	25.31	25.10	24.81	36.17	35.99	35.71
change	0.52	0.31	0.00	0.49	0.31	0.00
maximum active state	25.29	25.07	24.74	35.28	35.11	34.89
change	-0.02	-0.02	-0.07	-0.89	-0.88	-0.82
	height (mm)					
	1	2	3	4	5	6
unloaded	11.08	11.06	11.06	9.14	9.12	9.12
loaded	10.67	11.02	11.06	8.81	9.10	9.12
change	-0.41	-0.05	0.00	-0.33	-0.02	0.00
maximum active state	10.18	10.45	10.48	8.78	9.06	9.08
change	-0.49	-0.57	-0.58	-0.03	-0.04	-0.04
	width (mm)					
	1	2	3	4	5	6
unloaded	11.07	11.08	11.07	9.11	9.11	9.11
loaded	11.45	11.05	11.07	9.47	9.11	9.11
change	0.38	-0.03	0.00	0.36	-0.01	0.00
maximum active state	11.67	11.36	11.39	9.38	9.03	9.03
change	0.22	0.30	0.32	-0.09	-0.07	-0.08

Table 4-4 The pennation, volume, and pressure for the example computational experiments. Shown are the values at the unloaded, loaded, and maximum active state. Also shown are the change between the unloaded and loaded state, as well as between the loaded and maximum active state.

	pennation (°)					
	1	2	3	4	5	6
unloaded	22.94	22.93	22.93	8.82	8.82	8.82
loaded	21.97	22.61	22.93	8.49	8.72	8.82
change	-0.97	-0.32	0.00	-0.33	-0.09	0.00
maximum active state	19.08	19.61	19.88	7.53	7.67	7.72
change	-2.89	-3.00	-3.05	-0.96	-1.05	-1.10
	volume (mm3)					
	1	2	3	4	5	6
unloaded	2960.21	2960.52	2960.72	3041.88	3042.19	3042.45
loaded	2941.08	2948.93	2960.72	3024.98	3031.85	3042.45
change	-19.13	-11.59	0.00	-16.90	-10.34	0.00
maximum active state	3076.54	3083.08	3094.46	3193.11	3200.95	3213.54
change	135.46	134.15	133.74	168.13	169.10	171.09
	pressure (kPa)					
	1	2	3	4	5	6
unloaded	-13.5	-13.4	-13.4	13.7	13.8	13.9
loaded	-20.2	-17.5	-13.4	8.2	10.4	13.9
change	-6.7	-4.0	0.0	-5.4	-3.3	0.0
maximum active state	24.2	26.3	29.8	58.6	60.7	64.2
change	44.5	43.8	43.1	50.4	50.3	50.3

The strain-energy potentials differ between the computational experiments (Figure 4-8). The volumetric strain-energy potentials showed a tendency to decrease as external load increased. This is best shown in computational experiments with lower initial pennation angles (0°, 10°, and 20°). The active strain-energy potentials showed an increase as initial pennation angle increased for muscles at an initial length of 0.9 and 1.0, whereas this was not shown at initial muscle lengths of 1.1. The base material strain-energy potentials showed an increase as initial pennation angle increased for all initial muscle lengths. The passive strain-energy potentials were greatest for computational experiments with an initial muscle length of 1.1 and at lower initial pennation angles.

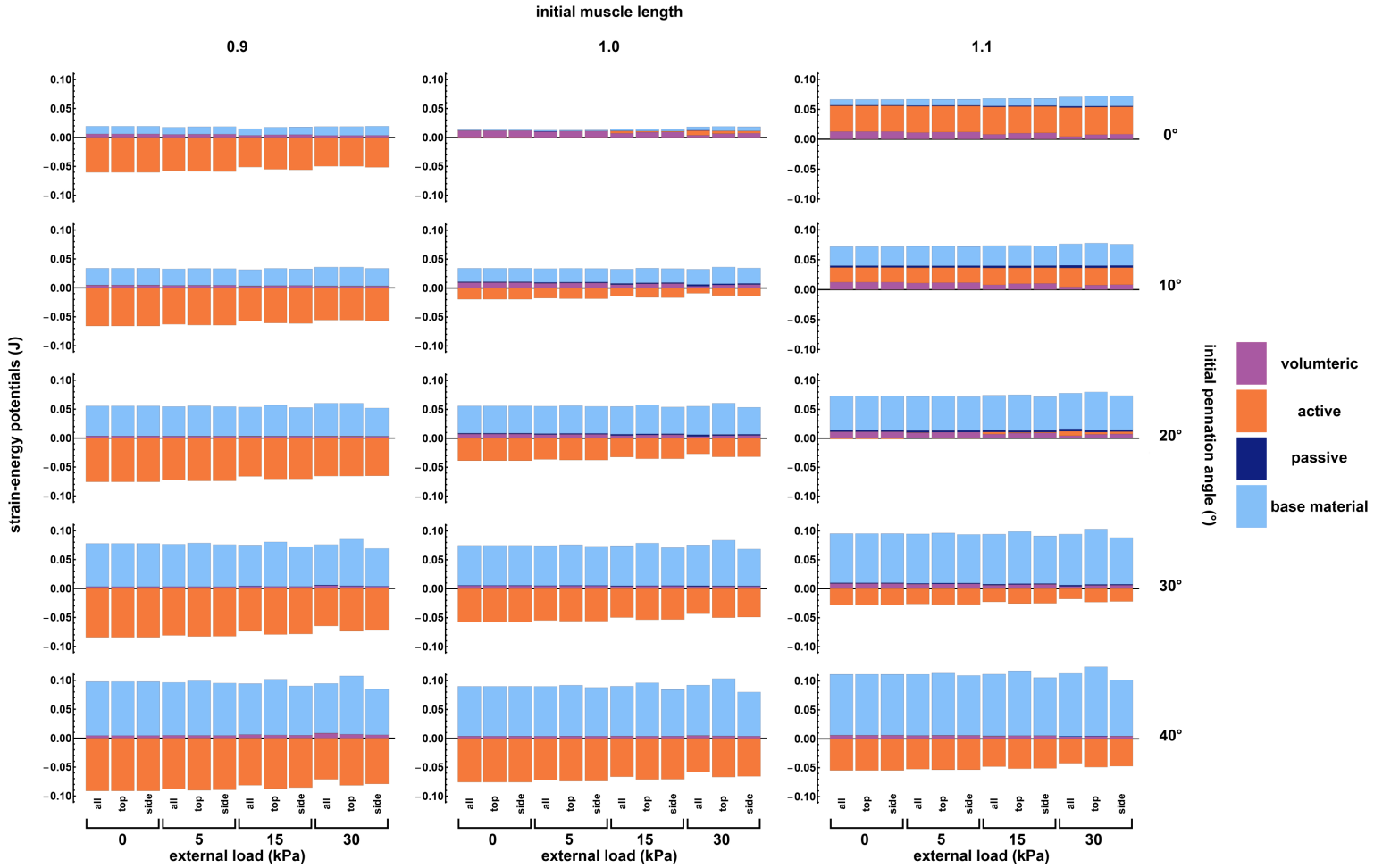

Figure 4-8 **Strain-energy potentials for the computational experiments at 100% activation. The computational experiments are separated by initial muscle length, initial pennation angle, external load, and loading direction. Shown are the volumetric (purple), active (orange), passive (dark blue), and base material (light blue) strain-energy potentials.**

4.4. Discussion

Muscle loading and maximum activation showed changes in muscle architecture and muscle force. The model showed that external loading caused a reduction in maximum muscle force. We showed that loading direction, initial pennation angle, and initial muscle length affect muscle force reduction.

4.4.1. Changes in muscle architecture

For computational experiments without compression the length and thickness decreased with activation and width increased. The decrease in thickness was also calculated in a model by Randhawa and Wakeling (2015) for the medial gastrocnemius. Further modelling of the medial gastrocnemius also showed decreases in muscle thickness (Rahemi *et al.*, 2014) as well as increases in width. In experimental work the muscle thickness was shown to remain constant with muscle activation (Narici *et al.*, 1996; Maganaris *et al.*, 1998). Recent work showed that muscle thickness decreased during walking and running (Hodson-Tole and Lai, 2019) indicating muscle decreased in thickness with increased activation in non-isometric conditions. Muscle loading resulted in an increase in muscle length when loaded from either the top, the sides, or all directions. The muscle thickness decreased when loaded from the top or all directions which was compensated by an increase in the width. The reverse was true for loading from the sides where thickness increased, and width decreased. Decreases in thickness as a result of loading where also found in physical experiments (Chapter 2; Ryan *et al.*, 2019). In these experiments muscle thickness increased with muscle activation after loading. Our example computational experiments showed that at 10° pennation there was a decrease in thickness only due to transverse loading in passive muscle and no change due to activation. In our 20° computational experiments we saw both thickness decreases because of transverse loading and activation. Many studies showed an increase in pennation angle with muscle activation for physical experiments (Narici *et al.*, 1996; Maganaris *et al.*, 1998; Randhawa and Wakeling, 2018) and models (Rahemi *et al.*, 2014; Randhawa and Wakeling, 2015). However, for our muscle blocks we found that pennation angle increased due to activation only for computational experiments with an initial pennation angle of 0° and 40°, pennation angle decreased for computational experiments with 10°, 20°, and 30° initial pennation angle. Rahemi *et al.* (2014) used a

similar model, however, with a different geometry. It is possible that the more accurate representation of the medial gastrocnemius as a parallelepiped had an effect on the pennation rotation.

4.4.2. Muscle force reduction

Previous studies showed that external transverse loading causes a reduction in muscle force. Siebert *et al.* (2014a) found a 13 % reduction in muscle force using a unidirectional load of 53 kPa (2.6 N) in rat models. A similar study was performed in humans (Chapter 2; Ryan *et al.*, 2019; Stutzig *et al.*, 2019) showing a 16 % decrease in muscle force with a maximum external transverse load of 29 kPa (98.1 N). A force reduction of 5 % was found using a 108.4 N multidirectional transverse load in humans (Siebert *et al.*, 2018). This is approximately a 1.8 kPa load assuming a calf girth of 40 cm (Nevill *et al.*, 2004) and equal width of the medial and lateral gastrocnemius. For our current study we chose a range of 5 (1.5 N), 15 (4.5 N), and 30 kPa (9.0 N) which was similar to that in chapter 2 and of Ryan *et al.* (2019) and Stutzig *et al.* (2019) in amount of pressure. For our highest load we found a force reduction of approximately 3.8% at 50% activation and 2.5% at 100% activation using the least square means of all variations of the computational experiments. Here the 50% is comparable to the human experiments that used twitch force (Chapter 2; Siebert *et al.*, 2018; Ryan *et al.*, 2019; Stutzig *et al.*, 2019), whereas the 100% is comparable to the rat experiments that used maximum muscle force (Siebert *et al.*, 2014a). This was lower than was found in the physical experiments done in chapter 2 and by Ryan *et al.* (2019) and Stutzig *et al.* (2019) and also underestimated the force reduction when compared to Siebert *et al.* (2014a). Force reduction was also underestimated when compared to Siebert *et al.* (2018) as our 5 kPa load gave a reduction of approximately 0.6 % compared to their 5 % at 1.8 kPa. Although the 1.8 kPa was a crude estimate of the load applied in those experiments.

In the previous section we include the force because the muscle force reduction was shown to be independent of local pressure (Siebert *et al.*, 2016). If this is the case, it becomes harder to compare all the experiments. A low force (2.6 N) applied to a small rat muscle (2.5 cm^2) (Siebert *et al.*, 2014a) resulted in a significant decrease in muscle force (13 %). Our model showed a decrease between 0.5 and 2.5 % at 50% and 100% activation for small forces (between 1.5 and 4.5 N) on a similar sized muscle (3 cm^2).

This suggests that our model underestimated the amount of force reduction causes by external transverse loading. For the experiments on human muscle the forces were much higher (98.1 and 108.4 N) and the muscles much larger. If indeed local force rather than local pressure determines muscle force reduction due to transverse loading then a comparison between the small muscle experiments and human muscle experiments should not be made.

Force reduction was shown to depend on local force rather than local pressure (Siebert *et al.*, 2016) and pressure differed between the unidirectional (Chapter 2) and multidirectional experiments (Chapter 3). However, using a larger surface area as was done with the multidirectional experiments did not only decrease the pressure but also off loaded a fraction of the force on areas other than the medial gastrocnemius. Therefore, not the full force would be loading the gastrocnemius and the force reduction would be expected to be lower.

4.4.3. Initial muscle length

The length of the medial gastrocnemius depends on the angle of both the ankle and the knee (Fukunaga *et al.*, 1996; Narici *et al.*, 1996; Herbert *et al.*, 2002). Muscle length played a role in force reduction as was shown in chapter 3. Experiments done in chapter 2 and by Ryan *et al.* (2019) and Stutzig *et al.* (2019) used longer initial muscle lengths because they had participants lying down with their knee fully extended. Experiments in chapter 3 were performed with muscle at a shorter initial muscle length because participants were seated and had their knee flexed at a 90° angle. The data from our computational experiments at 50% activation showed that there is a greater reduction in force for muscles with an initial length of 1.1 (4.5%) than at an initial length of 0.9 (2.4%) (Figure 4-7). We compare against 50% activation because twitch force was used in the physical experiments. The physical experiments showed that a shorter initial muscle length showed no reduction in muscle force (Chapter 3), whereas longer initial muscle length showed a 16% decrease in force (Chapter 2; Ryan *et al.*, 2019; Stutzig *et al.*, 2019). These results indicate that initial muscle length is part of the reason that muscle force is reduced due to transverse loading.

4.4.4. Loading direction

Our study in chapter 3 was not only performed with shorter initial muscle length but also with multidirectional loading (chapter 3) rather than unidirectional loading (Chapter 2; Ryan *et al.*, 2019; Stutzig *et al.*, 2019). Unidirectional transverse loading (Chapter 2; Ryan *et al.*, 2019; Stutzig *et al.*, 2019) caused a greater decrease in muscle force compared to multidirectional loading (Siebert *et al.*, 2018) even though the loading force used in both experiments was similar at 98.1 and 108.4 N, respectively. Data in figure 4-5 showed that direction of loading had a significant effect on the muscle force. Multidirectional loading resulted in a much greater decrease in muscle force than unidirectional loading. However, the results from the example computational experiments show that top loading leads to a greater reduction in muscle force than loading from all directions. The example computational experiments are a better approximation of the physical experiments because they more closely match the pennation angles measured for the physical experiments as well as the muscle lengths that were used. Data from figure 4-5 contains computational experiments with loads of 30 kPa. This would sum to a total load of 90 kPa on the geometry. As this is a higher load than was used in the multidirectional loading experiments it would result in greater muscle force reduction. Ideally the sum of loads on the geometry should be set up to balance between the different loading directions.

4.4.5. Initial pennation angle

For the computational experiments run with varying initial pennation angles we observed two main effects. The maximum force in the line of action of the muscle decreased as initial pennation angle increases. This holds with the theory that a smaller component of the fibre contractile force lies in the line of action of the muscle and therefore less force is produced in the line of action of the muscle. Furthermore, the computational experiments showed that the reduction in force due to transverse loading became less as initial pennation angle increased. This would indicate that muscle with higher pennations are more resilient to the effects of transverse loading. This matches the results obtained from previous experiments where muscle with higher initial pennation angles (chapter 3) showed no reduction of force as a result of transverse loading, whereas muscle with lower initial pennation angles (Chapter 2; Ryan *et al.*,

2019; Stutzig *et al.*, 2019) showed a significant decrease in muscle force because of transverse loading.

4.4.6. Comparison of physical experiments and example computational experiments

Similar to previous results the example computational experiments (Table 4-1, 4-2, 4-3) showed that external transverse loading led to a reduction in muscle force. Comparisons between the computational experiments and comparisons between the experiments performed in chapter 2, 3 and by Ryan *et al.* (2019) and Stutzig *et al.* (2019) showed similar results with the latter showing greater effects of transverse loading than the former. Results from the example computational experiments showed that changes in muscle architecture in the model happened as they did in the physical experiments. Lengths increased due to compression. Muscle contractions were nearly isometric. The most likely reason for the models to not be fully isometric is due to timing errors between changes in boundary conditions of the model and onset of muscle activation. For volume we saw nearly no increase as a result of muscle activation which showed that our model was nearly isovolumetric. Changes in internal pressure were calculated to increase between 24 and 64 kPa due to activation, which are similar values as have been measured in frog muscle, which were measured to be between 13 and 40 kPa at maximum activation (Hill, 1948).

4.4.7. Muscle energies

The volumetric strain-energy potentials (Figure 4-8) decreased as external transverse load was increased for a majority of the computational experiments. Therefore, it can be assumed that the force reduction due to transverse loading is linked to the energy that arises from changes in volume. The base material strain-energy potentials showed an increase with increases in initial pennation angle. Similarly, the thickness and width strains showed an increase with increased initial pennation angles. Therefore, we assume that base material strain-energy potentials are linked to the deformations that the base material undergoes due to muscle activation.

The work the muscle performed to lift the external transverse load calculated from the computational experiments was compared to that of previous experiments in

rats (Siebert *et al.*, 2014a) and humans (Chapter 2; Ryan *et al.*, 2019; Stutzig *et al.*, 2019). For the computational experiments the lifting work was only calculated for experiments with top loading as this would give the closest comparison to the rat and human experiments. In rat experiments the lifting work ranged from approximately 1204 to 1801 J m^{-3}. In the human block loaded experiments they ranged from 1224 to 5676 J m^{-3} and in the human sling loaded experiments the ranged from 2476 to 6360 J m^{-3}. Whereas, in the computational experiments the lifting work ranged from approximately 53 to 456 J m^{-3}. The lifting heights for the computational experiments were not measured. Instead the increase in muscle thickness between the loaded state and the maximum active state was used to calculate lifting work. The increases in thickness for the computational experiments were lower than the heights to which the external transverse loads were lifted in the physical experiments. This resulted in lower lifting work performed in the computational experiments. Both the rat and human experiments were done with muscle including aponeuroses and tendon contracting isometrically and therefore the muscle would have been able to shorten more than the computational experiments which were only muscle contracting isometrically. This would allow for greater bulging in the muscle thickness in the rat and human experiments and higher lifting heights of the external transverse load.

4.4.8. Limitations

Length was expected not to change with activation as we were running isometric contractions. However, transitions in boundary conditions between external loading and muscle activation resulted in near isometric muscle contractions. Due to human error timesteps were input with rounding errors that resulted in boundary conditions not being set. There was 5% strain in the muscle length during activation for computational experiments at optimal resting length.

For this project a block geometry was chosen to represent the muscle. Although research has shown that a block geometry can be representative of whole muscle (Wakeling *et al.*, 2020) there are elements not included that can change the results of the model. Using a parallelepiped geometry might better capture the natural shape of the medial gastrocnemius. Due to unsupported overhang in a parallelepiped muscle could lead to greater changes due to transverse loading in muscle thickness and pennation angle. Furthermore, not included in the study were the aponeuroses. With a stiffer tissue

such as the aponeuroses covering the top and bottom of the geometry there could be changes to the muscle deformations due to transverse loading and activation, as well as to force production. In a block geometry with pennate fibres not all of the fibres would insert into the fixed ends of the muscle along which the force is measured and therefore would not fully contribute to the muscle force. Unconnected fibres might still add to the muscle force through transmission through the base material (Kjaer, 2004), although it is not determined if this happens within this model. By adding aponeuroses to a parallelepiped geometry the contribution of all fibres should improve as all fibres would indirectly connect to the fixed faces along which the force is measured. It would also be possible to add a tendon to the study. It would make the computational experiments more comparable to physical experiments that have been performed, especially those in chapter 2 and 3 of this thesis. It would give the geometry more room to deform and we would possibly see changes in muscle architecture closer to those measured in physical experiments.

For this study we chose to simulate isometric muscle contractions with the exclusion of a tendon and aponeuroses. As such the force-velocity relationship did not play a role in the calculations. Adaptations to the model are being made for future projects to include tendon, aponeuroses, and the force-velocity relationship of muscle. Previous research has shown that it is possible to make the model dynamic in this way (Ross *et al.*, 2018). Making the model dynamic would also allow the inclusion of inertial effects of muscle mass. Muscle mass has been shown to change muscle performance in a muscle model (Ross and Wakeling, 2016).

To determine the stress-strain relationship of the base material data were taken from across-fibre compression experiments of muscle tissue (Wakeling *et al.*, 2020). As the fibre properties only come into play in the along-fibre direction, using data from across-fibre compression should yield mostly properties that represent the base material. However, direct measurement of base material, for instance muscle tissue with muscle fibres extracted from them, would give a more accurate, and possibly different, stress-strain relationship.

4.4.9. Conclusion

We are able to conclude that the reduction in force due to transverse loading was replicated in the computational experiments similar as was shown in previous physical experiments. The initial pennation angle, initial muscle length and the direction of transverse loading were independently varied throughout the computational experiments to determine their contribution to muscle force reduction as a result of external transverse loading. The amount of force reduction was shown to be dependent on initial pennation angle, initial muscle length and the direction of transverse loading.

Chapter 5.

Discussion

5.1. Thesis Summary

In chapter 2 we showed that, like the study done in rats (Siebert *et al.*, 2014a), we are able to affect the muscle's ability to produce maximum twitch force in humans. To determine this, we placed a significant amount of load on a portion of the muscle. At our highest load we were able to reduce the maximum twitch force by approximately 16%. No matter if you are a professional athlete or work a desk job, losing nearly a fifth of your strength would be a significant burden on performing routine tasks. However, the manner in which the muscle was loaded for these experiments does not relate to many real-life situations. With this being true we have to take into account that this was exploratory research. It was difficult to say whether a response to loading would be found, and therefore using the design that was chosen along with the relatively high loads would ensure that if muscle were to show any response to loading, this design would find that response. Furthermore, with finding such a strong result we were far more likely to find evidence of the mechanism behind the reduction in force. We found that there is a large decrease in muscle thickness and pennation angle due to initial passive loading, and transient changes during muscle activation were lower when higher loads were applied when loading the medial gastrocnemius. Likewise, it was shown that loading had an effect on the changes in fascicle thickness. Changes in muscle thickness that were observed in these experiments are relatively large compared the change in thickness that muscle undergoes during unloaded activation, where it is shown to be approximately zero for the medial gastrocnemius (Narici *et al.*, 1996; Maganaris *et al.*, 1998). The data seem to indicate that the muscle is attempting to restore its natural architecture as it is contracting, and that the restrictions on returning to that state are reducing the force that it is able to produce. This could further be explained by stating that the internal work that the muscle must do to change its shape reduces the energy that is available to perform work in the line of action of the muscle to contract.

The idea that led to this project was that muscle is not an isolated structure. It exists in an organism where it is surrounded by other structures, and through every day

activities loading of our muscles occurs. People are seated for extended periods of time, either behind a desk or in a car, they wear heavy backpacks, and dress in tight fitting clothing. It would be less than ideal if people were expending more energy performing tasks because they have to overcome the effects of loading on their muscles. What if leaning against the corner of a table with your leg suddenly caused you to collapse under your own weight? This is extremely unlikely to happen to a healthy person, however if the health of a person is compromised this might become more likely. So far, we discussed people performing everyday tasks, however for professional athletes every small advantage counts. Perhaps such advantages can be found by freeing muscle from loads such as those from compression garments. Different garments have been tested from socks to whole-body garments with loads of approximately 3 kPa (Sperlich *et al.*, 2010; Faulkner *et al.*, 2013). We can also consider soldiers during missions who have all manner of gear strapped to their body. For the purpose of research this is also an important finding to consider. During ultrasound measurements the probe needs to be pressed firmly against the skin to prevent air from disrupting the image. The pressure with which the probe is pressed on the skin needs to be considered as it could possibly deform the muscle (Herbert *et al.*, 1995; Bolsterlee *et al.*, 2015; Hirata *et al.*, 2017). Aside from deforming the muscle the load placed on the muscle should be considered as this could possibly distort force measurements. An ever-growing area of research is that of exoskeletons (Dollar and Herr, 2008; Sawicki *et al.*, 2020). Here it would also be wise to consider the effect that might occur from strapping hard object onto a person. External transverse loads or restrictions to transverse expansion limit the performance of muscle. Understanding these effects might help the design of clothing, the measuring of muscle, or the design of exoskeletons to minimize a possible loss of force.

5.1.1. Comparing unidirectional against multidirectional loading

The project in chapter 3 was performed for several purposes. One of which was to move towards a more realistic form of muscle loading by using a sling rather than a block to load the muscle. Furthermore, loading with a sling would allow for a more multidirectional loading of the muscle. This was thought to have a greater effect on the whole muscle and would lead to a clearer reduction in force. Loading using a sling has been shown to affect muscle force (Siebert *et al.*, 2018). It was, therefore, of interest to us to observe this reduction in muscle force using a sling while also imaging muscle

architecture using ultrasound. Furthermore, we had the participants change from a prone position to a seated position. This would give us a more natural orientation in which the calf muscles are used. This would also prevent any deformation of the muscle in the transverse direction as a result of gravity.

The results of the experiment were interesting. Where we previously had found reductions in force due to loading, here the data showed no reduction in force at all. The ultrasound similarly showed far less effect of loading on architecture than were found in previous experiments. For the pennation angle there was some significant difference between the unloaded and the 10kg trials under passive resting conditions. For muscle thickness there was significant difference between the unloaded posttest and the loaded trials. This shows that there is a clear difference in effect between the unidirectional loading of the block and the multidirectional loading of the sling.

5.1.2. The effect of muscle length

An important factor seems to be the muscle length at which the experiments are performed. In the prone position the knee is fully extended, and the muscle is at a longer length than it is when the knee is flexed at a 90° angle when participants are seated. Although not quantified, it was clear that the muscle felt less compliant when the knee was fully extended compared to when it was at a 90° angle indicating that the muscle under more tension when the knee was fully extended. The change in muscle length could have a significant effect on the range of the force-length relationship over which the gastrocnemius is acting. An issue that is encountered here is that there is not sufficient information about the force-length relationship of the gastrocnemii in humans. Kawakami and Fukunaga (2006) give some insight as to where on the force-length relationship the medial gastrocnemius is working depending on ankle and knee angles. However, it has also been shown that the force-length relationship shifts according to muscle activation level (Holt and Azizi, 2016). Literature shows that the medial gastrocnemius works on the ascending limb during maximum activation (Kawakami and Fukunaga, 2006). Muscle at shorter lengths would have the tendency to lengthen when compressed, whereas muscle at longer length would shorten (Sleboda and Roberts, 2019). For muscle at shorter lengths this would lead to a rise on the ascending limb of the force-length relationship at maximum activation and an increase in force potential. Whereas, for muscle at longer lengths at maximum activation there would be a decrease

down the ascending limb of the force-length relationship causing a decrease in force potential. The right shift of the force-length relationship when lowering activation would shift the force potential down for both lengthened and shortened muscle. The situation would remain the same as higher activation where shortened muscle losses force potential whereas lengthened muscle gains force potential. The only length changes measured in the experiments were the fascicle lengths. The accuracy of the fascicle length measurements was not high enough to draw any conclusions on the effects of length. Fascicle lengths for unloaded muscle at longer lengths was not measured and therefore we cannot say if fascicle lengths shortened as a result of loading. More accurate measurement and a more complete collection of data for all conditions are needed to determine the effects of length, as well as a better understanding of how the medial gastrocnemius muscle length relates to the force-length relationship.

5.1.3. Comparing force measurements

Of interest to note is the differences in the force plots between the block loaded and sling loaded experiments. The exact same method of muscle stimulation was used in both experiments. In both cases single pulse twitches were administered starting at 5 mA, slowly increasing the pulse until a plateau in the force was reached. The stimulation current at the force plateau was administered as a double pulse to elicit twitches for the main experiment. However, in the block loaded experiment with participants lying prone the average current used was approximately 30 mA, whereas in the sling loaded experiment where participants were seated the current averaged approximately 170 mA. In both experiments the location of the stimulation electrode was optimized to give the greatest contraction of the calf muscles. The difference in stimulation current used is clearly represented in the force plots, where the forces for the sling loaded experiments is nearly twice as high as the forces for the block loaded experiments. One explanation for this would be that the stimulated nerve moves deeper into the leg when the knee is at a 90° angle than when it is fully flexed, which would mean that a higher current is needed to stimulate the nerve. However, if this were the case, then higher current would lead to similar stimulation of the nerve and this should result in similar forces, which is not the case. The results from the muscle model would suggest that the reduction in force does not differ greatly between 50% and 100% activation which means the percentage of force reduction drops with higher activation. This would suggest at higher

activation the muscle is able to overcome the force reduction. This would match the results from our experiments where the sling loaded experiment with higher forces did not show force reduction whereas the block loaded experiment with the lower forces did show force reduction.

5.1.4. Transverse expansion of the muscle

Previous research showed that resistance to radial expansion limited muscle in the work that it could produce (Azizi *et al.*, 2017). In previous research the thickness of the medial gastrocnemius was found to be close to 20 mm (Narici *et al.*, 1996; Maganaris *et al.*, 1998), and was shown to not change in thickness during maximum voluntary contraction. In our unidirectional block loaded study compressed muscle at rest was measured between 12 and 14 mm in thickness depending on the load. For the lower loads the muscle thickness was able to recover to approximately 18 mm, close to what previous studies found. However, during testing ultrasound images were taken from nearly uncompressed muscle. Measurements of these images put the thickness of the medial gastrocnemius at 19.7 mm. Therefore, we can say that during our unidirectional block loaded experiments resistance to radial expansion does occur. In our multidirectional sling loaded study muscle thickness at rest under loaded conditions was between 18 and 19 mm, where the muscle thickness at rest under unloaded conditions was between 19 and 19.5 mm. At maximum twitch force the loaded trials muscle thickness increased to between 20 and 20.5 mm, and for the unloaded trials it increased to between 20.5 and 21 mm. Therefore, it would be fair to say that hardly any resistance to radial expansion occurred during the sling experiments. As such it is likely that muscle has a thickness at which it can operate at maximum force output, and during contraction it will always try to recover to this optimal thickness.

5.1.5. Pennation angle changes

At this point it would also be interesting to look at the other values that we got from our unloaded analysis of the experiments in chapter 2. The pennation of our unloaded muscle from the unidirectional block loaded experiments showed an average value of approximately 14° at rest. This is at least 2° higher than the loaded resting averages which were between 10° and 12°. In our multidirectional sling loaded study we found pennation angles of approximately 19° for the unloaded trials at rest, and

approximately 18.5° for the loaded trials. First, this shows that pennation angles in the unidirectional block loaded study where lower than those in the multidirectional sling loaded study, even for the unloaded trials. The difference in pennation angles between the two studies could have occurred due to physiological differences between the two tested groups. However, in both cases young, athletic adults were tested with a large number of participants per test group. A comparison was made between the unloaded, resting pennation angles of the unidirectional block study (14.4 ± 2.8°) and the multidirectional sling study (19.4 ± 1.9°) using an independent samples t-test. The test showed a significant difference between the two groups ($p < 0.05$). Due to this we assume the difference in pennation angle to be because of participant posture rather than physiological differences between the two tested groups. We assume the differences to be due to the prone position of the participants in the unidirectional block loaded study compared to having the knee flexed at 90° in the multidirectional sling study. In the unidirectional block study the pennation angle would be lower because of the muscle being stretch to a longer length, as well as gravity flattening the muscle. Secondly, in our multidirectional sling loaded study the loading showed to have little to no effect on the pennation angle at rest, and those values are close to the values found in previous literature (Narici *et al.*, 1996; Maganaris *et al.*, 1998). Important to note is the difference in change in pennation angle between rest and peak activation. In the unidirectional block loaded study the pennation changed by nearly 6°, whereas in the multidirectional sling loaded experiment it only changed by about 2° to 3°. This shows that in the unidirectional block loaded study the pennation is trying to recover from being compressed and increases to values that are close to those of the multidirectional sling loaded study. Whereas, in the multidirectional sling loaded study the pennations of the loaded trials are close to those of the unloaded trials, and both show similar changes in pennation. Meaning that in our multidirectional sling loaded study the pennation does not have to recover from being compressed. For both our experiments the peak active values of the pennation angles are far off from those found in literature, which shows values over 30° pennation. An explanation for this would be that the values in literature come from maximum voluntary contractions, whereas we used maximum force twitches where the muscle activation is much lower.

5.1.6. Muscular hydrostats

Comparing the fascicle dimensions between the two experiments from chapter 2 and 3 showed interesting data. In the block loaded experiment fascicle thickness was shown to increase during muscle activation and fascicle length is shown to decrease transiently. Compared to this, the sling loaded experiment showed a decrease in the fascicle thickness during muscle activation and a minor decrease in fascicle length followed by an increase in fascicle length as the muscle relaxed. Furthermore, fascicle lengths in passive muscle were found to be shorter in the sling experiment than in the block experiment. This is likely the result of the fascicles being compressed and being pushed to longer lengths.

Although several of these measurements were not proven to be statistically significant discussing them can be interesting. To explain one theory on these finding we give a short summary of work reported by Steven Vogel about muscular hydrostats. If you take a balloon and you wrap it with a helical mesh you can influence the shape changing capacities of the balloon (Vogel, 2003). A helical mesh with a very small angle relative to the long axis of the balloon will mainly prevent the balloon from getting longer when transversely compressed. A helical mesh with a large angle will prevent the balloon from getting thinner when it is transversely compressed. With an angle of 55° the balloon will resist changes in all directions when transversely compressed. Interestingly, with angles larger than this the balloon will get shorter when compressed, and with angles smaller than this the balloon will get longer.

The connective tissue throughout the muscle surrounding the fibres, fascicles, and whole muscle quite possibly have a helical pattern to them (Purslow and Trotter, 1994), and the angle of this helix depends on the length of the muscle. Research on fluid filled bladders surrounded by a helical mesh showed that the interaction of the helical mesh with the bladder resulted in a greater increase in passive force (Sleboda and Roberts, 2017). This shows that the helical mesh is preventing the deformation of the bladder. Furthermore, compression of models consisting of tubes with reinforced fibres arranged in a helical pattern show different results to compression due to a difference in fibre angle (Sleboda and Roberts, 2019). In models with lower fibre angle compression resulted in shortening of the tube, whereas, in models with higher fibre angles compression caused lengthening of the tube. Similarly, compression caused a reduction

in generated force for models with a high fibre angle, and an increase in force for models with a low fibre angle. Experiments were also run on semimembranosus muscles where the muscle was held at different lengths and compressed (Sleboda and Roberts, 2019). Compression of muscle at short lengths caused a decrease in force, whereas, compression of muscle at long lengths caused an increase in force.

Research has shown that the collagen fibres in the endomysium have distinct angles to them and that those angles change with muscle length (Purslow and Trotter, 1994) providing a helical mesh similar to what has been described above. Further research showed that collagen fibres in the epimysium form a helical pattern with an angle of approximately 55° for muscle at resting length (Purslow, 2010). This is important to our current studies because, depending on the muscle length, the muscle could be getting longer or shorter as we load it. This in turn would have an effect on where on the force-length relationship the muscle is working during the experiments and might give more insight as to why muscle force is reducing or not reducing depending on what position the participant is in.

Returning to the findings on fascicle dimensions this effect of helical connective tissue could explain the results that are shown. The fascicles are shorter in the multidirectional sling loaded study and the helices within the connective tissue would presumably have a large angle. As a result of the tension increase within the fascicle due to activation and this large helical angle the fascicle would get longer and thinner. In the block experiment the fascicles are longer, and we can assume the helical angle to be smaller. Tension increase in the fascicle would cause the fascicle to shorten and thicken. This would suggest that muscle fascicles behave like muscular hydrostats do. The main counterargument against this is important. Sarcomeres are arranged and move in the longitudinal direction of muscle fibres, and fibres run the length of muscle fascicles. Therefore, any contraction of sarcomeres due to muscle activation should lead to a shortening of a muscle fascicle. Even so, it seems to be an interesting area for further exploration.

5.1.7. Duration of architecture changes

The figures for pennation angle (Figure 2-3A, B; Figure 3-4A, B) and muscle thickness (Figure 2-3C, D; Figure 3-4C, D) both show the transient increase in

respectively pennation and thickness. However, the duration of the event differs between the two studies. The changes for the block loaded study span a shorter time (0.25 s) than the changes for the sling loaded study (0.4 s). An identical electrical stimulation was used in the two experiments, so this does not explain the difference. Higher currents were used in the sling experiments, which explains higher forces but does not explain longer durations. Another possible explanation could be that the muscles were stretched to different degrees. With the knee extended, as was the case in the block loaded study, the muscle would have been stretched tighter. Whereas, in the sling loaded study, with the knee bent, the muscle would have been much slacker. It was clear from palpating the muscle during the experiment that with extended knee the muscle felt stiffer than with flexed knee. The time it takes for the muscle to go from slack to taut would explain the longer time to reach the peak value. The addition of compliance in series with a muscle reduced the maximum twitch force and prolonged its duration (Hill, 1951; Mayfield *et al.*, 2015, 2016). This would confirm what was observed in our experiments. In the sling loaded study the resting muscle length is shorter and there would be more compliance in the Achilles tendon compared to the block loaded study where the resting muscle length was longer and the tendon would be less compliant. The reduction in twitch force was not observed because higher stimulation currents were used. However, we are possibly seeing the longer duration of the twitch due to the compliance.

5.1.8. Comparing the finite element model to physical experiments

In chapter 4 the finite element model showed reliable results when compared to physical experiments done in the past. The model was shown to be nearly isovolumetric similar as muscle has been shown to be (Abbott and Baskin, 1962). Pressures increase as a result of activation by similar amounts as have been reported previously (Hill, 1948). Compression resulted in decreases in muscle thickness and pennation angle as has been measured previously (Chapter 2; Ryan *et al.*, 2019). Finally, the force reduction as a result of external transverse loading can be seen in the computational experiments similar to physical experiments that were performed (Siebert *et al.*, 2014a, 2018; Chapter 2; Ryan *et al.*, 2019; Stutzig *et al.*, 2019).

In previous experiments it was established that pennation angles increase with muscle activation (Narici *et al.*, 1996; Maganaris *et al.*, 1998; Chapter 2; Ryan *et al.*, 2019). However, this was one aspect of muscle architecture that was not reflected in the

model. For the model the changes in pennation angle due to activation were minor between -1.5° and 1.5°, fluctuating between increases and decreases. An explanation for this discrepancy in pennation angle changes due to activation could be that our computational experiments did not include a tendon. Physical experiments will use isometric contraction of the muscle-tendon unit where the muscle is allowed to shorten because lengthening of the tendon keeps the muscle-tendon unit isometric. Our model was nearly isometric, but without the tendon the muscle showed minimal shortening during activation. As such the muscle would be unable to change pennation angle. Another possibility is that there is a mechanism to pennation angle rotation that was not being accounted for in our current model. Further development of the model would be able to give insight into whether the model can correctly replicate pennation angle rotations during muscle activation.

Comparisons to other models was difficult. Studies reported the use of different initial pennation angles (Chi *et al.*, 2010; Kinugasa *et al.*, 2016; Alipour *et al.*, 2017) but no changes in pennation angle were reported. Rahemi *et al.* (2015) mentions pennation rotations from the model, however changes are not reported. Studies have also reported muscle strains and deformations (Blemker *et al.*, 2005; Tang *et al.*, 2009; Alipour *et al.*, 2017) yet no values are presented for muscle thickness that can be compared to the measurements from the physical experiments performed in this thesis.

5.1.9. Example computational experiments compared to physical experiments

For our example computational experiments we selected experiments that best fit the physical experiments that were preformed previously in chapter 2 and by Ryan *et al.* (2019) and Stutzig *et al.* (2019) and those discussed in chapter 3. These are conditions with a lower pennation angle (10°), a longer initial muscle length (1.1), and transverse loading from the top for the block loaded experiments and a higher pennation angle (20°), a shorter initial muscle length (0.9), and transverse loading from all directions for the sling loaded experiments, respectively. To compare external load, we selected a 15 kPa and 5 kPa external load, respectively. This was done because in the computational experiments where load was applied from all directions a 5 kPa load was applied to each of the three surfaces summing up to a total of 15 kPa. This matched with the computational experiments where load was applied to only one surface and that load

was selected to be 15 kPa to match the other computational experiments. A load of 15 kPa was not the highest load that was applied during physical experiments which was 30 kPa and gave us the clearest results. However, the chosen loads gave the best comparison between computational experiments.

For both conditions of selected computational experiments we saw that transverse loading led to a reduction in muscle thickness. This matched the physical experiments where loading reduced muscle thickness. However, a greater reduction in muscle thickness was seen for the block loaded experiments compared to the sling loaded experiments which was not reflected in the computational experiments. For the models matching the seated experiments we saw a reduction in thickness due to activation and for the computational experiments matching the block loaded experiments we saw no change in thickness due to activation. These results do not match the physical experiments where activation led to an increase in muscle thickness. However, these results do match more closely to previous research which showed no significant change in thickness due to muscle activation (Narici *et al.*, 1996; Maganaris *et al.*, 1998).

The computational experiments show a reduction in pennation angle as a result of external loading. This matched the results from the physical experiments where loading caused a reduction in pennation angle. The difference in pennation angle change between the physical experiments was not matched by the models. The models matching the sling loaded experiments showed greater pennation angle change than the models matching the block loaded experiments. The opposite was found in the physical experiments. As for pennation angle changes due to activation we saw the opposite of what previous research has shown. The models showed a decrease in pennation angle due to muscle activation whereas previous research showed increases in pennation angle (Narici *et al.*, 1996; Maganaris *et al.*, 1998; Chapter 2; Ryan *et al.*, 2019).

Reduction in force matched well between the selected computational experiments and the physical experiments. Both conditions of the computational experiments showed a reduction in force as a result of external loading. The reduction in force was greater for the computational experiments matching the block loaded experiments which is similar to the results of the physical experiments where the block loaded experiments showed a greater reduction in muscle force.

There are a couple of reasons why the change in thickness and pennation angle do not match the results from the physical experiments. In the physical experiments we used isometric contractions of the whole muscle-tendon unit. Under these circumstances stretch in the tendon allows the muscle to shorten and still have the muscle-tendon unit be isometric. The allowed shortening of the muscle could allow the muscle to have greater rotation of the pennation angle which would also affect the change in thickness. Future experiments where a tendon is added to the model could give more insight into whether the allowed stretch of the tendon results in more change in pennation angle and muscle thickness. The block geometry used for the computational experiments did not match the parallelepiped geometry of a medial gastrocnemius nor did we have aponeuroses in our model. These could play a factor in the way that force is transmitted through the muscle and can affect the pennation angle rotation and the change in muscle thickness. Again, a shift towards more realistic models could give more insight into how pennation angle rotation and muscle thickness change work under externally loaded and activated conditions.

The physical experiments with sling loading of the medial gastrocnemius showed little to no reduction in muscle force especially when compared to the unidirectional block loading. This is however not reflected within the computational experiments where multidirectional loading is shown to have the greatest effect on force. A reason for this could be that the model loads the muscle in isolation whereas in the physical experiments the muscle is surrounded by the rest of the calf. In the physical experiments although the muscle is being loaded from multiple directions the sling is being supported by other sections of the calf. This means that the applied load is not applied to the medial gastrocnemius only but by the whole calf. Therefore, the applied loads in the physical experiment would be lower than expected and would explain why little to no reduction in force is measured. For this reason the comparisons made previously between the sling loaded experiments and the computational experiments with compression from all sides are not fair comparisons. In the computational experiments the full load is applied to the block, whereas in the experiments loading from all directions was limited. Finding a method by which the multidirectional load can be isolated to just the medial gastrocnemius could show a more pronounced effect of transverse loading on muscle force.

5.1.10. Comparison of muscle models

Different types of models have been used to study transverse loading of muscle. There was a geometrical model (Siebert *et al.*, 2012) that solves for dimension changes while maintaining constant volume, showing how transverse dimensions change under transversely loaded contractions. Another model was a force model (Siebert *et al.*, 2014b; Siebert *et al.*, 2018) that balanced the forces between the longitudinal muscle force and the transverse load by including a gearing ratio, showing that muscle force is reduced due to transverse loading. A physical, hydrostatic model (Sleboda and Roberts, 2019) was used to describe length changes and force reduction due to transverse loading using a helically wrapped, water filled tube. The model presented in chapter 4 of this thesis used the minimization of an energy equation to describe dimension changes and muscle force reduction in a finite element model. The geometrical model (Siebert *et al.*, 2012) and force model (Siebert *et al.*, 2014b; Siebert *et al.*, 2018) both showed an increase in muscle thickness due to activation, whereas the energy model (chapter 4) showed an increase in thickness only for models with an initial pennation of 0° and 10°. Models with an initial pennation of 20° or greater showed a reduction in thickness. For force reduction the force model (Siebert *et al.*, 2014b; Siebert *et al.*, 2018), physical, hydrostatic model (Sleboda and Roberts, 2019), and energy model (chapter 4) showed similar results. These models showed a reduction in force. However, the hydrostatic model showed a reduction in force only for muscle at shorter lengths, and the energy model showed in increase in force for models with an initial pennation angle of 40°. A difference between the geometrical and force models compared to the energy model is that they used optimized parameters. No such optimization was used in the energy model however results were similar to the other models. Results from the models and experimental work done in chapter 2 and by Ryan *et al.* (2019) match up well. The increase in muscle thickness shown in geometrical model was found in the experimental work. The experimental work also showed the reduction in force that was shown by the force, hydrostatic, and energy models. The results of the models did not match the results found in the experiments presented in chapter 3 of this thesis as changes in thickness were minimal and no reduction in force was measured. The energy model presented in chapter 4 was run using a series of initial conditions with regards to length and pennation angle. This showed that the results of the model depend heavily on the initial conditions used. As such inconsistencies between the four models discussed

above are to be expected as well as inconsistencies between the models and the experimental work.

5.2. Avenues of Future Research

5.2.1. Muscle length measurement

It would be of a lot of interest to study how muscle length changes as it is loaded at different knee and ankle angles. It should be possible to use ultrasound to image the muscle tendon junction of the Achilles tendon and the medial gastrocnemius while loading passive muscle over a range of different knee and ankle angles. By the direction the muscle tendon junction is moving you would be able to tell whether the muscle is getting longer or shorter. Quite possibly the muscle tendon junction at the knee would also have to be imaged to determine whether the muscle is not displacing as a whole due to the loading. However, it is uncertain whether the muscle tendon junction at the knee can be properly imaged and perhaps it is unnecessary because the tendon at the knee is much shorter and stiffer than the Achilles tendon. In conjunction with the measurements of muscle length it would be worth measuring fascicle thickness and length as well. A range of different muscle lengths would mean that we would also be working with different fascicle lengths. As such we would be able to determine the behaviour of the fascicle dimensions as they activate at different lengths. Measurement of muscle length and changes in muscle length due to loading could add valuable information to better understand force reduction in muscle as a result of transverse loading. Previous research predicts through models that muscle will lengthen or shorten as a result of transverse loading depending on the angle of the fibres in the extracellular matrix (Sleboda and Roberts, 2019). It would be informative if this could be shown for *in vivo* muscle as well. Furthermore, this is linked to changes in muscle force output due to transverse loading and can therefore help to better understand this effect on muscle.

5.2.2. Effects of fat accumulation

In the ongoing study of muscle loading an area of further investigation is the accumulation of fat in and around muscle, or intramuscular adipose tissue and intermuscular adipose tissue. Intramuscular adipose tissue, also known as intramyocellular triglyceride, occurs as droplets within muscle fibres. The occurrence of

these fat droplets is strongly linked to insulin resistance and is studied in research relating to diabetes and obesity (Goodpaster *et al.*, 2000; Sinha *et al.*, 2002). Although the accumulation of fat within muscle fibres is interesting and the effect on fibre contractions could be studied further, it is in no way related to the theme of our current projects. Intermuscular adipose tissue is the fat found within and between muscle groups (Kim *et al.*, 2004; Vettor *et al.*, 2009). Intermuscular adipose tissue is found in all individuals and can increase due to pathological reasons, a sedentary lifestyle, and aging (Vettor *et al.*, 2009). As intermuscular adipose tissue increases in and around muscle there is the possibility that this will result in compression of the muscle or prevent it from expanding in the transverse direction. The assumption that adipose tissue can restrict the bulging of muscle seems reasonable because the stiffness of adipose tissue (shear modulus = 7.5 kPa (Geerligs *et al.*, 2008)) is greater than of muscle tissue (shear moduli ±6 kPa //; ±1.6 kPa $\perp$ (Gennisson *et al.*, 2010)) according to their respective shear moduli with muscle at rest. It should be noted though that for muscle the shear modulus in the longitudinal direction increased greatly when the muscle is activated. Therefore, a comparison between the behaviour and functionality of muscle with low amounts of intermuscular adipose tissue and muscle with high amounts could give insight into whether adipose tissue results in a natural occurrence of force reduction due to compression. A method to test this could be to use rat models. Subjects could be tested in lean conditions after which they could be fed a high caloric diet to increase intermuscular adipose tissue after which they could be retested. It should be possible to use magnetic resonance imaging to estimate the volume of adipose tissue which could be used to adjust the data for a more accurate result. Results could determine whether intermuscular adipose tissue should be an area targeted by medical professionals to increase mobility for certain individuals.

5.2.3. Errors in ultrasound imaging

An error might occur in the data of the ultrasound imaging when the probe has to be positioned against the muscle. Bolsterlee *et al.* (2016) compared ultrasound data with MRI data to determine misalignment of the ultrasound probe. They showed that a range of alignments can lead to correct ultrasound data, however, they recommend orienting the probe perpendicular to the skin and parallel to the tibia. Obtaining and maintaining a proper alignment would depend on how tightly the probe is strapped or pressed against

the muscle during recording. In the experiments in chapter 2 this error did not occur as the probe was integrated into the external load. However, this did leave us unable to collect ultrasound data during the unloaded trials. In the sling experiment this error was minimized by placing the probe on a flexible arm which would allow the probe to be positioned against the muscle. It was possible to place the probe in such a position that it barely pressed against the muscle, and flexibility in the arm allowed the probe to move as the muscle bulged and pushed against it. However, because the contact between the probe and the muscle has to be airtight it was not possible to completely prevent the probe from deforming the muscle. For future research it would be an advantage if this type of error could be minimized further. There exist many types of temporary adhesive solutions such as skin glues and double-sided tapes. In the case of the temporary glue or tape it should be determined what the ease of removing them is, as well as whether they are transparent to the ultrasound. This would allow for the probe to be attached reliably and easily, and not interfere with the muscle. A strong adhesive bond would furthermore allow for more freedom of movement by the participant and would allow for more dynamic studies such as walking trials.

5.2.4. Muscle force measurement from ultrasound

A long-term goal in human biomechanics is to measure muscle force through non-invasive methods. As opposed to animal experiments, the use of traditional methods such as tendon buckles and force transducers is problematic (Komi, 1990). Measurements from force plates and dynamometers are difficult to relate to muscle forces. Estimates of muscle moment arms are prone to error (An *et al.*, 1984; Maganaris *et al.*, 1998b; Olszewski *et al.*, 2015; Fletcher and MacIntosh 2018) and measured forces could be the result of multiple muscles coactivating (Sirin and Patla, 1987; Ivanenko, Poppele and Lacquaniti, 2004; McLean and Goudy, 2004). Studies have looked at other methods to measure muscle force, such as electromyography (EMG). Though EMG and force correlate well at low intensity or slow, isometric contractions, for high intensity contractions EMG plateaus while force continues to rise (Sejersted *et al.*, 1984). Passive forces are not represented in EMG, and therefore EMG does not represent the total muscle force (Baumann *et al.*, 1979). Chemical processes in the muscle do not account for the total volume changes that occur during isometric contraction (Hill, 1948). It was shown that pressure changes in the muscle account for

the majority of the volume changes. In frog gastrocnemius pressures were measured between 100-300 mm Hg during contraction. Other studies showed that there is a strong positive correlation between intramuscular pressure and joint torque in humans (Sylvest and Hvid, 1959), and this correlation exists for both submaximal and maximal contractions (Baumann *et al.*, 1979; Sejersted *et al.*, 1984; Aratow *et al.*, 1993; Ateş *et al.*, 2018). The idea was put forward that intramuscular pressure, as an alternative to EMG, could be used to determine muscle force (Baumann *et al.*, 1979). In chapter 3 we have shown that, according to both previous research as well as our results, muscle fascicles are curved. Calculation of fascicle curvatures show promising results and further refinement of the method could allow for more accurate measurements of curvatures. We also showed that a relationship exists between fascicle curvature and intramuscular pressure through the law of Laplace. If intramuscular pressure could be an alternative to EMG measurements, then perhaps it would be possible to correlate fascicle curvature with muscle force in a non-invasive manner. Attempts to determine muscle force from ultrasound imaging has been shown before. Previous research shows that EMG, ankle joint angle, and ankle joint moments can be determined from ultrasound data with an accuracy of approximately 50% (Cunningham and Loram, 2020). It would therefore seem possible that through more detailed analysis of muscle architecture from ultrasound data a non-invasive method of measuring muscle force could be achieved.

5.2.5. Extracellular matrix restrictions to bulging due to aging

The extracellular matrix (ECM) consists primarily of collagen fibrils and accounts for 1-10% of skeletal muscle (Kjær, 2004; Kragstrup *et al.*, 2011). It provides mechanical support for vessels and nerves and gives the muscle its passive elastic response (Kjaer, 2004). Within the ECM we find advanced glycation end products (AGEs). AGEs are a result of continuous chemical reactions within the body and increase as a result of aging (Baynes, 2001; Kragstrup *et al.*, 2011). Due to AGEs nonspecific cross-linking occurs within the ECM and this leads to stiffening and more resistance to load (Kjaer, 2004; Kragstrup *et al.*, 2011).

The ECM surrounds the fibres, fascicles, and muscle. As such, the result of a stiffer ECM would lead to a restriction in the amount of bulging that these structures could undergo. Restrictions to bulging have been shown to reduce the power production of muscles (Azizi *et al.*, 2017) and could play a role in why external loading reduces

muscle force. Therefore, a stiffer ECM could be part of the reason behind the reduced force output in aging individuals. As such, an interesting continuation on the research discussed in this thesis would be to determine the elastic properties of the ECM, how much the elasticity is affected by aging, and what effect all this has on the force production of fibres or muscles.

To determine the elasticity of the ECM it would have to be separated from other elements within the muscle. This is possible through a method of cell-maceration (Ohtani *et al.*, 1988; Nishimura *et al.*, 1994). This isolates the ECM in such a way that it is possible to image it using scanning electron microscopy. Using cell-maceration it might be possible to obtain an isolated ECM that can be used to perform compression tests to determine the stress-stretch relationship (Takaza, Moerman and Simms *et al.*, 2013; Mohammadkhah, Murphy and Simms *et al.*, 2016).

It is possible to degrade the ECM in smooth bronchial muscle, which has been shown to increase muscle shortening (Bramley *et al.*, 1995). A similar procedure could be attempted on aged skeletal muscle. Skeletal muscle could be treated with collagenase to degrade the ECM. Measurements of muscle force before and after treatment could show whether muscle force increases when the ECM is degraded. Assuming an increase in force is found the increase in muscle force would have to be linked to transverse expansion of fascicles or the whole muscle. Measuring transverse expansion of fascicles would be possible through ultrasound imaging (Chapter 2; Chapter 3; Wakeling and Randhawa, 2014; Randhawa and Wakeling, 2018; Ryan *et al.*, 2019).

References

Abbott, B.C., Baskin, R.J., (1962). Volume changes in frog muscle during contraction. *J. Physiol.*, 161, 379.

Agu, O., Hamilton, G., Baker, D. (1999) Graduated compression stockings in the prevention of venous thromboembolism, *Brit. J. Surg.*, 86, pp. 992-1004

Alipour, M., Mithraratne, K., Fernandez, J. (2017) A diffusion-weighted imaging informed continuum model of the rabbit triceps surae complex, *Biomech. Model. Mechanobiol.*, 16, pp. 1729-1741

Allison, G.T. (2003) Trunk muscle onset detection technique for EMG signals with ECG artefact, *J. Electromyogr. Kines.*, 13, pp. 209–216

An, K.N., Takahashi, K., Harrigan, T.P., Chao, E.Y. (1984) Determination of Muscle Orientations and Moment Arms, *J. Biomech. Eng.*, 106, pp. 280-282.

An, K.N., Hui, F.C., Morrey, B.F., Linscheid, R.L., Chao, E.Y. (1981) Muscles Across the Elbow Joint: A Biomechanical Analysis, *J. Biomech.*, 14, pp. 659-669.

Anderson, F.C., Pandy, M.G. (2001) Static and dynamic optimization solutions for gait are practically equivalent, *J. Biomech.*, 34, pp. 153-161.

Aratow, M., Ballard R.E., Crenshaw A.G., Styf J., Watenpaugh D.E., Kahan N.J., Hargens A.R., (1993). Intramuscular pressure and electromyography as indexes of force during isokinetic exercise. *J. Appl. Physiol.*, 74, 2634-2640.

Arnold, E. M., Ward, S.R., Lieber, R.L., Delp, S.L. (2010) A model of the lower limb for analysis of human movement, *Ann. Biomed.I Eng.*, 38, pp. 269-279.

Arndt, D., Bangerth, W., Davydov, D., Heister, T., Heltai, L., Kronbichler, M., Maier, M., Pelteret, J.P., Turcksin, B, Wells, D. (2017) The deal.II Library, Version 8.5**,** *J. Numer. Math.*, 25, pp. 137-146.

Ateş, F., Davies, B.L., Chopra, S., Coleman-Wood, K., Litchy, W.J., Kaufman, K.R., (2018). Intramuscular Pressure of Tibialis Anterior Reflects Ankle Torque but Does Not Follow Joint Angle-Torque Relationship. *Front. Physiol.*, 9, 1-9.

Azizi, E., Deslauriers A.R., Holt N.C., Eaton C.E., (2017). Resistance to radial expansion limits muscle strain and work. *Biomech. Model. Mechanobiol.*, 16, 1633-1643.

Azizi, E., Brainerd, E.L., Roberts, T.J. (2008) Variable gearing in pennate muscles, *P. Natl. Acad. Sci. USA*, 105, pp. 1745-1750

Azizi, E., Halenda, G.M., Roberts, T.J. (2009) Mechanical properties of the gastrocnemius aponeurosis in wild turkeys, *Integr. Comp. Biol.*, 49, pp. 51-58

Bailey, A. J., Restall, D.J., Sims, T.J., Duance, V.C. (1979) Meat tenderness: Immunofluorescent localisation of the isomorphic forms of collagen in bovine muscles of varying texture, *J. Sci. Food Agric.*, 30, pp. 203-210

Bangerth, W., Hartmann, R., Kanschat, G. (2007) Deal.II - -A general-purpose object-oriented finite element library, *ACM T. Math. Software*, 33, pp. 1-27.

Baskin, R.J., Paolini, P.J., (1967). Volume change and pressure development in muscle during contraction. *Am. J. Physiol.*, 213, 1025-1030.

Baumann, J.U., Sutherland, D.H., Hänggi, A. (1979) Intramuscular pressure during walking: an experimental study using the wick catheter technique, *Clin. Orthop. Relat. Res.*, 145, pp. 292-299.

Baynes, J.W. (2001) The role of AGEs in aging: Causation or correlation, *Exp. Gerontol.*, 36, pp. 1527-1537.

Benjamin, M., Ralphs, J.R. (2000) The cell and developmental biology of tendons and ligaments, *Int. Rev. Cytol.*, 196, pp. 85-130

Blemker, S.S., Delp, S.L. (2005) Three-dimensional representation of complex muscle architectures and geometries, *Ann. Biomed.I Eng.*, 33, pp. 661–673.

Blemker, S.S., Pinsky, P.M., Delp, S.L. (2005) A 3D model of muscle reveals the causes of nonuniform strains in the biceps brachii, *J. Biomech.*, 38, pp. 657-665

Bolsterlee, B., Candevia, S.C., Herbert, R.D., (2016). Ultrasound imaging of the human medial gastrocnemius muscle: how to orient the transducer so that muscle fascicles lie in the image plane. *J. Biomech.*, 49, 1002-1008.

Bolsterlee, B., Veeger H.E., van der Helm F.C., Gandevia S.C., Herbert R.D., (2015). Comparison of measurements of medial gastrocnemius architectural parameters from ultrasound and diffusion tensor images. *J. Biomech.*, 48, 1133-1140.

Bramley, A.M., Roberts, C.R., Schellenberg, R.R. (1995) Collagenase increases shortening of human bronchial smooth muscle in vitro, *Am. J. Respir. Crit. Care Med.*, 152, pp. 1513-1517

Brand, R.A., Pedersen, D.R., Friederich, J.A. (1986) The sensitivity of muscle force predictions to changes in physiologic cross-sectional area, *J. Biomech.*, 19, pp. 589-596

Brandjes, D.P.M., Büller, H.R., Heijboer, H., Huisman, M.V., de Rijk, M., Jagt, H., van ten Cate, J.W. (1997) Randomised trial of effect of compression stockings in patients with symptomatic proximal-vein thrombosis, *Lancet*, 349, pp. 759-762

Brukner, P., Connell, D. (2016) Serious thigh muscle strains: Beware the intramuscular tendon which plays an important role in difficult hamstring and quadriceps muscle strains, *Br. J. Sports Med.*, 50, pp. 205-208

Butz, T. (2006) *Fourier Transformation for Pedestrians*. Berlin: Springer Berlin Heidelberg.

Chi, S.W., Hodgson, J, Chen, J.S., Edgerton, V.R., Shin, D.D., Roiz, R.A., Sinha, S. (2010) Finite element modeling reveals complex strain mechanics in the aponeuroses of contracting skeletal muscle, *J. Biomech.*, 43, pp. 1243-1250

Cobb, M. (2002) Timeline: exorcizing the animal spirits: Jan Swammerdam on nerve function., *Nat. Rev. Neurosci.*, 3, pp. 395-400.

Cooke, R. (1997) Actomyosin interaction in striated muscle, *Physiol. Rev.*, 77, pp. 671-697.

Cresswell, A.G., Löscher, W.N., Thorstensson, A. (1995) Influence of gastrocnemius muscle length on triceps surae torque development and electromyographic activity in man, *Exp. Brain Res.*, 105, pp. 283-290

Cronin, N.J., Carty, C.P., Barrett, R.S., Lichtwark, G. (2011) Automatic tracking of medial gastrocnemius fascicle length during human locomotion, *J. Appl. Physiol.*, 111, pp. 1491-1496

Cunningham, R. (2015) *The application of b-mode ultrassonography for analysis of human skeletal muscle*. PhD Thesis.

Cunningham, R.J., Loram, I.D. (2020) Estimation of absolute states of human skeletal muscle via B-mode ultrasound imaging and deep convolutional neural networks, *J. R. Soc. Interface*, 17, pp. 1-12.

Cutts, A. (1988) The range of sarcomere lengths in the muscles of the human lower limb., *J. Anat.*, 160, pp. 79-88.

Damon, B.M., Ding, Z., Anderson, A.W., Freyer, A.S., Gore, J.C. (2002) Validation of diffusion tensor MRI-based muscle fiber tracking, *Magn. Reson. Med.*, 48, pp. 97-104

Darby, J., Hodson-Tole, E.F., Costen, N., Loram, I.D. (2012) Automated regional analysis of B-mode ultrasound images of skeletal muscle movement., *J. Appl. Physiol.*, 112, pp. 313–327

Darby, J., Li, B., Costen, N., Loram, I., Hodson-Tole, E. (2013) Estimating skeletal muscle fascicle curvature from B-mode ultrasound image sequences, *IEEE Trans. Biomed. Eng.*, 60, pp. 1935-1945.

Dick, T. J. M., Biewener, A. A., Wakeling, J. M. (2017) Comparison of human gastrocnemius forces predicted by Hill-type muscle models and estimated from ultrasound images, *J. Exp. Biol.*, 220, pp. 1643-1653.

Dollar, A.M., Herr, H. (2008) Lower extremity exoskeletons and active orthoses: Challenges and state-of-the-art, *IEEE Trans. Robot.*, 24, pp. 144-158

Duda, R. O., Hart, P. E. (1972) Use of the Hough Transformation to Detect Lines and Curves in Pictures, *Commun. ACM*, 15, pp. 11-15.

Elliott, D.H. (1965) Structure and function of mammalian tendon, *Biol. Rev.*, 40, pp. 392-421.

Eng, C.M., Azizi, E., Roberts, T.J. (2018) Structural determinants of muscle gearing during dynamic contractions, *Integr. Comp. Biol.*, 58, pp. 207-218

Epstein, M., Herzog, W. (1998) *Theoretical Models of Skeletal Muscle Biological and Mathematical Considerations*. Chichester: Wiley.

Ettema, G. J. C., Huijing, P. A. (1994) Frequency response of rat gastrocnemius medialis in small amplitude vibrations, *J. Biomech.*, 27, pp. 1015-1022.

Di Fabio, R.P. (1987) Reliability of computerized surface electromyography for determining the onset of muscle activity, *Phys. Ther.*, 67, pp. 43-48

Faulkner, J.A., Gleadon, D., McLare, J., Jakeman, J.R. (2013) Effect of lower-limb compression clothing on 400-m sprint performance, *J. Strength Cond. Res.*, 27, pp. 669-676.

Fialka, O., Cadik, M. (2006) FFT and convolution performance in image filtering on GPU. *Tenth International Conference on Information Visualisation (IV'06)*, pp. 609-614.

Finni, T., Hodgson J.A., Lai A.M., Edgerton V.R., Sinha S., (2003). Mapping of movement in the isometrically contracting human soleus muscle reveals details of its structural and functional complexity. *J. Appl. Physiol.*, 95, pp. 2128-2133.

Fletcher, J. R., MacIntosh, B. R. (2018) Estimates of Achilles Tendon Moment Arm Length at Different Ankle Joint Angles: Effect of Passive Moment, *J. Appl. Biomech.*, pp. 1-22.

Folland, J. P., Williams, A. G. (2007) The adaptations to strength training: Morphological and neurological contributions to increased strength, *Sports Med.*, 37, pp. 145-168.

de Brito Fontana, H.D., Han, S., Sawatsky, A., Herzog, W., (2018). The mechanics of agonistic muscles. *J. Biomech.*, 79, 15-20.

de Brito Fontana, H., de Campos, D., Sawatsky, A., Han, S.W., Herzog, W. (2020) Why do muscles lose torque potential when activated within their agonistic group?, *J. Exp. Biol.*, 223, pp. 1-5

Fox, S. I. (2006) *Human Physiology*. Ninth. New York: McGraw-Hill.

Frangi, A. F., Niessen, W.J., Vincken, K.L., Viergever, M.A. (1998) Multiscale vessel enhancement filtering, *Medial Image Computing and Computer-Assisted Invervention - MICCAI'98. Lecture Notes in Computer Science*, 1496, pp. 130-137.

Friederich, J.A., Brand, R.A. (1990) Muscle fiber architecture in the human lower limb, *J. Biomech.*, 23, pp. 91-95.

Fukunaga, T., Ichinose, Y., Ito, M., Kawakami, Y., Fukashiro, S. (1997) Determination of fascicle length and pennation in a contracting human muscle in vivo, *rapid commun.*, 82, pp. 2941-2949

Fukunaga, T., Roy, R.R., Shellock, F.G., Hodgson, J.A., Edgerton, V.R. (1996) Specific tension of human plantar flexors and dorsiflexors., *J. Appl. Physiol.*, 80, pp. 158-165.

Fukunaga, T., Roy, R. R., Shellock, F.G., Hodgson, J.A., Day, M.K., Lee, P.L., Kwong-Fu, H., Edgerton, V.R. (1992) Physiological cross-sectional area of human leg muscles based on magnetic resonance imaging, *J. Orthop.*, 10, pp. 928-934.

Gans, C., Bock, W.J. (1965) The functional significance of muscle architecture - a theoretical analysis, *Rev. Anat. Embryol. Cell Biol.*, 38, pp. 115-142

Geerligs, M., Peters, G.W.M., Ackermans, P.A.J., Oomens, C.W.J., Baaijens, F.P.T. (2008) Linear viscoelastic behavior of subcutaneous adipose tissue, *Biorheology*, 45, pp. 677-688.

Gefen, A., Megido-Ravid, M., Itzchak, Y., Arcan, M. (2000) Biomechanical analysis of the three-dimensional foot structure during gait: A basic tool for clinical applications, *J. Biomech. Eng.*, 122, pp. 630-639.

Gennisson, J. L., Deffieux, T., Macé, E., Montaldo, G., Fink, M., Tanter, M. (2010) Viscoelastic and anisotropic mechanical properties of in vivo muscle tissue assessed by supersonic shear imaging, *Ultrasound Med. Biol.*, 36, pp. 789-801.

Gerus, P., Rao, G., Berton, E. (2015) Ultrasound-based subject-specific parameters improve fascicle behaviour estimation in Hill-type muscle model, *Comput. Methods Biomech Biomed. Engin.*, pp. 116-123

Gielen, A.W.J., Oomens, C.W.J., Bovendeerd, P.H.M., Arts, T., Janssen, J.D. (2000) A finite element approach for skeletal muscle using a distributed moment model of contraction, *Comput. Methods Biomech Biomed. Engin.*, 3, pp. 231-244

Gillies, A. R., Lieber, R.L. (2011) Method for decellularizing skeletal muscle without detergents or proteolytic enzymes, *Tissue Engineering - Part C: Methods*, 17, pp. 383-389.

Goodpaster, B. H., Theriault, R., Watkins, S.C., Kelley, D.E. (2000) Intramuscular lipid content is increased in obesity and decreased by weight loss, *Metabol. Clin. Exp.*, 49, pp. 467-472.

Gordon, A. M., Homsher, E., Regnier, M. (2000) Regulation of contraction in striated muscle, *Physiol. Rev.*, 80, pp. 853-924.

Gordon, A.M., Huxley, A.F., Julian, F.J., (1966). The variation in isometric tension with sarcomere length in vertebrate muscle fibres. *J. Physiol.*, 184, 170-192.

Hara, H., Hamanaka, N., Yoshida, M., Ikehata, N., Tachibana, S., Nakakawaji, K., Mihara, M. (2019) Variability in compression pressure of multi-layer bandaging applied by lymphedema therapists, *Support. Care Cancer*, 27, pp. 959-963

Heinemeier, K.M., Olesen, J.L., Haddad, F., Langberg, H., Kjaer, M, Baldwin, K.M., Scherling, P. (2007) Expression of collagen and related growth factors in rat tendon and skeletal muscle in response to specific contraction types, *J. Physiol.*, 582, pp. 1303-1316

van der Helm, F. C. T. (1994) A finite element musculoskeletal model of the shoulder mechanism, *J. Biomech.*, 27, pp. 551-569.

Herbert, R. D., Moseley, A.M., Butler, J.E., Gandevia, S.C. (2002) Change in length of relaxed muscle fascicles and tendons with knee and ankle movement in humans, *J. Physiol.*, 539.2, pp. 637-645.

Herbert, R.D., Gandevia S.C., (1995). Changes in pennation with joint angle and muscle torque: in vivo measurements in human brachialis muscle. *J. Physiol.*, 484, 523-532.

Herbert, R. D., Moseley, A.M., Butler, J.E., Gandevia, S.C. (2002) Change in length of relaxed muscle fascicles and tendons with knee and ankle movement in humans, *J. Physiol.*, 539, pp. 637-645.

Hill, A.V (1951) The effect of series compliance on the tension developed in a muscle twitch, *Proc. R. Soc. B Biol. Sci.*, 138, pp. 325-329

Hill, A.V., (1948). The pressure developed in muscle during contraction. *J. Physiol.*, 107, 518-526.

Hill, A. V., (1938). The heat of shortening and the dynamic constants of muscle. *Proc. R. Soc. B Biol. Sci.*, 126, 136-195.

Hirata, K., Kanehisa, H., Miyamoto, N. (2017) Acute effect of static stretching on passive stiffness of the human gastrocnemius fascicle measured by ultrasound shear wave elastography, *Eur. J. Appl. Physiol.*, 117, pp. 493-499

Hodges, P.W., Bui, B.H. (1996) A comparison of computer-based methods for the determination of onset of muscle contraction using electromyography, *Electroencephalogr. Clin. Neurophysiol.*, 101, pp. 511-519

Hodson-Tole, E. F., Lai, A. K. M. (2019) Ultrasound-derived changes in thickness of human ankle plantar flexor muscles during walking and running are not homogeneous along the muscle mid-belly region, *Sci. Rep*., 9, pp. 1-11.

Hodson-Tole, E. F., Wakeling, J. M., Dick, T. J. M. (2016) Passive muscle-tendon unit gearing is joint dependent in human medial gastrocnemius, *Front. Physiol.*, 7, pp. 1–8.

Holt, N.C., Danos, N., Roberts, T.J., Azizi, E. (2016) Stuck in gear: age-related loss of variable gearing in skeletal muscle, *J. Exp. Biol.*, 219, pp. 998-1003

Holt, N. C., Azizi, E. (2016) The effect of activation level on muscle function during locomotion: Are optimal lengths and velocities always used?, *Proc. Royal Soc. B*, 283, pp. 1-7.

Hough, P. V. C. (1962) A method and means for recognition complex patterns, *US Patent*.

Hutchinson, J.R., Rankin, J.W., Rubenson, J., Rosenbluth, K.H., Siston, R.A., Delp, S.L. (2015) Musculoskeletal modelling of an ostrich (Struthio camelus) pelvic limb: Influence of limb orientation onmuscular capacity during locomotion, *PeerJ*, 2015, pp. 1-52

Hutton, D. V. (2004) *Fundamentals of Finite Element Analysis*. New York: McGraw-Hill.

Huxley, A. F., Niedergerke, R. (1954) Interference microscopy of living muscle fibres, *Nature*, 173, pp. 971-973.

Huxley, H., Hanson, J. (1954) Changes in cross-striations of muscle during contractions and stretch and their structural interpretation, *Nature*, 173, pp. 973-976.

Illingworth, J., Kittler, J. (1988) A survey of the hough transform, *Comput. Vis. Graph. Image Process.*, 44, pp. 87-116.

Infantolino, B.W., Neuberger, T., Challis, J.H., (2012). The arrangement of fascicles in whole muscle. *Anat. Rec.*, 295, 1174-1180.

Irving, T.C., Konhilas, J., Perry, D., Fischetti, R., de Tombe, P.P. (2000) Myofilament lattice spacing as a function of sarcomere length in isolated rat myocardium, *Am. J. Physiol. Heart Circ. Physiol.*, 279, pp. 2568-2573.

Ivanenko, Y. P., Poppele, R. E., Lacquaniti, F. (2004) Five basic muscle activation patterns account for muscle activity during human locomotion, *J. Physiol.*, 556, pp. 267-282.

James, J. F. (2011) *A Student's Guide to Fourier Transforms*. Third. Cambridge: Cambridge University Press.

Jenkyn, T.R., Koopman, B., Huijing, P., Lieber, R.L., Kaufman, K.R. (2002) Finite element model of intramuscular pressure during isometric contraction of skeletal muscle, *Phys. Med. Biol.*, 47, pp. 4043-4061

Jiang, H., van Zijl, P.C.M., Kim, J., Pearlson, G.D., Mori, S. (2006) DtiStudio: Resource program for diffusion tensor computation and fiber bundle tracking, *Comput. Methods Programs Biomed.*, 81, pp. 106-116.

Johansson, T., Meier, P., Blickhan, R. (2000) A finite-element model for the mechanical analysis of skeletal muscles, *J. Theor. Biol.*, 206, pp. 131-149

Katz, B. (1939) The relation between force and speed in muscular contraction, *The J. Physiol.*, 96, pp. 45-64.

Kawakami, Y., Abe T., Kuno S., Fukunaga T., (1995). Training-induced changes in muscle architecture and specific tension. Eur. *J. Appl. Physiol. Occup. Physiol.*, 72, 37-43.

Kawakami, Y., Fukunaga, T., (2006). New insights into in vivo human skeletal muscle function. *Exerc. Sport Sci. Rev.*, 34, 16-21.

Kawakami, Y., Ichinose, Y., Fukunaga, T. (1998) Architectural and functional features of human triceps surae muscles during contraction., *J. Appl. Physiol.*, 85, pp. 398-404.

Kawakami, Y., Abe, T., Fukunaga, T. (1993) Muscle-fiber pennation angles are greater in hypertrophied than in normal muscles, *J. Appl. Physiol.*, 74, pp. 2740-2744

Kim, J., Heshka, S., Gallagher, D., Kotler, D.P., Mayer, L., Albu, J., Shen, W., Freda, P.U., Heymsfield, S.B. (2004) Intermuscular adipose tissue-free skeletal muscle mass: Estimation by dual-energy X-ray absorptiometry in adults, *J. Appl. Physiol.*, 97, pp. 655-660.

Kinugasa, R., Yamamura, N., Sinha, S., Takagi, S. (2016) Influence of intramuscular fiber orientation on the Achilles tendon curvature using three-dimensional finite element modeling of contracting skeletal muscle, *J. Biomech.*, 49, pp. 3592-3595

Kjaer, M. (2004) Role of Extracellular Matrix in Adaptation of Tendon and Skeletal Muscle to Mechanical Loading, *Physiol. Rev.*, 84, pp. 649-698.

Kjær, M., Langberg, H., Heinemeier, K., Bayer, M.L., Hansen, M., Holm, L., Doessing, S., Kongsgaard, M., Krogsgaard, M.R., Magnusson, S.P. (2009) From mechanical loading to collagen synthesis, structural changes and function in human tendon, *Scand. J. Med. Sci. Sports*, 19, pp. 500-510

Kojic, M., Mijailovic, S., Zdravkovic, N. (1998) Modelling of muscle behaviour by the finite element method using hills three-element model, *Int. J. Numer. Meth. Eng.*, 43, pp. 941-953

Komi, P. V (1990) Relevance of in vivo force measurements to human biomechanics, *J. Biomech.*, 23, pp 23-34.

Konow, N., Collias, A., Biewener, A.A. (2020) Skeletal Muscle Shape Change in Relation to Varying Force Requirements Across Locomotor Conditions, *Front. Physiol.*, 11, pp. 1-11

Kragstrup, T. W., Kjaer, M., Mackey, A. L. (2011) Structural, biochemical, cellular, and functional changes in skeletal muscle extracellular matrix with aging, *Scand. J. Med. Sci. Spor.*, 21, pp. 749-757.

Labeit, S., Kolmerer, B. (2014) Titins : Giant Proteins in Charge of Muscle Ultrastructure and Elasticity, *Science*, 270, pp. 293-296.

Lansdown, D.A., Ding Z., Wadington M., Hornberger J.L., Damon B.M., (2007). Quantitative diffusion tensor MRI-based fiber tracking of human skeletal muscle. *J. Appl. Physiol.*, 103, 673-681.

Lee, S.S.M., Arnold, A.S., de Boef Miara, M., Biewener, A.A., Wakeling, J.M. (2013) Accuracy of gastrocnemius muscles forces in walking and running goats predicted by one-element and two-element Hill-type models, *J. Biomech.*, 46, pp. 2288-2295

van Leeuwen, J. L., Spoor, C. W. (1992) Modelling mechanically stable muscle architectures, *Philos. T. R. Soc.*, 336, pp. 275-292.

Li, H., Linke W.A., Oberhauser, A.F., Carrion-Vasquez, M., Kerkvliet, J.G., Lu, H., Marszalek, P.E., Fernandez, J.M. (2002) Reverse engineering of the giant muscle protein titin, *Nature*, 418, pp. 998-1002.

Li, L., Tong, K.Y., Hu, X.L., Hung, L.K., Koo, T.K.K. (2009) Incorporating ultrasound-measured musculotendon parameters to subject-specific EMG-driven model to simulate voluntary elbow flexion for persons after stroke, *Clin.l Biomech.*, 24, pp. 101-109

Lichtwark, G. A., Wilson, A. M. (2008) Optimal muscle fascicle length and tendon stiffness for maximising gastrocnemius efficiency during human walking and running, *J. Theor. Biol.*, 252, pp. 662-673.

Lichtwark, G.A., Bougoulias, K., Wilson, A.M. (2007) Muscle fascicle and series elastic element length changes along the length of the human gastrocnemius during walking and running, *J. Biomech.*, 40, pp. 157-164

Lichtwark, G.A., Wilson, A.M. (2005) A modified Hill muscle model that predicts muscle power output and efficiency during sinusoidal length changes, *J. Exp. Biol.*, 208, pp. 2831-2843

Lieber, R. L., Fridén, J. (2000) Functional and Clinical Significance of skeletal muscle architecture, *Muscle Nerve*, 23, pp. 1647-1666

Linder-Ganz, E., Shabshin, N., Itzchak, Y., Gefen, A. (2007) Assessment of mechanical conditions in sub-dermal tissues during sitting: A combined experimental-MRI and finite element approach, *J. Biomech.*, 40, pp. 1443-1454

Lloyd, D. G., Besier, T. F. (2003) An EMG-driven musculoskeletal model to estimate muscle forces and knee joint moments in vivo, *J. Biomech.*, 36, pp. 765-776.

Logan, D. L. (2007) *A First Course in the Finite Element Method*. fourth. Toronto: Thomson.

van Loocke, M., Lyons, C.G., Simms, C.K., (2008). Viscoelastic properties of passive skeletal muscle in compression: Stress-relaxation behaviour and constitutive modelling. *J. Biomech.*, 41, 1555-1566.

Maganaris, C.N., (2003). Force-length characteristics of the in vivo human gastrocnemius muscle. *Clin. Anat.*, 16, 215-223.

Maganaris, C.N., Baltzopoulos, V. (1998) Changes in Achilles tendon moment arm from rest to maximum isometric plantarflexion, *J. Physiol.*, 510, pp. 977-985.

Maganaris, C.N., Baltzopoulos, V., Sargeant, A.J. (2002) Repeated contractions alter the geometry of human skeletal muscle., *J. Appl. Physiol.*, 93, pp. 2089-2094.

Maganaris, C.N., Baltzopoulos, V., Sargeant, A.J., (1998). In vivo measurements of the triceps surae complex architecture in man: Implications for muscle function. *J. Physiol.*, 512, 603-614.

Magnusson, S.P., Hansen, P., Aagaard, P., Brønd, J., Dyhre-Poulsen, P, Bojsen-Moller, J., Kjaer, M. (2003) Differential strain patterns of the human gastrocnemius aponeurosis and free tendon, in vivo, *Acta Physiol. Scand.*, 177, pp. 185-195

Mayfield, D.L., Lichtwark, G.A., Cronin, N.J., Avela, J., Cresswell, A.G. (2015) Doublet potentiation in the triceps surae is limited by series compliance and dynamic fascicle behavior, *J. Appl. Physiol.*, 119, pp. 807-816

Mayfield, D.L., Launikonis, B.S., Cresswell, A.G., Lichtwark, G.A. (2016) Additional in-series compliance reduces muscle force summation and alters the time course of force relaxation during fixed-end contractions, *J. Exp. Biol.*, 219, pp. 3587-3596

McLean, L., Goudy, N. (2004) Neuromuscular response to sustained low-level muscle activation: within- and between-synergist substitution in the triceps surae muscles, *Eur. J. Appl. Physiol.*, 91, pp. 204-216.

Millman, B.M. (1998) The filament lattice of striated muscle, *Physiol. Rev.*, 78, pp. 359-391

Miyoshi, T., Kihara, T., Koyama, H., Yamamoto, S.I., Komeda, T. (2009) Automatic detection method of muscle fiber movement as revealed by ultrasound images, *Med. Eng. Phys.*, 31, pp. 558-564

Mohammadkhah, M., Murphy, P., Simms, C.K. (2016) The in vitro passive elastic response of chicken pectoralis muscle to applied tensile and compressive deformation, *J. Mech. Behav. Biomed. Mater.*, 62, pp. 468-480

Moore, C.L., Copel, J.A. (2011) Point-of-Care Ultrasonography, *N. Engl. J. Med.*, 364, pp. 749-757.

Mori, S., van Zijl, P.C.M. (2002) Fiber tracking: principles and strategies - a technical review, *NMR Biomed.*, 15, pp. 468-480.

Moss, R.L. (1979) Sarcomere length-tension relations of frog skinned muscle fibres during calcium activation at short lengths, *J. Physiol.*, 292, pp. 177-192.

Muramatsu, T., Muraoka, T., Kawakami, Y., Shibayama, A., Fukunaga, T. (2002) In vivo determination of fascicle curvature in contracting human skeletal muscles, *J. Appl. Physiol.*, 92, pp. 129-134.

Namburete, A.I.L., Rana, M. and Wakeling, J.M. (2011) Computational methods for quantifying in vivo muscle fascicle curvature from ultrasound images, *J. Biomech.*, 44, pp. 2538-2543.

Narici, M.V., Binzoni T., Hiltbrand E., Fasel J., Terrier F., Cerretelli P., (1996). In vivo human gastrocnemius architecture with changing joint angle at rest and during graded isometric contraction. *J. Physiol.*, 496, 287-297.

Nevill, A.M., Stewart, A.D., Olds, T., Holder, R. (2004) Are adult physiques geometrically similar? The dangers of allometric scaling using body mass power laws, *Am. J. Phys. Anthropol.*, 124, pp. 177-182.

Nielsen, P.M.F., le Grice, I.J., Smail, B.H., Hunter, P.J. (1991) Mathematical model of geometry and fibrous structure of the heart, *Am. J. Physiol. Heart Circ. Physiol.*, 260, pp 1365-1378.

Nishimura, T., Hattori, A., Takahashi, K. (1994) Ultrastructure of the Intramuscular Connective Tissue in Bovine Skeletal Muscle, *Cells Tissues Organs*, 151, pp. 250-257.

O'Neill, M.C., Lee, L.F., Larson, S.G., Demes, B., Stern, J.T., Umberger, B.R. (2013) A three-dimensional musculoskeletal model of the chimpanzee (Pan troglodytes) pelvis and hind limb, *J. Exp. Biol.*, 216, pp. 3709-3723

Oehlert, G. (2010) A first course in design and analysis of experiments. W.H. Freeman. (Creative Commons License) http://users.stat.umn.edu/~gary/Book.html.

Ohtani, O., Ushiki, T., Taguchi, T., Kikuta, A. (1988) Collagen Fibrillar Networks as Skeletal Frameworks: A Demonstration by Cell-Maceration/Scanning Electron Microscope Method, *Arch. Histol. Cytol.*, 51, pp. 249-261

Olszewski, K., Dick, T.J.M., Wakeling, J.M. (2015) Achilles tendon moment arms: The importance of measuring at constant tendon load when using the tendon excursion method, *J. Biomech.*, 48, pp. 1206-1209.

Oomens, C.W.J., Maenhout, M., van Oijen, C.H., Drost, M.R., Baaijens, F.P. (2003) Finite element modelling of contracting skeletal muscle, *Philos. Trans. R. Soc. B: Biol. Sci.*, 358, pp. 1453-1460

Pandy, M.G., Zajac, F.E., Sim, E., Levine, W.S. (1990) An optimal control model for maximum-height human jumping, *J. Biomech.*, 23, pp. 1185-1198.

Pelteret, J., McBride, A. (2012) The deal.II tutorial step-44: Three-field formulation for non-linear solid mechanics, *Zenodo*.

Pillen, S., Arts, I.M.P., Zwarts, M.J. (2008) Muscle ultrasound in neuromuscular disorders, *Muscle Nerve*, 37, pp. 679-693.

Podlozhnyuk, V. (2007) Image convolution with CUDA. *NVIDIA Corporation white paper*. 2097.

Powell, P.L., Roy, R.R., Kanim, P., Bello, M.A., Edgerton, V.R. (1984) Predictability of skeletal muscle tension from architectural determinations in guinea pig hindlimbs, *J. Appl. Physiol. Respir. Environ. Exerc. Physiol.*, 57, pp. 1715-1721.

Purslow, P.P. (2010) Muscle fascia and force transmission, *J. Bodyw. Mov. Ther.*, 14, pp. 411-417.

Purslow, P.P., Trotter, J.A. (1994) The morphology and mechanical properties of endomysium in series-fibred muscles: variations with muscle length, *J. Muscle Res. Cell M.,* 15, pp. 299-308.

Rack, P.M.H., Westbury, D.R. (1969) The effects of length and stimulus rate on tension in the isometric cat soleus muscle, *J. Physiol.*, 204, pp. 443-460.

Rahemi, H. (2015) Structural Mechanics of Skeletal Muscles Contractions: Mechanistic Findings Using a Finite. PhD Thesis.

Rahemi, H., Nigam, N., Wakeling, J.M. (2015) The effect of intramuscular fat on skeletal muscle mechanics: implications for the elderly and obese., *J. R. Soc. Interface*, 12, pp. 1-8.

Rahemi, H., Nigam, N., Wakeling, J.M., (2014). Regionalizing muscle activity causes changes to the magnitude and direction of the force from whole muscles – a modelling study. *Front. Physiol.*, 5, 1-10.

Ramsey, R.W., Street, S.F. (1940) The isometric length-tension diagram of isolated skeletal muscle fibers of the frog, *J. Cell. Physiol.*, 15, pp. 11-34.

Rana, M., Hamarneh, G., Wakeling, J.M. (2014) 3D curvatures of muscle fascicles in triceps surae., *J. Appl. Physiol.*, 117, pp. 1388-1397.

Rana, M., Hamarneh, G., Wakeling, J.M., (2013). 3D fascicle orientations in triceps surae. *J. Appl. Physiol.*, 115, 116-125.

Rana, M., Hamarneh, G., Wakeling, J.M., (2009). Automated tracking of muscle fascicle orientation in B-mode ultrasound images. *J. Biomech.*, 42, 2068-2073.

Rana, M., Wakeling, J.M., (2011). In-vivo determination of 3D muscle architecture of human muscle using free hand ultrasound. *J. Biomech.*, 44, 2129-2135.

Randhawa, A., Wakeling, J.M. (2015) Multidimensional models for predicting muscle structure and fascicle pennation, *J. Theor. Biol.*, 382, pp. 57-63.

Randhawa, A., Wakeling, J.M. (2018) Transverse anisotropy in the deformation of the muscle during dynamic contractions, *J. Exp. Biol.*, 221, pp 1-12.

Randhawa, A., Wakeling, J.M., (2013). Associations between muscle structure and contractile performance in seniors. *Clin. Biomech.*, 28, 705-711.

Rehorn, M.R., Blemker, S.S. (2010) The effects of aponeurosis geometry on strain injury susceptibility explored with a 3D muscle model, *J. Biomech.*, 43, pp. 2574-2581

Reinhardt, L., Siebert, T., Leichsenring, K., Blickhan, R., Böl, M., (2016). Intermuscular pressure between synergistic muscles correlates with muscle force. *J. Exp. Biol.*, 219, 2311-2319.

Rennerfelt, K., Lindorsson, S., Brisby, H., Baranto, A., Zhang, Q. (2019) Effects of Exercise Compression Stockings on Anterior Muscle Compartment Pressure and Oxygenation During Running: A Randomized Crossover Trial Conducted in Healthy Recreational Runners, *Sports Med.*, 49, pp. 1465-1473.

Rode, C., Siebert, T., Blickhan, R. (2009) Titin-induced force enhancement and force depression: A “sticky-spring” mechanism in muscle contractions?, *J. Theor. Biol*., 259, pp. 350-360.

Röhrle, O., Pullan, A.J. (2007) Three-dimensional finite element modelling of muscle forces during mastication, *J. Biomech.*, 40, pp. 3363-3372

Ross, S.A., Ryan, D.S., Dominguez, S., Nigam, N. ,Wakeling, J.M. (2018) Size, history-dependent, activation and three-dimensional effects on the work and power produced during cyclic muscle contractions, *Integr. Comp. Biol.*, 58, pp 232-250

Ross, S.A., Wakeling, J.M. (2016) Muscle shortening velocity depends on tissue inertia and level of activation during submaximal contractions, *Biol. Lett.*, 12, p. 1-4.

Rowe, R. W. D. (1981) Morphology of perimysial and endomysial connective tissue in skeletal muscle, *Tissue and Cell*, 13, pp. 681-690

Ryan, D.S., Stutzig, N., Siebert, T., Wakeling, J.M. (2019) Passive and dynamic muscle architecture during transverse loading for gastrocnemius medialis in man, *J. Biomech.*, 86, pp. 160-166.

Ryu, J., Nishimura, T.H. (2009) Fast image blurring using Lookup Table for real time feature extraction. *2009 IEEE International Symposium on Industrial Electronics*, pp. 1864-1869.

Sandercock, T.G., Heckman, C.J. (1997) Doublet potentiation during eccentric and concentric contractions of cat soleus muscle, *J. Appl. Physiol.*, 82, pp. 1219-1228.

Sawicki, G.S., Beck, O.N., Kang, I., Young, A.J. (2020) The exoskeleton expansion: Improving walking and running economy, *J. NeuroEng. Rehabil*., 17, pp. 1-9

Schenk, P., Siebert, T., Hiepe, P., Güllmar, D., Reichenbach, J.R., Wick, C., Blickhan, R., Böl, M., (2013). Determination of three-dimensional muscle architectures: Validation of the DTI-based fiber tractography method by manual digitization. J. Anat., 223, 61-68.

Schindelin, J., Arganda-Carreras, I., Frise, E., Kaynig, V., Longair, M., Pietzsc, T., Preibisch, S., Rueden, C., Saalfeld, S., Schmid, B., Tinevez, J., White, D.J., Hartenstein, V., Eliceiri, K., Tomancak, P., Cardona, A. (2009) ‘Fiji - an Open platform for biological image analysis’, *Nat. Methods*, 9.

Schmid, L., Klotz, T., Siebert, T., Röhrle, O. (2019) Characterization of Electromechanical Delay Based on a Biophysical Multi-Scale Skeletal Muscle Model, *Front. Physiol.*, 10

Sejersted, O.M., Hargens, A.R., Kardel, K.R., Blom, P., Jensen, Ø., Hermansen L. (1984) Intramuscular fluid pressure during isometric contraction of human skeletal muscle, *J. Appl. Physiol. Respir. Environ. Exerc. Physiol.*, 56, pp. 287-295.

Seydewitz, R., Siebert, T., Böl, M. (2019) On a three-dimensional constitutive model for history effects in skeletal muscles, *Biomech. Model. Mechanobiol.*, 18, pp. 1665-1681.

Shen, B. and Sethi, I.K. (1996) Convolution-based edge detection for image/video in block DCT domain. *J. Vis. Commun. Image R.*, 7, pp. 411-423.

Siebert, T., Eb, E., Ryan, D.S., Wakeling, J.M., Stutzig, N. (2018) Impact of multidirectional transverse calf muscle loading on calf muscle force in young adults, *Front. Physiol.*, 9, pp. 1-8.

Siebert, T., Günther, M., Blickhan, R. (2012) A 3D-geometric model for the deformation of a transversally loaded muscle, *J. Theor. Biol*., 298, pp. 116-121.

Siebert, T., Rode, C., Till, O., Stutzig, N., Blickhan, R., (2016). Force reduction induced by unidirectional transversal muscle loading is independent of local pressure. *J. Biomech.*, 49, 1156-1161.

Siebert, T., Stutzig, N., Rode, C., (2018). A hill-type muscle model expansion accounting for effects of varying transverse muscle load. *J. Biomech.*, 66, 57-62.

Siebert, T., Till, O., Stutzig, N., Gunther M., Blickhan R., (2014a). Muscle force depends on the amount of transversal muscle loading. *J. Biomech.*, 47, 1822-1828.

Siebert, T., Till, O., Blickhan, R., (2014b). Work partitioning of transversally loaded muscle: experimentation and simulation. *Comput. Methods Biomech. Biomed. Engin.*, 17, 217-229.

Sinha, R., Dufour, S., Petersen, K.F., LeBon, V., Enoksson, S., Ma, Y., Savoye, M., Rothman, D.L., Shulman, G.I., Caprio, S. (2002) Assessment of Skeletal Muscle Triglyceride Content by 1H Nuclear Magnetic Resonance Spectroscopy in Lean and Obese Adolescents, *Diabetes*, pp. 1022-1027.

Sinha, S., Sinha, U., Edgerton, V.R. (2006) In vivo diffusion tensor imaging of the human calf muscle, *J. Magn. Reson. Imaging*, 24, pp. 182-190

Sirin, A.V., Patla, A.E. (1987) Myoelectric changes in the triceps surae muscles under sustained contractions - Evidence for synergism, *Eur. J. Appl. Physiol.*, 56, pp. 238-244.

Sleboda, D.A., Roberts, T.J. (2019) Internal fluid pressure influences muscle contractile force, *Proc. Natl. Acad. Sci.*, pp 1772-1778.

Sleboda, D.A., Roberts, T.J., (2017). Incompressible fluid plays a mechanical role in the development of passive muscle tension. *Biol. Lett.*, 13, 1-5.

Soeller, C. and Cannell, M.B. (1999) 'Examination of the transverse tubular system in living cardiac rat myocytes by 2-photon microscopy and digital image-processing techniques', *Circ. Res.*, 84, pp. 266–275

Sperlich, B., Haegele, M., Achtzehn, S., Linville, J., Holmberg, H.C., Mester, J. (2010) Different types of compression clothing do not increase sub-maximal and maximal endurance performance in well-trained athletes, *J. Sports Sci.*, 28, pp. 609-614

Stark, H., Schilling, N. (2010) A novel method of studying fascicle architecture in relaxed and contracted muscles, *J. Biomech.*, 43, pp. 2897-2903

Stefanati, M. Villa, C., Torrente, Y., Matas, J.F.R. (2020) A mathematical model of healthy and dystrophic skeletal muscle biomechanics, *J. Mech. Phys. Solids*, 134

Stokes, I.A.F., Gardner-Morse, M., Henry, S.M., Badger, G.J. (2000) Decrease in trunk muscular response to perturbation with preactivation of lumbar spinal musculature, *Spine*, 25, pp. 1957-1964

Stutzig, N., Ryan, D., Wakeling, J.M., Siebert, T. (2019) Impact of transversal calf muscle loading on plantarflexion, *J. Biomech.*, 85, pp. 37-42.

Sylvest, O., Hvid, N. (1959) Pressure measurements in human striated muscles during contraction, *Scand. J. Rheumatol.*, 5, pp. 216-222.

Takaza, M., Moerman, K.M., Simms, C.K. (2013) Passive skeletal muscle response to impact loading: Experimental testing and inverse modelling, *J. Mech. Behav. Biomed. Mater.*, 27, pp. 214-225

Tang, C. Y., Zhang, G., Tsui, C. P. (2009) A 3D skeletal muscle model coupled with active contraction of muscle fibres and hyperelastic behaviour, *J. Biomech.*, 42, pp. 865-872

Teran, J., Blemker, S., Thow Ng Thow Hing, V., Fedkiw, R., (2003) Finite volume methods for the simulation of skeletal muscle, *Proceedings of the 2003 ACM SIGGRAPH/Eurographics Symposium on Computer Animation, SCA 2003*, pp. 68-75.

Ternifi, R., Kammoun, M., Pouletaut, P., Subramaniam, M., Hawse, J.R., Bensamoun, S.F. (2020) 'Ultrasound image processing to estimate the structural and functional properties of mouse skeletal muscle', *Biomed. Signal Process. Control*., 56, pp. 1-5.

Vettor, R., Milan, G., Franzin, C., Sanna, M., De Coppi, P., Rizzuto, R., Federspil, G. (2009) The origin of intermuscular adipose tissue and its pathophysiological implications, *Am. J. Physiol. Endocrinol. Metab.*, 297, pp. 987-998.

Vogel, S. (2003) *Comparative Biomechanics*. Princeton: Princeton University Press.

Wakeling, J.M., Lee, S.S.M., Arnold, A.S., de Boef Miara, M., Biewener, A.A. (2012) A muscle's force depends on the recruitment patterns of its fibers, *Ann. Biomed. Eng.*, 40, pp. 1708-1720

Wakeling, J.M., Jackman, M., Namburete, A.I., (2013). The effect of external compression on the mechanics of muscle contraction. *J. Appl. Biomech.*, 29, pp. 360-364.

Wakeling, J.M., Randhawa, A., (2014). Transverse strains in muscle fascicles during voluntary contraction: A 2D frequency decomposition of B-mode ultrasound images. *Int. J. Biomed. Imaging*, 2014, pp. 1-9.

Wakeling, J.M., Ross, S.A., Ryan, D.S., Bolsterlee, B., Konno, R., Dominguez, S., Nigam, N. (2020) The energy of muscle contraction. I. Tissue force and deformation during isometric contractions. Unpublished

Wang, H., Wu, Y., Lin, K., Shiang, T. (2009) Noninvasive analysis of fascicle curvature and mechanical hardness in calf muscle during contraction and relaxation, *Man. Ther.*, 14, pp. 264-269

Wick, C., Böl, M., Müller, F., Blickhan, R., Siebert, T., (2018). Packing of muscles in the rabbit shank influences three-dimensional architecture of M. soleus. *J. Mech. Behav. Biomed. Mater.*, 83, 20-27.

Wickiewicz, T.L., Roy, R.R., Powell, P.L., Edgerton, V.R. (1983) Muscle architecture of the human lower limb, *Clin. Orthop. Relat. Res.*, pp. 275-283.

Williamson, F. (1980) 'Richard courant and the finite element method: A further look', *Hist. Math.*, 7, pp. 369–378.

Winters, T.M., Takahashi, M., Lieber, R.L., Ward, S.R. (2011) Whole muscle length-tension relationships are accurately modeled as scaled sarcomeres in rabbit hindlimb muscles, *J. Biomech.*, 44, pp. 109-115.

Yeoh, O.H. (1993). Some forms of the strain energy function for rubber. *Rubber Chem. Tech.*, 66, 754-771

Yucesoy, C.A., Koopman, B.H.F.J.M., Huijing, P.A., Grootenboer, H.J. (2002) Three-dimensional finite element modeling of skeletal muscle using a two-domain approach: Linked fiber-matrix mesh model, *J. Biomech.*, 35, pp. 1253-1262

Zajac, F. E. (1989) Muscle and tendon: properties, models, scaling, and application to biomechanics and motor control., *Crit. Rev. Biomed. Eng.*, pp. 359-411.

Zhao, H., Zhang, L. (2011) Automatic Tracking of Muscle Fascicles in Ultrasound Images Using Localized Radon Transform. *IEEE Transactions on Biomedical Engineering*, 58, pp. 2094-2101.

Zhou, Y., Zheng, Y. P. (2008) Estimation of Muscle Fiber Orientation in Ultrasound Images Using Revoting Hough Transform (RVHT), *Ultrasound Med. Biol.*, 34, pp. 1474-1481

Appendix

The data collected from the computational experiments performed using the finite element method were more extensive than what was presented in chapter 4. To give a full representation of the data collected we include this appendix. Shown are the least square means of the energy, force, fibre stretch, pressure, volume, pennation angle, and muscle strain which are plotted against the activation, compression, initial pennation angle, and initial muscle length. The results are shown for loading from all directions (Figure A1-A2), loading from top (Figure A3-A4), loading from the side (Figure A5-A6), and no loading (Figure A7-A8).

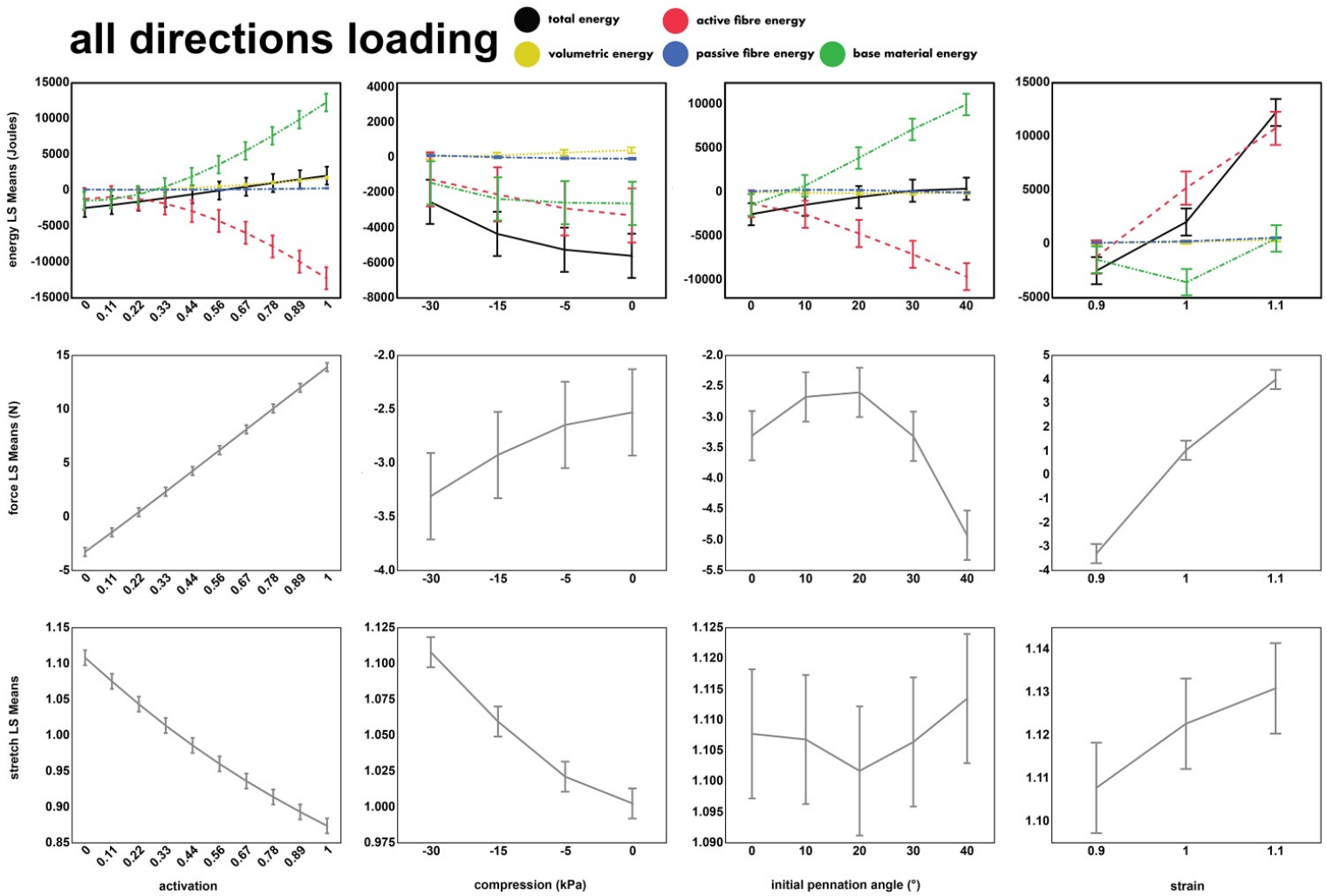

Figure A1 **Main effects plots for the muscle models loaded from all directions. The figure shows the energies, forces, and stretch as a function of activation, compression, initial pennation angle, and initial muscle length. Error bars represent the standard error of the least squares means.**

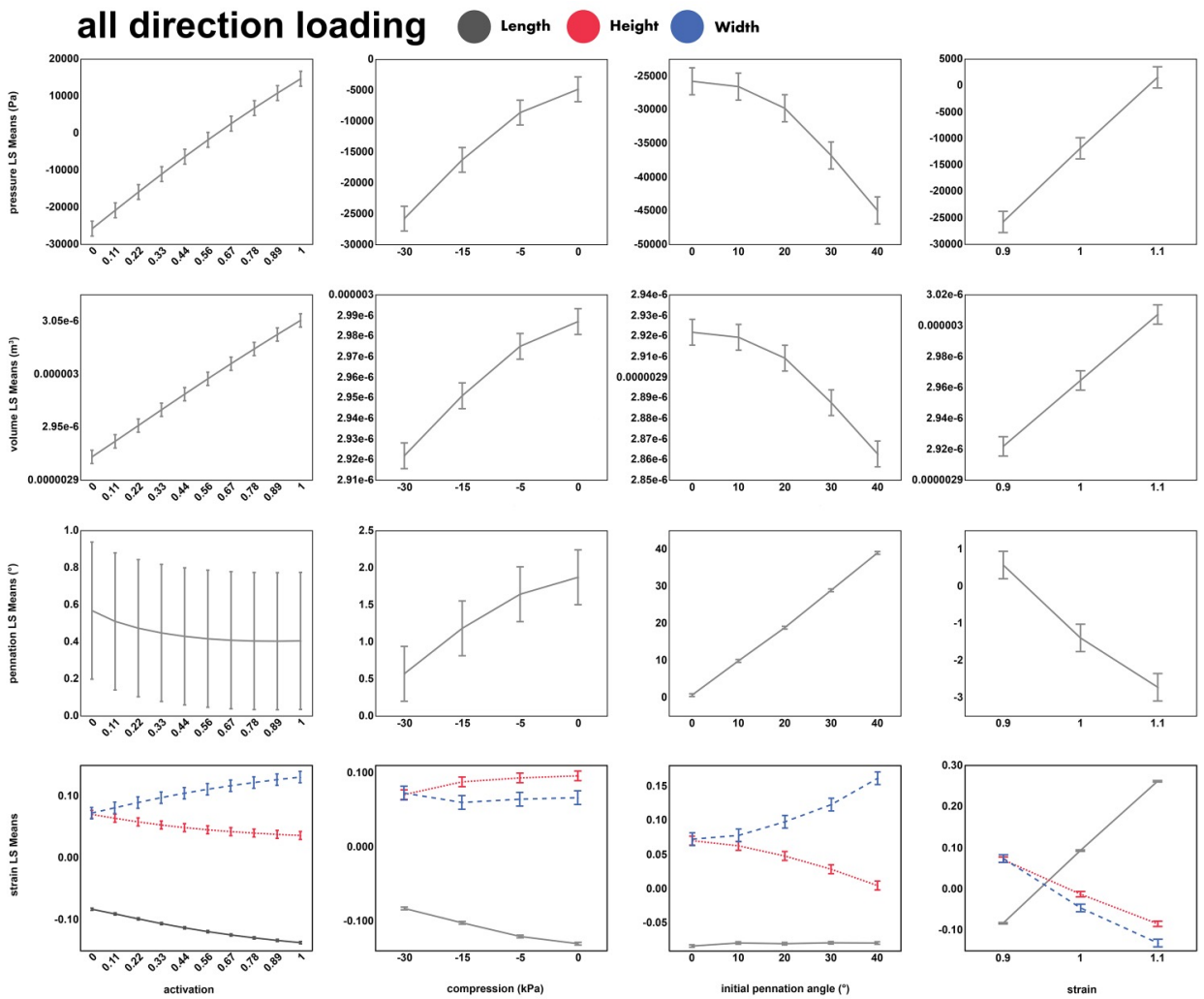

Figure A2 **Main effects plots for the muscle models loaded from all directions. The figure shows the pressure, volume, pennation angle and strain as a function of activation, compression, initial pennation angle, and initial muscle length. Error bars represent the standard error of the least squares means.**

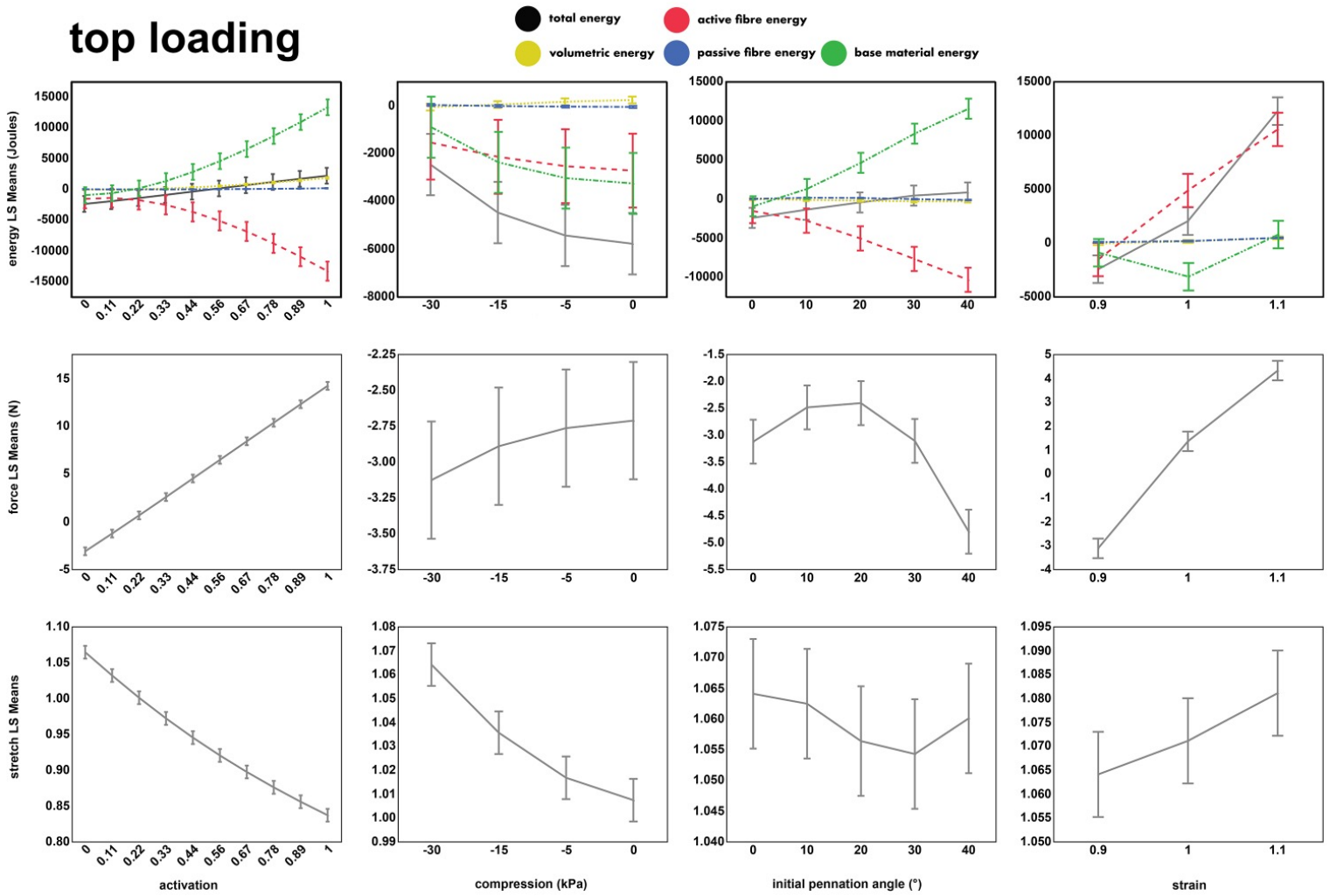

Figure A3 **Main effects plots for the muscle models loaded from the top. The figure shows the energies, forces, and stretch as a function of activation, compression, initial pennation angle, and initial muscle length. Error bars represent the standard error of the least squares means.**

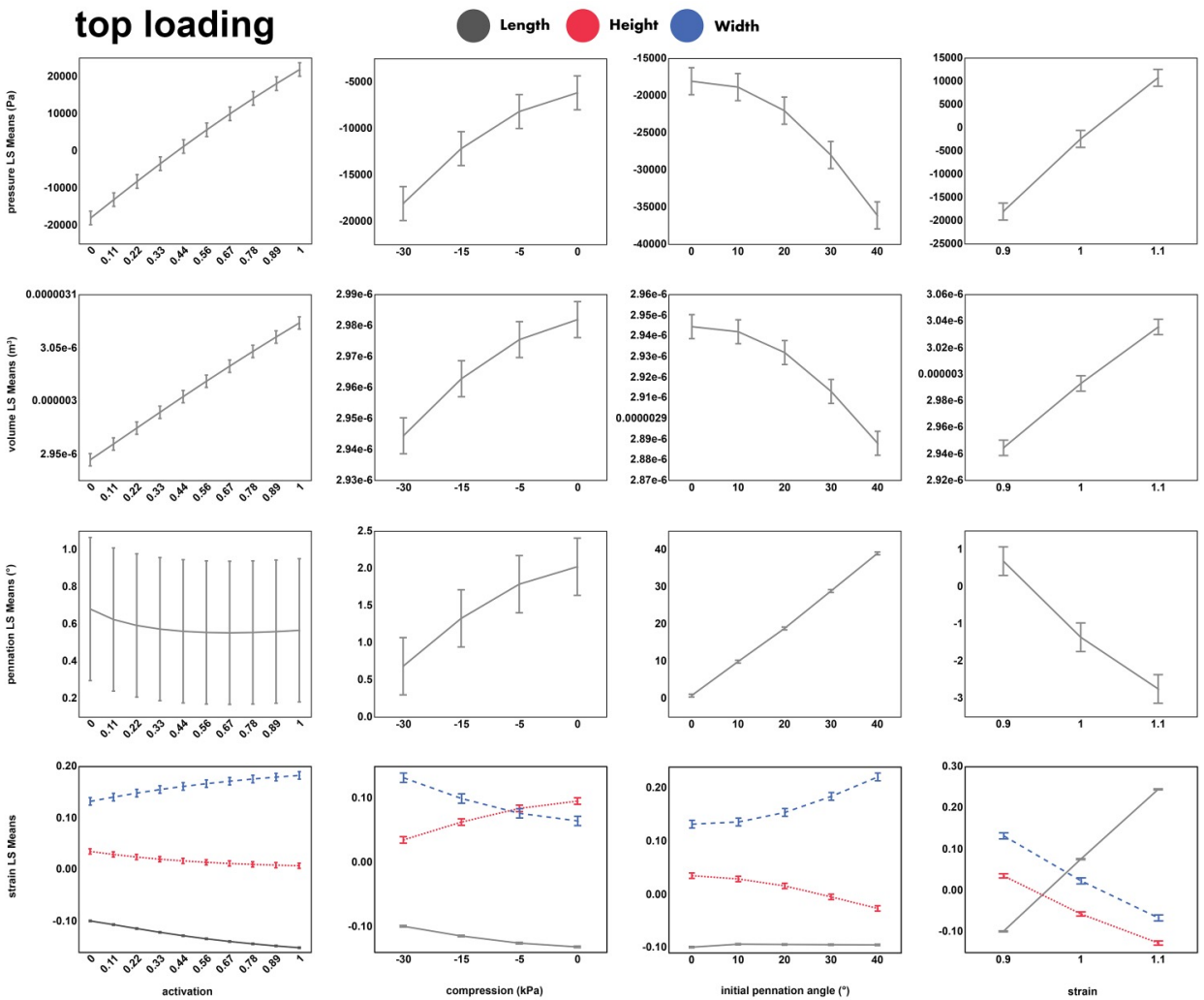

Figure A4 **Main effects plots for the muscle models loaded from the top. The figure shows the pressure, volume, pennation angle and strain as a function of activation, compression, initial pennation angle, and initial muscle length. Error bars represent the standard error of the least squares means.**

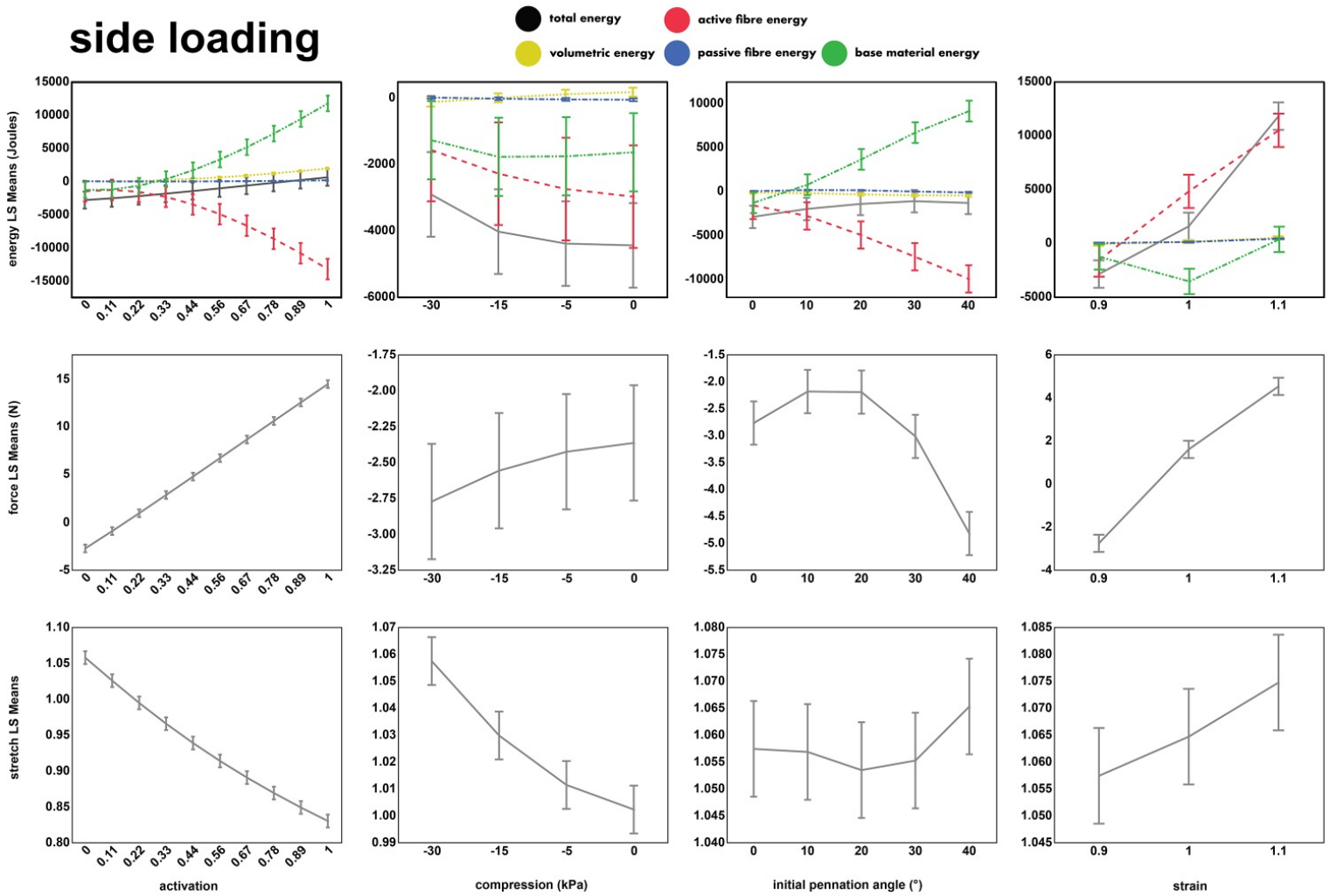

Figure A5 **Main effects plots for the muscle models loaded from the side. The figure shows the energies, forces, and stretch as a function of activation, compression, initial pennation angle, and initial muscle length. Error bars represent the standard error of the least squares means.**

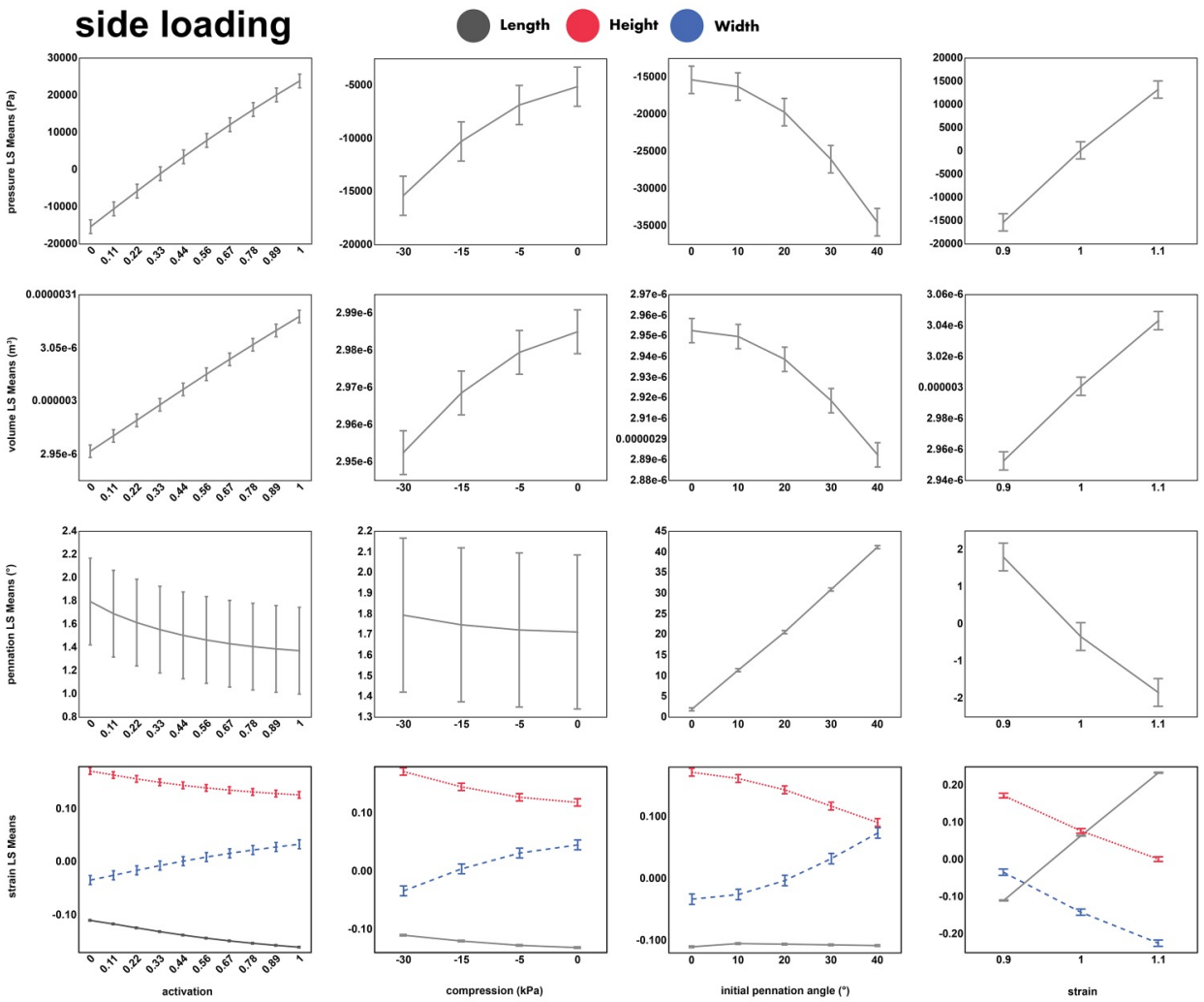

Figure A6 **Figure A2 Main effects plots for the muscle models loaded from the side. The figure shows the pressure, volume, pennation angle and strain as a function of activation, compression, initial pennation angle, and initial muscle length. Error bars represent the standard error of the least squares means.**

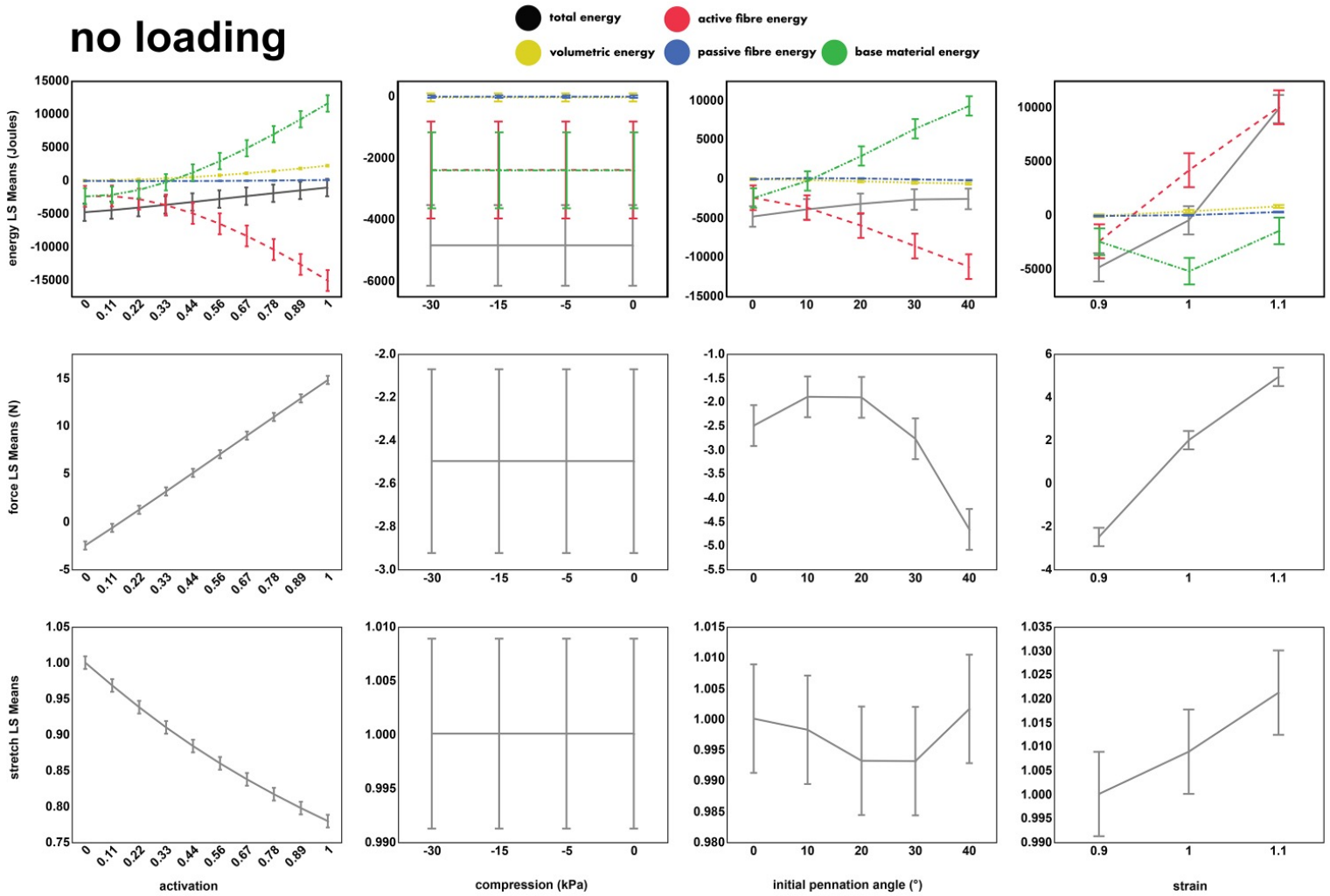

Figure A7 **Main effects plots for the muscle models without loading. The figure shows the energies, forces, and stretch as a function of activation, compression, initial pennation angle, and initial muscle length. Error bars represent the standard error of the least squares means.**

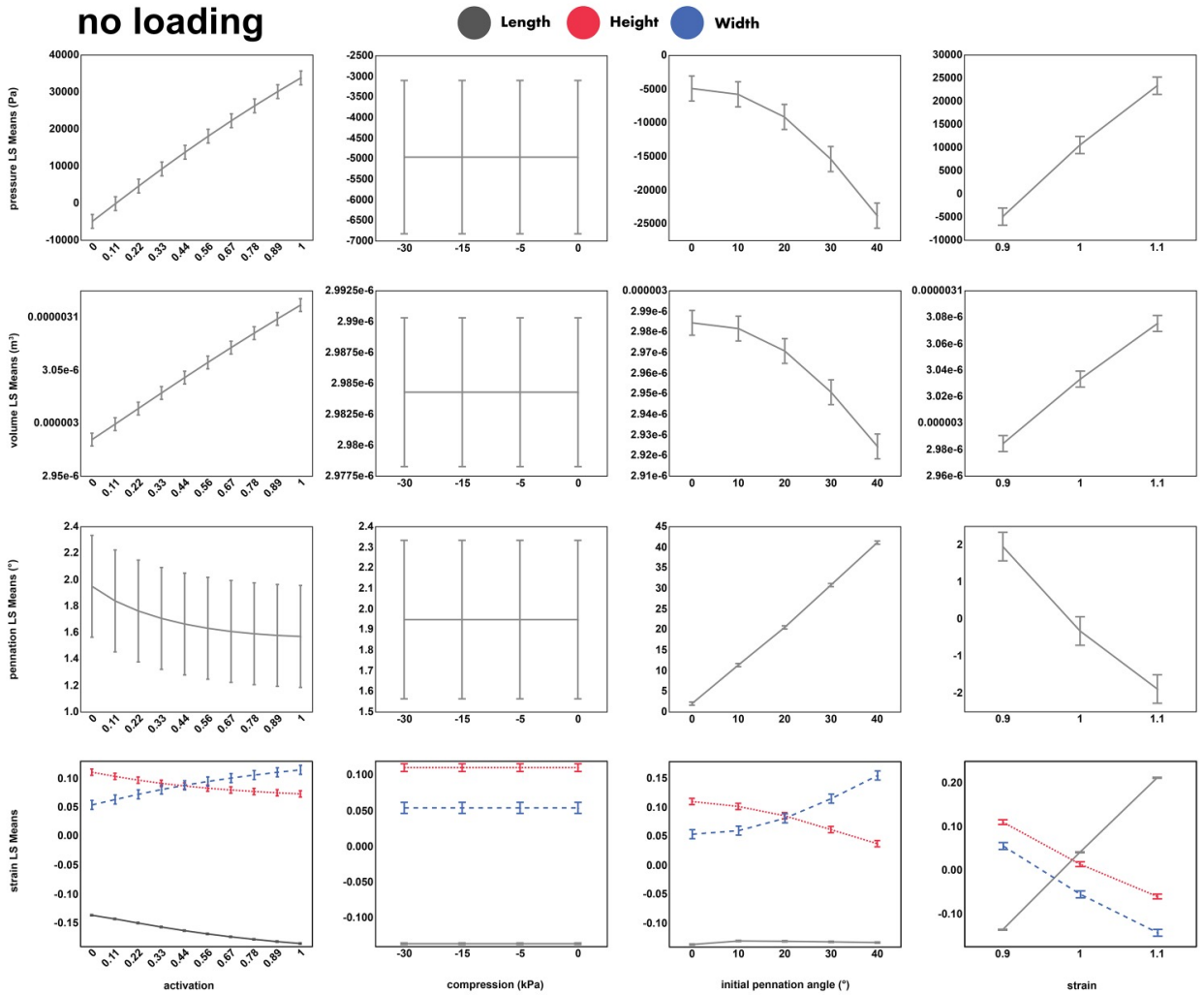

Figure A8 **Main effects plots for the muscle models without loading. The figure shows the pressure, volume, pennation angle and strain as a function of activation, compression, initial pennation angle, and initial muscle length. Error bars represent the standard error of the least squares means.**